Title
Interrogating the Role of Spatial Organization in Receptor Function: Eph-Ephrin Signaling in Breast Cancer

Author
Nair, Pradeep

Publication Date
2010

Peer reviewed|Thesis/dissertation

Interrogating the Role of Spatial Organization in Receptor Function: Eph-Ephrin Signaling in Breast Cancer

by

Pradeep M. Nair

A dissertation submitted in partial satisfaction of the

requirements for the degree of

Doctor of Philosophy

in

Chemistry

in the

Graduate Division

of the

University of California, Berkeley

Committee in charge:

Professor Jay T. Groves, Chair
Professor Carolyn R. Bertozzi
Professor Ming C. Hammond
Professor Kevin E. Healy

Spring 2010

Interrogating the Role of Spatial Organization in Receptor Function: Eph-Ephrin Signaling in Breast Cancer

by

Pradeep M. Nair

Abstract

Interrogating the Role of Spatial Organization in Receptor Function: Eph-Ephrin Signaling in Breast Cancer

by

Pradeep M. Nair

Doctor of Philosophy in Chemistry

University of California, Berkeley

Professor Jay T. Groves, Chair

Cells in living tissue integrate multiple signals from their environment to govern numerous aspects of both healthy and diseased behavior. The cell membrane serves as an exquisite functional filter that regulates information transmission between a cell and its surrounding environment. This viscoelastic plasma membrane, which allows lateral diffusion while restricting the orientation of signaling molecules within the plane of a phospholipid bilayer, is uniquely well suited to make sense of the myriad biochemical, mechanical, and spatial cues that constantly stimulate receptors on the cell surface. The chemical basis for the cell membrane, a fluid phospholipid bilayer, can be used to create a supported membrane that retains these properties while allowing precise control over the physical and chemical aspects of signaling molecules on the supported membrane surface.

Cell communication is critical for proper maintenance of multicellular organisms, and tumorigenesis can occur when communication is not properly controlled. Cancerous cells often display a vastly altered array of cell surface receptors compared to normal cells, and the abnormal signaling that these receptors trigger has grave consequences for the fate of the cell and the organism as a whole. The dynamics by which these receptors bind to ligands within the environment are not well understood because the cell membrane is a chemically heterogeneous and physically irregular surface that is difficult to study *in vivo*. Here we recapitulate signaling events that occur in live cancer cells using the supported membrane to present laterally mobile ligands to receptor-expressing human breast cancer cells.

This platform allows for precise control of the spatial organization of signaling molecules on the supported membrane surface, as well as a detailed examination of subsequent changes in signaling events within living cells. Using this approach we observe receptor reorganization responses that are strongly linked to tissue invasion and our observations reveal a mechanism by which cells respond to the spatial and mechanical aspects of their environment.

I dedicate this to my family, for their unwavering love and support.

Contents

List of Figures

List of Tables

Acknowledgments

I would like to acknowledge everyone who has provided me with support and encouragement, both to inspire my graduate endeavors and to make my time here an exciting and enlightening experience throughout. My cousin Gopal Sarngadharan first taught me to search out answers for myself. Professor Brooks Pate showed amazing patience and was an exciting advisor in college who motivated me to continue down the research path. David Kavulak and James Johns both made the transition to graduate school far less daunting. The entire Groves lab has provided the ideal collaborative research environment, and I must thank several members here. Professor Jay T. Groves has always been an encouraging advisor, allowing me to explore my own ideas, ready to help right the ship when things go off course, and clairvoyant enough to ensure they rarely do. Professor Khalid Salaita, with whom I worked closely on much of the work presented here, has never been anything short of the perfect mentor, labmate, or friend. His constant energy and enthusiasm was contagious and inspiring and his guidance was instrumental to my own success as a student. I would also like to thank Dr. Bryan Jackson, Dr. Nathan Clack, Professor Martin Forstner, and Professor Jwa-Min Nam, who all welcomed me into the lab and made sure I got off to a fast start as a researcher. I must also thank Dr. Hans-Christian Aasheim for graciously providing the monomeric ephrin-A1 used in chapter 3, Alexander Smoligovets and Dr. Cheng-Han Yu, who performed the transfections discussed in chapter 4, and Professor Marcus Textor, Dr. Mirjam Ochsner, Elizabeth Xu, and Julia Ying, who worked with me on projects not discussed here. Niña Hartman, despite her spritely quirks, has always provided a supportive and friendly ear and made daily lab life far more entertaining.

Chapter 1

Supported Membranes to Study Intercellular Communication in Cancer

1.1 Abstract

Cell communication occurs through a precisely regulated series of chemical reactions that begin with activation of receptors at the cell membrane surface and culminate with changes in the expression or localization of biomolecules such as proteins or sugars. The physical context in which activating ligands are presented to the cell is a key regulator in proper signaling, but this is often a difficult factor to address *in vitro*. In the case of juxtacrine signaling, where both receptor and ligand reside on apposed cell membranes, the orientations of the signaling molecules are highly constrained and the likelihood of clustering is significantly higher than in the case of paracrine signaling, where ligands are freely floating in solution. This results in completely different binding dynamics even for chemically identical receptor-ligand pairs, and can drastically alter the outcome of receptor stimulation. The supported membrane serves as an ideal experimental scaffold on which to display natively membrane-bound ligands to receptor-expressing cells. This platform is amenable to several conventional biochemical assays to measure the bulk response of activated receptors. Furthermore, the planar geometry of the cell-supported membrane interface allows for high-resolution microscopic techniques to directly visualize receptor-ligand binding interactions and subsequent downstream signaling events as they occur in living cells. The supported membrane is used here to present activating ligands to live human breast cancer cells displaying receptors implicated in tumor progression and invasion.

1.2 Cell Communication in a Diverse Physical Microenvironment

Cells in living tissue integrate multiple signals from their environment to govern numerous aspects of their behavior. Signaling molecules can be presented in a variety of different physical contexts (Figure 1.1).[1] The interstitial fluid surrounding cells in a multicellular organism can contain soluble ligands such as growth factors or cytokines that bind to receptors on a cell membrane, leading to paracrine signaling. Proteins and sugars presented in the extracellular matrix, responsible for the physical properties of different tissues, can also stimulate receptors on the cell surface. Finally direct cell-cell contact can lead to juxtacrine signaling, where cognate receptor-ligand pairs are presented on apposed cell membranes.[2]

Each signaling modality is characterized by unique physical characteristics. The extracellular matrix provides immobile anchorage points for cell adhesion, as well as ligand-aggregating domains that cluster receptors on the cell surface.[3] Receptors engaging ligands displayed on adjacent cell membranes may encounter resistance to movement of receptor-ligand complex generated by the membrane or the cytoskeleton of the ligand-displaying cell. Furthermore the orientation of both receptor and ligand will be highly constrained by the planar membranes displaying each. On the other hand, freely floating ligands in solution have no such orientational constraint, and since there is no physical tether between the ligand and another cell, transport of receptor-ligand complex will depend only on forces generated by the receptor-expressing cell. These mechanical differences in ligand display modalities can affect receptor

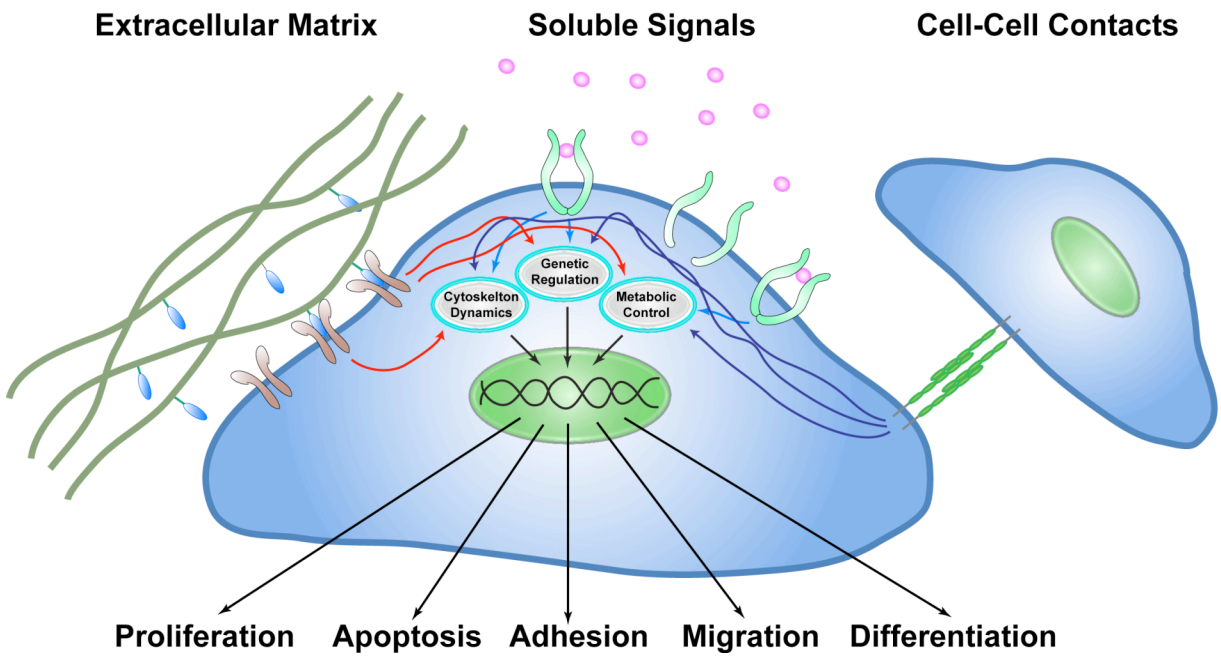

Figure 1.1: Cells integrate signals from a variety of physical contexts

responses such as clustering,[4] endocytosis,[5] or conformational change,[6] all of which may alter cell signaling.

1.3 The Cell Membrane is the Gatekeeper

The organelle that makes sense of all these potential signaling mechanisms is the cell membrane. As the barrier between the extracellular environment and the cytosol, it is responsible for transducing signals from outside the cell into biochemical changes within the cell, and vice versa. In this sense the cell membrane serves as a functional filter that allows the cell to respond to the myriad physical and chemical aspects of its microenvironment.

The cell membrane is a fluid phospholipid bilayer with a precisely controlled mixture of proteins, sugars, and lipids and it serves as a viscoelastic surface through which signals are transmitted.[3] Signaling molecules on the cell membrane are laterally fluid, but fixed within the plane of the bilayer. This constrains the available degrees of freedom for membrane-anchored receptors, making local enhancement of concentration far more probable than in solution,[7] and thus changing the kinetics of clustering at the membrane surface.

Organization of signaling molecules within the cell membrane is controlled through a variety of mechanisms. The phospholipid bilayer is composed of two leaflets of phospholipids oriented with their phosphate groups pointed outwards and their aliphatic groups inwards. This orientation allows the hydrophilic phosphate groups to face the cytosol and the extracellular space, and creates a hydrophobic region that separates the two. The length of this hydrophobic region depends on the makeup of the aliphatic tails. Longer, straighter tails will result in a longer hydrophobic region, and vice versa. In this manner proteins can be segregated to areas of the membrane with hydrophobic regions of the same length as their own transmembrane domains.

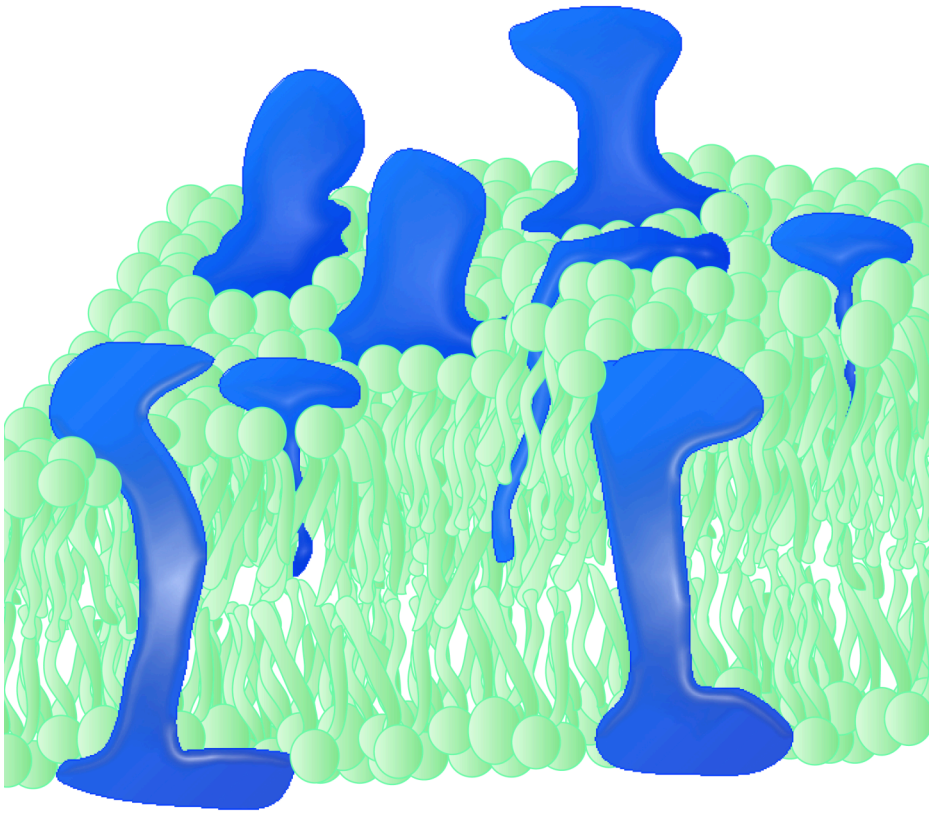

Figure 1.2: Cell membranes are complex
The cell membrane is an irregular, heterogeneous mixture of lipids, proteins, and sterols.

This minimizes hydrophobic mismatch that would otherwise lead to significant organization of water molecules around exposed hydrophobic residues, decreasing the allowed degrees of these molecules as well as the overall entropy of the system.[8,9]

In addition to thermodynamic considerations from the lipid molecules within the plasma membrane, some biomolecules within the cell membrane are physically tethered to the cytoskeleton, allowing rapid and direct reorganization of the membrane surface. Other molecules are indirectly linked to the cytoskeleton through a series of adaptor proteins that may be selectively activated to allow for modulated control of organization through the cytoskeleton.[3]

1.4 Miscommunication at the Membrane Interface Can Lead to Cancer

Cell communication is critical for proper tissue homeostasis, and tumorigenesis can occur when communication is not properly controlled. Malignant cells have evolved a unique set of behaviors that allow them to evade the various control mechanisms that multicellular organisms use to regulate intercellular signaling. Specifically, cancerous cells require no exogenous growth factor stimulation, become insensitive to growth-inhibitory and apoptotic signals, gain limitless replicative potential, develop their own vasculature, and eventually gain the ability to leave their

primary tissue and colonize new tissue in distant sites within the organism, through a process known as metastasis.[10]

With such drastic changes in intercellular signaling, it is no surprise that cancerous cells display a vastly altered array of cell surface receptors compared to normal cells[11], including loss of the intercellular adhesion molecule E-cadherin[12,13] and altered expression or activity of members of the ErbB[14] or Eph[15,16] receptor tyrosine kinase (RTK) families. These receptors trigger abnormal signaling events that have grave consequences for the fate of the cell and the organism as a whole. Many of the most successful cancer therapeutics target these same signaling molecules,[17,18] and are able to discriminate healthy from cancerous cells.

The potential therapeutic value to understanding the signaling of membrane-bound receptors has led to increased interest in understanding the dynamics by which these receptors bind to, and are activated by, their cognate ligands. However the cell membrane is a chemically heterogeneous and physically irregular surface that is difficult to study *in vivo*. Study of signaling events which begin at the cell surface requires the development of a platform that recapitulates the relevant degrees of freedom of the native system, but allows for the direct observation and manipulation of ligand binding and subsequent signaling events within live cells.

1.5 Probing the Influence of Membrane Organization in Signaling

Signaling has conventionally been studied using biochemical assays such as flow cytometry, western blotting, immunoprecipitation, or comparative genomic hybridization that probe relative concentrations of biomolecules as a function of cell stimulation. However an emerging motif in cell signaling is that the spatial organization of biomolecules within the cell membrane is a key component of properly regulated signaling,[1920] and these techniques are insensitive to this organization.

Microscopy allows for direct visualization of spatial organization within a single focal plane. With the advent of fluorescent proteins and organic dyes that can be covalently attached to target biomolecules, optical microscopy is now ideally suited to probe organization of labeled signaling molecules within live cell-cell junctions. However while fluorescence microscopy is well suited to detect labeled molecules within a single plane, the resolution with which this organization can be studied at the interface between two live cell membranes is limited. Direct visualization of this interface can only be performed with relatively poor resolution because the cell-cell contact zone is a dynamic and irregular interface, only part of which will fall within the well-defined focal plane of a high resolution optical microscope.

Further complicating the signaling landscape is the fact that the cell-cell interface is a chemically heterogeneous mixture made up of phospholipids, sphingolipids, cholesterol, integral proteins, membrane-anchored proteins, and a diverse array of glycosylated signaling elements (Figure 1.2).[21] At any given instant each of these molecules may interact with binding partners on the apposed cell surface, obscuring the effects of a single binding event. For these reasons it is necessary to design an experimental platform that is capable of measuring the effects of spatial organization for a single signaling cascade in isolation. Using a bottom-up approach, this

platform could then be augmented with additional signaling molecules to examine potential cross talk between different signaling pathways.

Design of such a platform requires the ability to perturb spatial organization at length scales relevant to juxtacrine signaling, and to then observe cellular response. Cell communication is sensitive to the lateral organization of signaling molecules at length scales ranging from single molecules[22-24] to the entire size of the cell,[25] so an ideal experimental platform must allow perturbation and observation across these length scales as well.

1.6 Developing a Model Cell Membrane

The biochemical results of receptor stimulation have largely been studied by presenting cells with soluble derivatives of ligands displayed *in vivo*. While this method of receptor activation is technically facile and has yielded tremendous insight into the products of receptor stimulation, it fails to accurately reflect the physical context in which juxtacrine or extracellular matrix signaling events occur. This can lead to drastic differences in response based solely on the physical aspects of ligand presentation, even with chemically identical presentation.[25-27] Physiologically relevant models of cell surface signaling must retain the lateral mobility available to signaling molecules presented on live cell membranes in order to accurately recapitulate the dynamics that occur *in vivo*.[28]

The chemical basis for the cell membrane is a phospholipid bilayer made up of two leaflets of phospholipids in an aqueous solution. Such a surface can be deposited onto a clean, hydrophilic glass substrate to form a supported phospholipid bilayer, or supported membrane for short, separated from the glass surface by a layer of water molecules 1 nm in height.[29] Neighboring phospholipids within a fluid supported membrane undergo van der Waals attractions between their aliphatic chains. When the temperature is below the gel-fluid transition temperature, these interactions are strong enough to prevent rotation of the phospholipids, and thus exchange of neighboring van der Waals attractions. This freezes the bilayer into the gel phase, where phospholipid lateral diffusion is not allowed. Above the transition temperature however, phospholipid molecules have enough kinetic energy to overcome these van der Waals attractions and allow lateral diffusion within the bilayer.[8]

1.7 Using the Supported Membrane to Study Cell Signaling Events

Signaling molecules can be anchored to phospholipids within a fluid supported membrane through several chemical or biochemical approaches.[26,30-32] Proteins in such a functionalized supported membrane retain the mobility characteristics of their anchoring lipid molecules, but are constrained to the plane of the supported membrane. This platform thus recapitulates the relevant degrees of freedom for signaling molecules presented on cell membranes, but in a far more controlled chemical microenvironment. In addition to serving as a scaffold upon which signaling molecules may be anchored, the supported membrane is a biocompatible surface with which cells expressing receptors of interest can be engaged.[33]

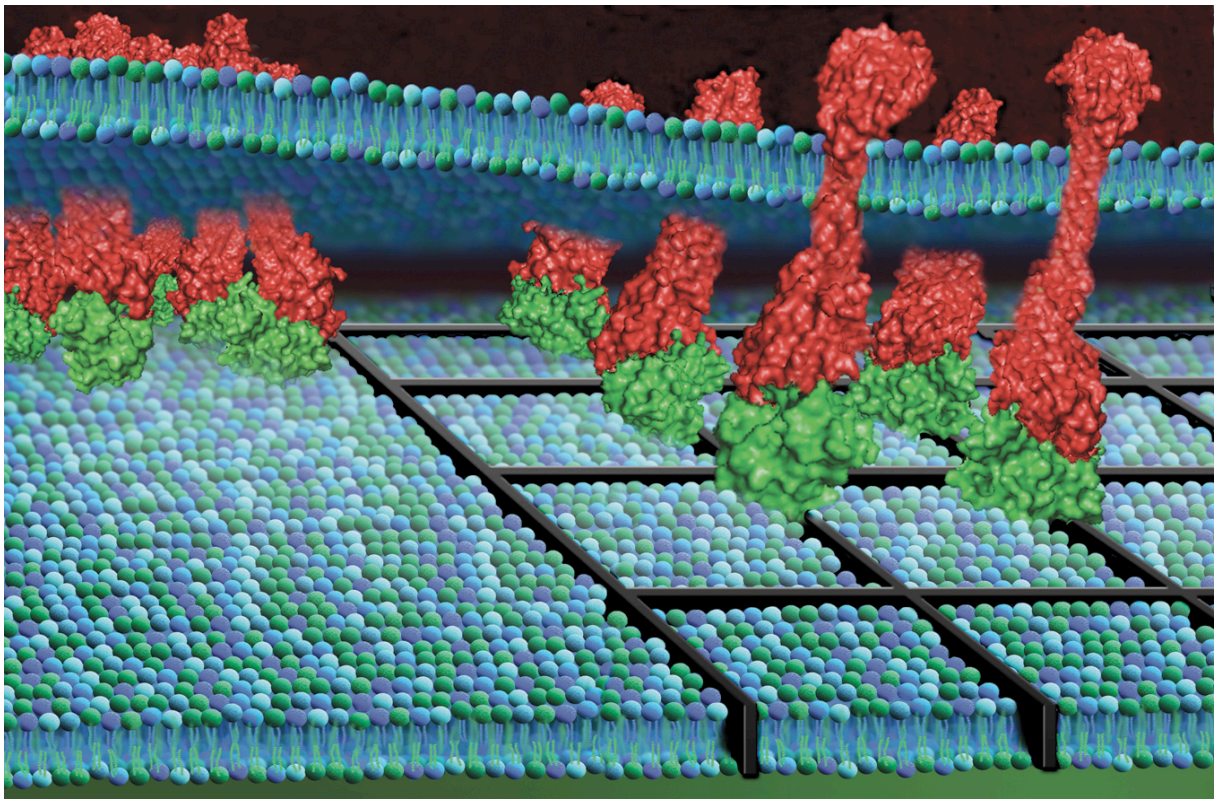

Figure 1.3: The hybrid cell-supported membrane interface
A schematic cross-section of a live cell (top) interacting with a supported membrane (bottom) through receptor-ligand binding events. The supported membrane provides a flat plane ideal for microscopic imaging and can be patterned with metal lines (black lines, right) that serve as diffusion barriers for membrane-anchored ligands and can thus alter the lateral organization of receptor-ligand complex within the interface.

The solid silica support on which supported membranes are deposited is amenable to several micro- and nanofabrication techniques that allow for lithographically defined constraints to laterally mobile receptor-ligand clusters. Pre-formed lipid bilayers can be "blotted" away through the use of an oxidized poly(dimethysiloxane) (PDMS) stamp. Alternatively, oxidized PDMS can be "inked" with either phospholipid vesicles (to form supported membrane patches)[34] or proteins (to create patterns of proteins adsorbed to exposed glass surfaces that restrict lipid diffusion)[35] before supported membrane deposition, creating protein or lipid corrals with micron-scale resolution. Metal lines as narrow as 20 nm in width that act as lipid diffusion barriers can also be deposited onto the underlying glass substrate using electron-beam lithography.[25] Patterned metal thin films can also be used to protect glass surfaces during protein deposition, then lifted off in a mildly basic aqueous solution. When vesicles are deposited onto this surface, supported membranes will form over the newly exposed glass, leaving a patterned protein-lipid hybrid surface with a lithographically defined resolution of 200 nm.[36] These lithographic techniques, as well as others primarily developed by the semiconductor industry but amenable to silica substrates, make the supported membrane the ideal platform to study the influence of lateral organization on signaling processes that originate from membrane-bound receptors (Figure 1.3).[20,25,37]

If a cell displaying receptors of interest is engaged with a supported membrane displaying

its cognate ligands, one can directly visualize the behavior of the cell, as well as the organization of labeled molecules both at the membrane junction and within the cell using a variety of microscopic techniques. The supported membrane provides a flat, well-defined plane that is amenable to several types of high-resolution optical microscopy.[38] Reflection interference contrast microscopy (RICM) can be used to image the hybrid cell-supported membrane junction. If the molecules of interest are labeled with fluorescent molecules, then epifluorescence, total internal reflection fluorescence (TIRF), or confocal microscopy can be used for direct visualization of signaling dynamics.[39]

The supported membrane can also be used with certain conventional biochemical approaches that are typically used to determine the extent of cell signaling. Cells can be allowed to engage a supported membrane, and then removed from the surface either by chemical trypsinization or by mechanical scraping. These cells can then be lysed and their protein content can be assayed using gel electrophoresis or western blotting to determine relative levels of protein expression based on supported membrane functionalization. In a similar fashion, genetic expression levels can be measured by purifying ribonucleic acid (RNA) from cells engaged with functionalized supported membranes, and then measuring gene expression across the entire human genome using array comparative genomic hybridization (array CGH).[40] In this manner one can determine changes in gene transcription between populations of cells engaged with different surfaces.

1.8 Juxtacrine Signaling at Hybrid Interfaces

Cell communication is a complex series of carefully regulated chemical reactions that determine cell migration, differentiation, proliferation and apoptosis. However cells in a multi-cellular organism do not function in isolation. Rather, they integrate physical aspects of their proximal microenvironment with chemical signals produced by other cells. While the chemical makeup of these signals provides significant insight into cellular decision-making, biochemical content alone is not sufficient to explain how cells interact with each other or with their microenvironment. The spatial organization of signaling molecules has emerged as a key component in cellular communication as well, and so new experimental tools capable of probing the effects of spatial organization on signaling must be developed.

In chapter 2, I describe the design of a platform that allows for the functional presentation of the natively soluble ligand, epidermal growth factor (EGF), to live mammary epithelial cells. The platform allows for presentation of a stimulating ligand on a fluid surface and characterization of subsequent changes in cell morphology.

In chapter 3, I utilized the supported membrane platform to present the natively membrane-anchored ligand ephrin-A1 to live human breast cancer cells. The monomeric form of this ligand is inactive in solution, while a synthetically cross-linked derivative of ephrin-A1 stimulates its receptor, EphA2, when presented in solution.[27] However both ephrin-A1 monomer and ephrin-A1 dimer were active on the surface of a fluid supported membrane. This is evidence that the lateral fluidity of the cell membrane, allowing for local enrichment of receptor-ligand complex on the membrane surface, is a key component of Eph-ephrin signaling *in vivo*.

In chapter 4, utilizing the supported membrane functionalized with ephrin-A1, I characterized the response of an invasive human breast cancer cell line to fluid membrane-anchored ephrin-A1, and observed radial transport of Eph-ephrin complex within the cell-supported membrane junction. When radial transport was mechanically hindered, these cells recruited significantly lower levels of metalloprotease and displayed dramatically altered cytoskeleton morphology. Finally, Eph-ephrin radial transport was measured across a panel of mammary epithelial cell lines, revealing a strong correlation between the ability of a cell to transport Eph-ephrin complex and its ability to invade foreign tissue, and this radial transport phenotype was linked to global changes in protein expression and organization.

This work demonstrates a fundamentally new technique to probe the effects of spatial organization in intercellular events that are known to play a role in tissue invasion. Many new questions have emerged from these findings, concerning the functional roles of receptor organization on the cell surface in general, as well as the specific mechanism by which EphA2 activation responds to physical parameters of ligand presentation. Furthermore, this work has demonstrated the utility of nanopatterned supported membranes to study juxtacrine signaling events in a controlled microenvironment. In chapter 5 I will describe some of the most pressing questions raised by this work, many of which are well suited to further study using the techniques developed here.

Chapter 2

A Fluid Membrane-Based Soluble Ligand-Display System for Live-Cell Assays

2.1 Abstract

Membrane-tethered epidermal growth factor (EGF) is found to modulate substrate attachment and spreading of human breast epithelial cells by signaling interactions with epidermal growth factor receptor (EGFR). In a newly implemented system, the fluidity of the supported membrane enables localized enrichment of ligand density in a configuration that reflects cognate-receptor distribution on the cell surface. This technique provides a means to control soluble ligand exposure within a parallel-surface array format.

2.2 Introduction

Cell communication modulates numerous biological processes including proliferation, apoptosis, motility, invasion and differentiation.[41-43] Correspondingly, there has been significant interest in the development of surface display strategies for the presentation of signaling molecules to living cells.[35,43-52] This effort has primarily focused on naturally surface-bound ligands, such as extracellular matrix components and membranes-bound signaling molecules. Soluble ligands (e.g. growth factors and cytokines) play an important role in intercellular communications,[53] and their display in a surface-bound format would be of great utility in the design of array-based live cell assays. Recently, several cell microarray systems that display cDNA, RNAi, or small molecules in a surface array format were proven to be useful in accelerating high-throughput functional genetic studies and screening therapeutic agents.[54-56] These surface display methods provide a flexible platform for the systematic, combinatorial investigation of genes and small molecules affecting cellular processes and phenotypes of interest. In an analogous sense, it would be an important advance if one could display soluble signaling ligands in a surface assay format that allows for systematic, patterned presentation of soluble ligands to live cells. Such a technique would make it possible to examine cellular phenotypes of interest in a parallel format with soluble signaling ligands as one of the display parameters.

Herein we report a ligand-modified fluid supported lipid bilayer (SLB)[45,49,57-61] assay system that can be used to functionally display soluble ligands to cells *in situ* (Figure 2.1A). The method benefits from the naturally fluid state of the supported membrane, which allows surface-linked ligands to diffuse freely in two dimensions. Ligands can become enriched beneath cells, by reaction-diffusion processes, and may also adopt spatial configurations reflecting those of their cognate receptors on the cell surface (Figure 2.1B). This provides a significant benefit over conventional cell signaling and culturing systems[35,46,50,62] that present inflexible distributions of signaling molecules. In this study, we observe marked differences in the response of cells to membrane surface displayed soluble ligands as a function of membrane fluidity. Tethering of soluble signaling molecules to fluid supported membranes opens up opportunities to use already developed membrane fabrication technologies[45,49,57-61] to present soluble components within a surface array format.

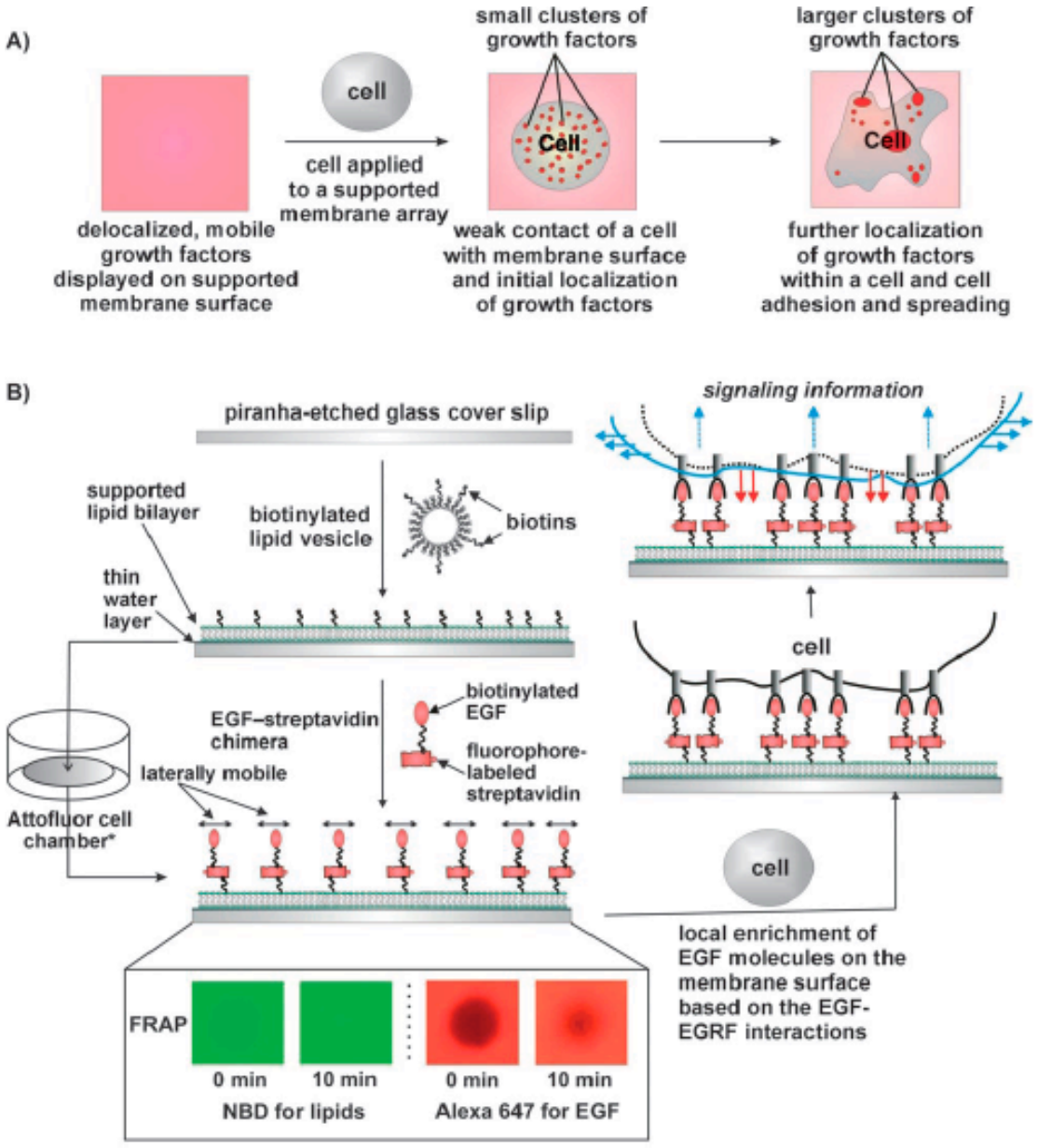

Figure 2.1: Presenting fluid EGF
A) Conceptual schematic of the fluid membrane-based soluble-ligand display strategy. **B)** Membrane-tethered EGF-based cell assay. Fluorescence recovery after photobleaching (FRAP) demonstrates mobility of lipids and EGF within supported membrane.

We chose epidermal growth factor (EGF) and the EGF receptor (EGFR) as a prototypic signaling system to evaluate the SLB platform. EGFR is a member of the type-I (ErbB) receptor tyrosine kinases (RTKs) and is activated by a number of ligands from the EGF family.[14,63,64] This results in receptor dimerization and a cascade of signaling events culminating in a number of biologic end points including proliferation.[64,65] ErbB de-regulation is a common event in human cancer where EGFR and a second family member, ErbB2, have become targets for directed therapeutic interventions such as Tarceva™, Herceptin™ and Iressa™.[17] It is clear that molecular understanding of EGFR and ErbB2 has a translational impact, and a more detailed

understanding of the molecular interactions of these molecules may yield further clinical benefit. However, the mechanism by which ErbB signaling is translated into specific biologic responses at the phenotypic level is poorly understood. Recent insights into the molecular mechanisms of EGFR signaling suggest that localization of EGFR on the cell membrane enhances receptor dimerization and clustering which is pre-requisite for ligand binding and activation of receptor kinase activity.[64,65] Applying the fluid membrane-tethered ligand display method reported herein to the EGF-EGFR system has clear benefits. The system allows for fast local enrichment of EGF induced by the EGF-EGFR interactions, facile *in situ* monitoring of fluorescently labeled EGF and temporal analysis of cellular phenotypes in a surface assay format. Moreover, with no ligand in solution, background fluorescence is minimal.

2.3 Results

2.3.1 Fluid Membrane-Tethered Epidermal Growth Factor

The design of an EGF-modified fluid SLB (EGF-SLB) assay is outlined in Figure 1B. To measure the fluidity of lipid bilayers (DMOPC, 1,2-dimyristoleoyl-*sn*-glycero-3-phosphocholine) with and without substrate-bound EGF, a focal region of the membrane was photobleached and fluorescence from NBD-PC (1-acyl-2-{12-[(7-nitro-2-1,3-benzoxadiazol-4-yl)amino]lauroyl}-*sn*-glycero-3-phosphocholine) lipids or Alexa Fluor 647-modified EGF was monitored. Photobleached regions for both bare lipids (green) and fluorescent EGF (red) recovered fluorescence, indicating they are fluid (Figure 2.1B, inset) though notably, EGF was slightly less fluid than NBD-modified lipids. Since there are four biotin-binding sites per streptavidin, and two should be this decrease in fluidity may be due to cross-linked streptavidin bound to multiple biotinylated lipids on the SLB surface.

2.3.2 Engaging Cells with Membrane-Anchored EGF

As a practical test of this system, we examined EGF-EGFR interactions between the EGF-SLB and live cells. We chose the immortal, non-transformed breast epithelial cell line, MCF10a, for this purpose as these cells express EGFR and are dependent on EGF signaling for proliferation and survival (all the cells in this paper refer to MCF-10a cells). We applied MCF-10a cells in serum-free, growth factor free DMEM/F-12 media (~300,000 cells per ml) to an EGF-SLB array and to a streptavidin-modified lipid membrane without EGF molecules. The cells were incubated at 37 ºC for 20 hr after which they were gently washed with DMEM/F-12 media and visualized by epifluorescence microscopy. Analysis of membranes post-washing revealed attachment of cells to the EGF-SLB array but not to the streptavidin-modified lipid membrane (Figure 2.2) suggesting EGF-dependent attachment of cells to the lipid surface. However, it was unclear whether direct ligand-receptor interaction alone was responsible for cell-membrane attachment, or whether EGFR signaling modulated cell attachment to the EGF-SLB via secondary mechanisms. To investigate whether the direct binding of EGF to EGFR facilitated attachment we added a competing antibody for EGFR (mAb225) to the cells. The presence of 3 ng/mL competing antibody reduced the number of cells attached to the membrane by 94% after 20 hrs (Figure 2.2, bottom left panel). This confirmed the specificity of the EGF-EGFR interactions and that it is required for cell-to-EGF-SLB attachment. EGF stimulation of

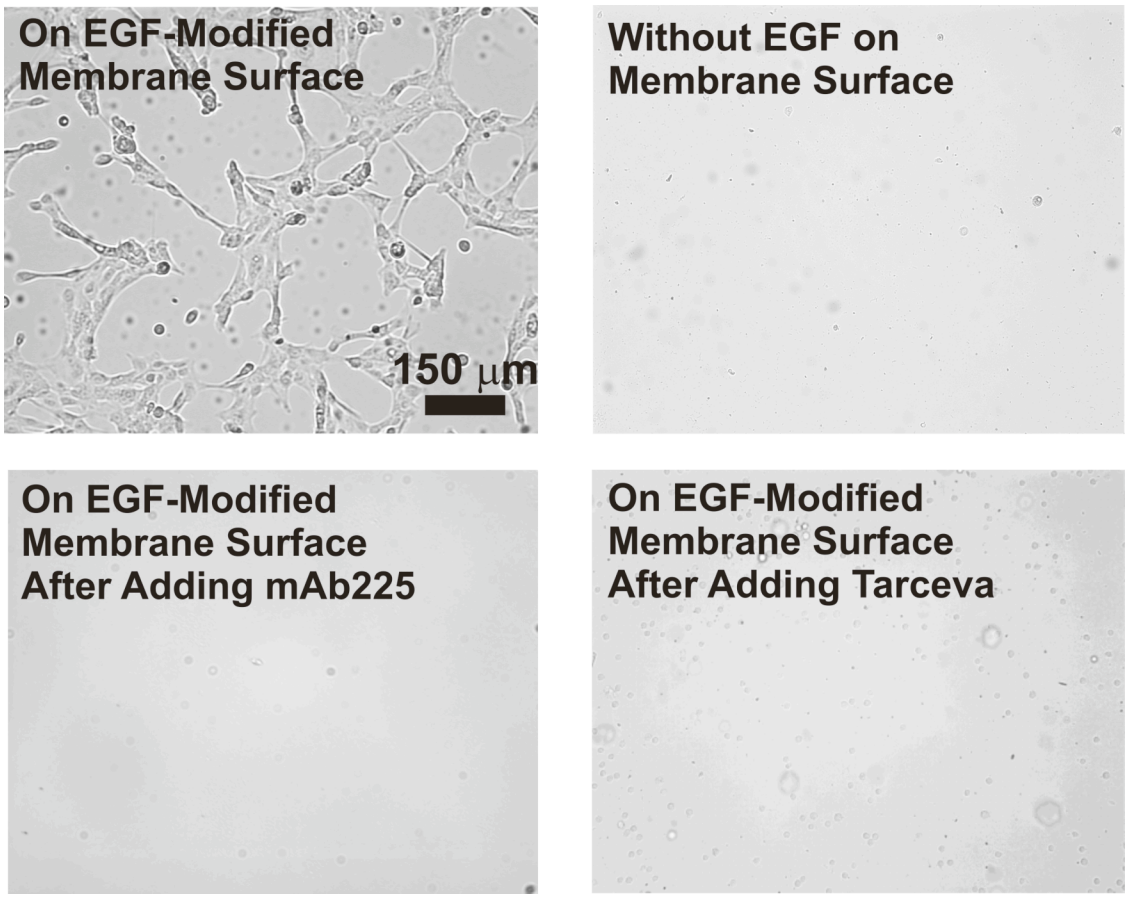

Figure 2.2: MCF-10A cells on supported membranes

EGFR kinase activity signaling activates a number of downstream pathways, some of which regulate cytoskeletal molecules, cell attachment and motility.[14,17,63-65] Therefore, we next tested if EGFR kinase activity is required for attachment by treating cells with Tarceva™, a specific kinase inhibitor of EGFR. When the assay was performed in the presence of Tarceva™, there was a significant reduction in the number of cells attached to the membrane (Figure 2.2, bottom right panel) confirming that activation of EGFR kinase activity is required for cell attachment.

To understand the temporal and spatial kinetics of the EGF-EGFR interaction, time-lapse experiments were employed to observe cell attachment to the EGF–SLB and subsequent EGF localization. This dynamic interaction was monitored using bright field microscopy to image cells and epifluorescence microscopy to image the EGF-coupled Alexa Fluor 647 (Figure 2.3). Cells were observed to weakly adhere to the surface as early as 80 min post plating. At this time, EGF was still randomly distributed across the surface. By 100 min, EGF molecules were observed to cluster into small focal points, which increased in size in a temporal fashion. These small clusters began to form larger clusters at around 150 min (Figure 2.3A). After 20 hr, a cell is spreading and adhered to the surface with many distinctive EGF clusters (Figure 2.3B). These clusters are reminiscent of focal adhesions required for cell-attachment to substratum. Since these EGF clusters appear to lie partially out of the supported membrane plane, as determined by focusing the microscope at different positions, we suspect that these clusters could be endocytosed EGFRs with bound EGFs and fluorophore labels. Since natural triggering of EGFR

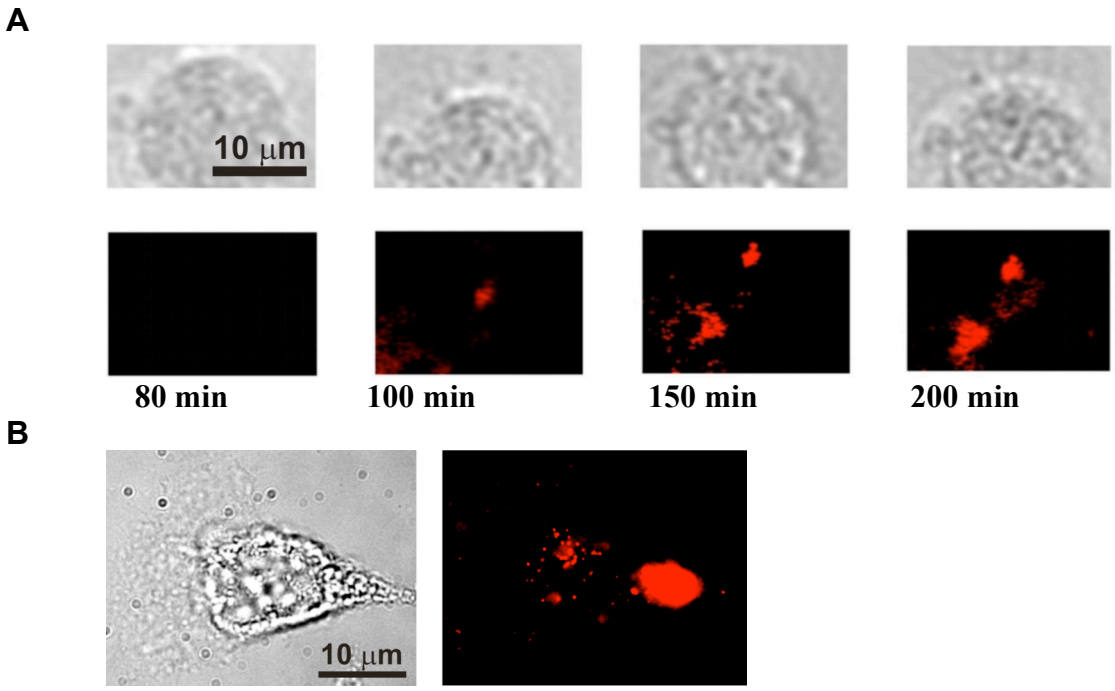

Figure 2.3: Cell clustering of fluid EGF
A) Bright field and fluorescence images showing clustering of EGF at the cell-supported membrane interface.
B) Bright field and fluorescence images of a cell on an EGF-modified SLB after 20 hr incubation at 37 ^{o}C.

by EGF is followed by endocytosis, we interpret this observation as further support of signaling functionality of membrane-tethered EGF. It should also be noted that cells cannot apply tensile forces to membrane adhesion sites; the fluid membrane will simply flow under such forces.[45] The stretched cell attachment phenotype (Figure 2.2 and Figure 2.3B) clearly indicates the presence of tensile forces, suggesting that the cells are anchored to the underlying solid substrate through focal adhesion sites. Formation of these focal adhesions likely involves remodeling of the surface by secretion of ECM proteins.

Clustering of EGFR on the cell surface is a pre-requisite for signal activation by ligand binding and is dependent on ligand diffusion across the SLB.[64,65] Therefore, we hypothesized that increasing the fluidity of membrane-tethered EGF would facilitate this process. To test this hypothesis, we directly compared the DMOPC-based system to the DPPC (1,2-dipalmitoyl-*sn*-glycero-3-phosphocholine)-based system, as DMOPC is much more fluid than DPPC (at 37^{o}C, the diffusion constant for DMOPC is 9 $\mu m^2 s^{-1}$ and the diffusion constant for DPPC is 0.1 $\mu m^2 s^{-1}$; Avanti Polar Lipids, Inc., Alabaster, AL).[66,67] Cells were applied to DMOPC- or DPPC-based EGF-SLB doped with the same concentration of biotinylated lipids using our standard procedure (see Methods), and EGF localization and cell attachment were observed after 20 hrs by bright field and epifluorescence microscopy. Cells adhered to the DMOPC EGF-SLB exhibited increased cell spreading, indicative of a motile phenotype, compared to the DPPC EGF-SLB (Figure 2.4). Cells attached to the DMOPC-based EGF-SLB surface displayed EGF clusters at the location where the cells were adhered. In contrast, fewer EGF clusters were found where cells were attached to the DPPC membrane arrays (Figure 2.4). These results suggest that supported membrane fluidity facilitates localized clustering of EGF, which is essential for its signaling functionality.

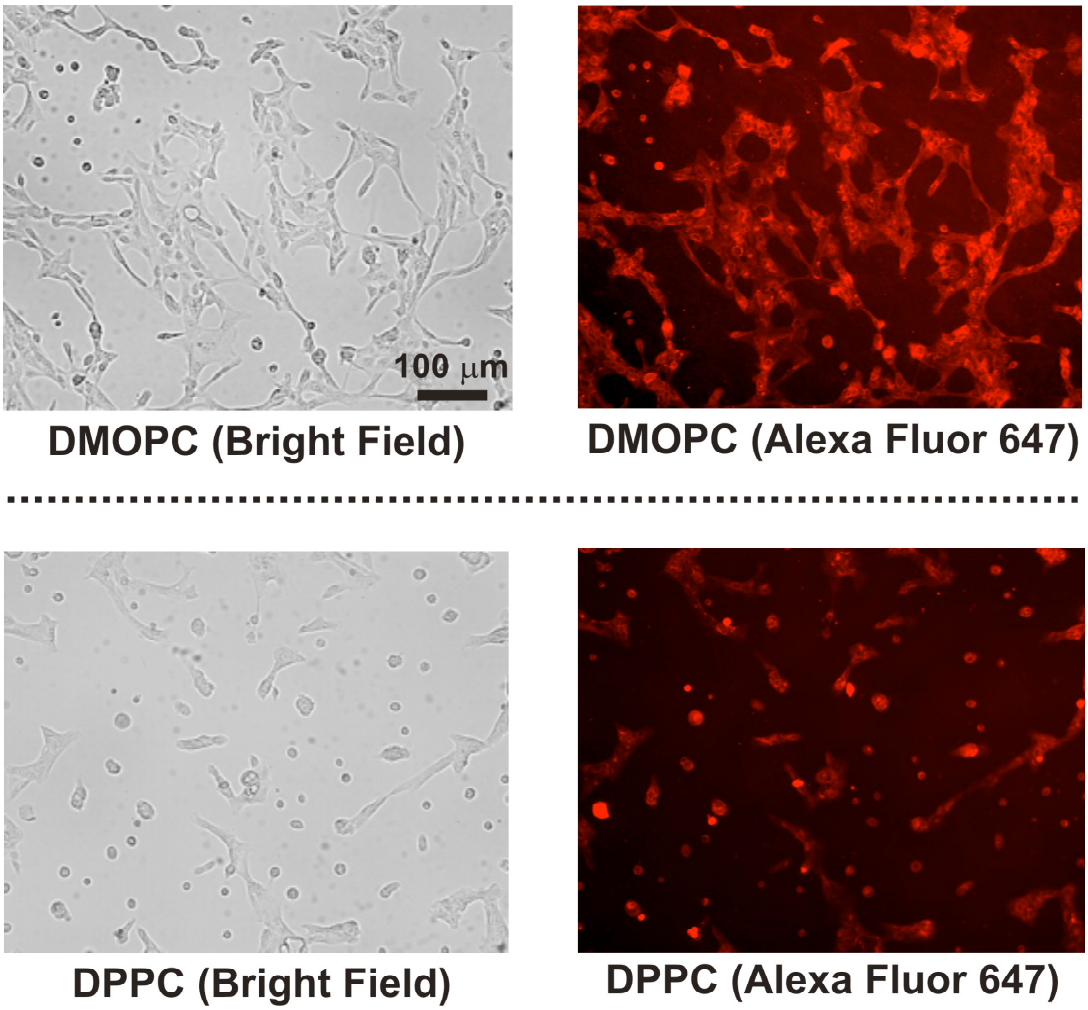

Figure 2.4: Fluid vs. immobile EGF
Cells cultured at 37 ^{o}C for 20 hrs on fluid (DMOPC, top panels) and non-fluid (DPPC, bottom panels) supported membranes.

2.4 Discussion

We have demonstrated the utility of fluid SLBs for the presentation of soluble signaling ligands to cells in culture. We found that membrane-tethered EGF is sufficient to promote cell adhesion and the fluidity of membrane-tethered ligands enhances its efficacy. Dynamic local enrichment of EGF molecules by reaction-diffusion processes was observed. The stretched morphology of the cells and the existence of focal adhesions suggest that the underlying substrate has been locally remodeled by ECM secretion. This process however, is triggered by membrane-displayed EGF. Through competition by inhibitory antibodies and EGFR kinase inhibitors, we demonstrated that this is an EGF-EGFR interaction-dependent phenotype and that kinase activation of the EGFR is also required. By studying the temporal adhesion of cells to EGF-SLB it is clear that full adhesion takes several hours, suggesting signaling through EGFR up-regulates a genetic program stimulating cell-adhesion.

This fluidity-based soluble ligand display system offers an experimental environment in which one can monitor dynamic reorganization and endocytosis of soluble ligands on a planar

platform in the absence of ligands in solution. By eliminating ligands in solution, improved observation of soluble signaling molecules is possible because background fluorescence intensity is minimal in this system.

The ligand display strategy reported herein provides a new dimension to controlling soluble ligand exposure to cells in culture. Display of soluble signaling ligands in an array format allows for the utilization of developed membrane array technologies to present soluble ligands to cells in various configurations. We anticipate this strategy will be useful in understanding the biology of ligand-receptor interactions as well as developing patterned soluble ligand-based high-throughput cell screening assays for medical diagnostic and cell biological applications. This simple system is expected to be applicable to other soluble ligands such as other growth factors, cytokines, and hormones as well as membrane-bound ligands (e.g. ephrins).

2.5 Methods

2.5.1 Lipid Membrane Preparation

Biotinylated lipid vesicles along with NBD-modified vesicles were prepared using existing methods.[57-59,61] In short, the desired lipids were dissolved in chloroform, and then the chloroform was evaporated using a rotary evaporator. The lipids were thoroughly dried under nitrogen gas and then hydrated with 1 mL of water. The hydrated lipids were extruded through 100 nm-sized pore filters and stored at 4 ^{o}C until the day of the experiments. Then, the vesicles (3 mol% biotin-modified DPPE, 2 mol% NBD-modified PC, and 95 mol% DMOPC purchased from Avanti Polar Lipids, Inc., Alabaster, AL) were allowed to warm to room temperature. Next they were ruptured on a piranha-etched microscopic cover glass (Fisher Scientific, Pittsburgh, PA) in 25 mM NaCl solution. The resulting lipid-bilayered glass substrate, immersed in NaCl solution, was sealed in an Attofluor cell chamber (Invitrogen Corp., Carlsbad, CA).

For the studies using DPPC, the initial lipid concentrations of the vesicles were 3 mol% biotin-modified DPPE, 2 mol% NBD-modified PC, and 95 mol% DPPC. After extruding through 100 nm-sized pore filters, the vesicles were extruded through 30 nm-sized pore filters so they would be smaller and easier to rupture. Before rupturing the vesicles, they were heated to 50 ^{o}C, as was the spreading solution and the NaCl salt solution. The piranha-etched microscopic cover glass was also heated above 50 ^{o}C. All of these heating steps were required to ensure the lipids were in the fluid phase while the bilayer was being formed. All other steps remained the same as when using DMOPC.

2.5.2 Membrane Functionalization

EGF conjugated to streptavidin and Alexa Fluor 647 (150 μl at 100 μg/ml; Invitrogen Corp., Carlsbad, CA) was incubated in the biotinylated membrane-modified glass substrate for 45 min at room temperature. The conjugate supplied by Invitrogen Corp. had an average EGF:Alexa Fluor 647-streptavidin ratio of 1:1, leaving three binding sites on each streptavidin to bind to a membrane-bound biotin molecule. This allowed attachment of EGF molecules to the membrane via streptavidin-biotin interactions. The NaCl salt solution immersing the SLB was then exchanged by washing the Attofluor cell chamber three times with DMEM/F-12 media (GIBCO, Invitrogen Corp., Carlsbad, CA). This washing step served the dual purpose of

removing unbound EGF-streptavidin-Alexa Fluor 647 molecules and immersing the SLB in media that was suitable for the desired cells to survive, while still retaining membrane fluidity.

2.5.3 Cell Culture

A human breast epithelial cell line, MCF-10a, was cultured in serum-rich media consisting of DMEM/F-12 media (GIBCO, Invitrogen Corp., Carlsbad, CA), hydrocortisone (500 ng/mL), horse serum (5% vol/vol), bovine insulin (0.01 mg/mL), and EGF (20 ng/mL). The day of the experiments, they were treated with trypsin-EDTA, washed twice with 1x PBS, centrifuged, and $3x10^5$ of the cells were re-suspended in 1 mL for each experiment. These 1 mL aliquots were then incubated in a 37 ^oC water bath until they were added to the EGF-SLB.

2.5.4 Cell Engagement

MCF-10a cells were added to the Attofluor cell chamber (1 mL at $3x10^5$ cells/mL). The chamber was then wrapped in parafilm, with holes to allow oxygen into the chamber, and the cells were incubated at 37 ^oC for 20 hours. After the incubation period, the Attofluor cell chamber was washed three times with DMEM/F-12 media to remove any non-adhered MCF-10a cells. The cells were then imaged using bright field and epifluorescence microscopy.

For the studies to count cells adhered to EGF-SLBs, the initial lipid concentrations were as before, but with an additional 2 mol% of the primary lipid constituent substituted for 2 mol% NBD-PC (3 mol% biotin-modified DPPE and 97 mol% DMOPC or DPPC). After the 20-hour incubation of the cells on the EGF-SLBs, the chamber was washed three times with DMEM/F-12 media as before, to remove non-adhered cells. Then the cells were stained with Hoechst 33342 (100 μl at 1 μg/ml) for 10 minutes and the chamber was washed four more times with DMEM/F-12 media to remove any unbound Hoechst 33342. Then the cells were imaged using bright field and epifluorescence microscopy.

For the studies with Tarceva™ and mAb225, the cells were incubated with either Tarceva™ or mAb225 for 45 minutes in a 37 ^oC water bath before being added to the EGF-SLB. All other steps were as before.

2.5.5 Optical Microscopy

We used a TE300 Nikon inverted microscope with a mercury arc lamp for epifluorescence illumination and a 100 W halogen lamp for bright field illumination. Figure 3A was taken with a Hamamatsu Orca CCD camera (Hamamatsu Corp., Hamamatsu City, Japan) and figures 2, 3B, and 4 were taken with a CoolSnap HQ CCD camera (Roper Scientific, Inc., Tucson, AZ). SimplePCI (Compix, Inc. Imaging Systems, Cranberry Township, PA) and MetaMorph (Molecular Devices Corp., Downington, PA) software was used to collect and analyze the images, which were then further processed using Adobe Photoshop 7.0. Alexa Fluor 647 was imaged using a Cy5 filter cube and NBD was imaged using an NBD/HPTS filter cube. For the cell counting studies Hoechst 33342 was imaged using a DAPI/Hoechst/AMCA filter cube. All filter cubes were purchased from Chroma Technology Corp., Rockingham, VT.

Chapter 3

Membrane-Bound Ephrin-A1 Signaling *In Vitro*

3.1 Abstract

Activation of the EphA2 receptor by the membrane-tethered ligand, ephrin-A1, has been shown to determine modulate the adhesion of a cell to its surrounding extracellular matrix. The human metastatic breast cancer cell line MDA-MB-231, expressing the EphA2 receptor on its cell membrane, displays an invasive, spread morphology when cultured on a supported lipid bilayer (SLB). When the SLB is functionalized with ephrin-A1, MDA-MB-231 cells cluster and internalize the ligand. These cells also revert to a rounded, non-invasive morphology when presented with fluid ephrin-A1 on a SLB. When these cells were presented with soluble ephrin-A1 monomer, they were unable to cluster the ligand and the EphA2 receptor was not activated, as measured by receptor degradation. When ephrin-A1 was covalently attached to the surface, MDA-MB-231 cells were unable to cluster or internalize the ligand and they did not display a phenotypic change in response to the ephrin-A1. The fluidity of the supported membrane enables localized enrichment of ligand density in a configuration reflecting cognate receptor distribution on the cell surface. Clustering is necessary for functional presentation of ephrin-A1 and this technique provides a means to control membrane-bound ligand exposure within a parallel surface array format.

3.2 Introduction

Cell-cell interactions are responsible for a wide array of cell behaviors ranging from cell growth and proliferation to apoptosis.[1,68] To better understand cell-cell communication and the interaction of a cell with the extracellular matrix (ECM), much work has focused on developing surface display strategies for the presentation of signaling molecules to living cells. These display strategies include covalent attachment, non-specific adsorption, electrostatic immobilization, coordination chemistry, as well as incorporation within a synthetic fluid membrane.[25,35,43,45,46,49,50,52,69,70] Although the chemical composition of the presented ligands may be identical, factors such as ligand orientation, density and two-dimensional (2D) mobility can all drastically alter the biological activity of surface-bound proteins.[50,61] The cell membrane is a dynamic environment allowing two-dimensional diffusion and clustering of signaling molecules and among the different display strategies, the synthetic fluid membrane is the most physiologically relevant display strategy for *in vitro* presentation of natively membrane-bound proteins.

Ephrin-A1 (EA1) is a glycosylphophatidylinositol (GPI) anchored ligand that binds to the EphA2 receptor found on the membranes of apposed cells. EA1-EphA2 signaling is a subject for scrutiny because EphA2 is overexpressed in several types of cancers such as ovarian and breast cancers.[28,71-73] Furthermore, overexpression of EphA2 can promote tumorigenesis in nontransformed human mammary epithelial cells.[74] On the other hand, activation of the EphA2 receptor has been shown to negatively regulate tumor growth and survival and much work has focused on activating EphA2 with ephrin ligands.[18,75] Both EphA2 and EA1 are membrane-bound proteins, and monomeric EA1 ($EA1_m$) is inactive when presented in solution.[27] *In vitro* presentation of EA1 has typically been accomplished by use of a soluble recombinant made up of two extracellular domains of EA1 each linked to one heavy chain of the Fc fragment of an antibody. Under non-reducing conditions, the two Fc fragments will form a disulfide bond, artificially cross-linking the extracellular domains of EA1 to form an EA1 dimer ($EA1_d$).[27] Since

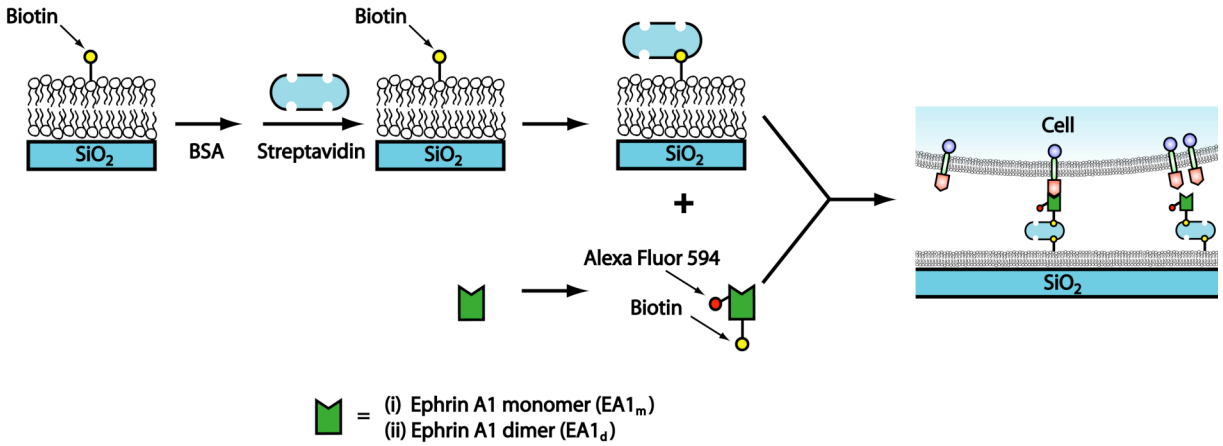

Figure 3.1: Presenting fluid ephrin-A1 to cells
Biotinylated phospholipids were incorporated into SLBs formed on silica substrates. Non-specific binding to the SLB surfaces was blocked with bovine serum albumin (BSA). Surfaces were then incubated with streptavidin then a fluorescently labeled and biotinylated ligand, either $EA1_m$ or $EA1_d$. These surfaces were then used to display fluid ligand to live receptor-expressing cells.

EA1 must be dimerized to activate EphA2 in solution, it has been hypothesized that clustering of ephrin ligands is required to activate EphA2.[15,16,24] The complete inactivity of $EA1_m$ when presented in solution highlights the importance of developing synthetic surfaces that recapitulate the essential characteristics of the native membrane.

Herein we describe use of a supported lipid bilayer (SLB) to present membrane-tethered ephrin-A1 (Figure 3.1). The SLB system has been demonstrated to be an effective platform to functionally present a variety of signaling molecules to cells.[25,69,76] The SLB is a natural choice for physiologically relevant presentation of natively membrane-bound signaling molecules *in vitro*.

After forming an ephrin-A1-functionalized SLB (EA1-SLB), human metastatic cancer cells displaying the EphA2 receptor were cultured on these substrates and their response to EA1-SLB (proliferation, adhesion, spreading, EphA2 activation) was observed. These responses were compared to the responses of the same cells to a bare SLB lacking EA1 (SLB), as well as to human non-metastatic cancer cells lacking EphA2. Use of the SLB platform to present EA1 to cells allows for local enrichment of the ligand induced by EphA2-EA1 interactions. Epifluorescence and bright field microscopy can be utilized to allow for *in situ* visualization of EA1 as well as the cellular response to this functionalized surface. Furthermore, with no ligand in solution, background fluorescence is minimal.

3.3 Results

3.3.1 Ephrin-A1-Modified Supported Lipid Bilayer

The design of an ephrin-A1-modified fluid SLB (EA1-SLB) is outlined in Figure 1. To measure the fluidity of lipid bilayers (1,2-dimyristoyl-*sn*-glycero-3-phosphocholine, DMPC) with and without substrate-bound ephrin-A1 dimer ($EA1_d$) or ephrin-A1 monomer ($EA1_m$), a focal region of the membrane was photobleached and fluorescence from NBD (lipids alone) or Alexa Fluor 594 ($EA1_d$ or $EA1_m$) was monitored. Initial experiments showed immobile fractions

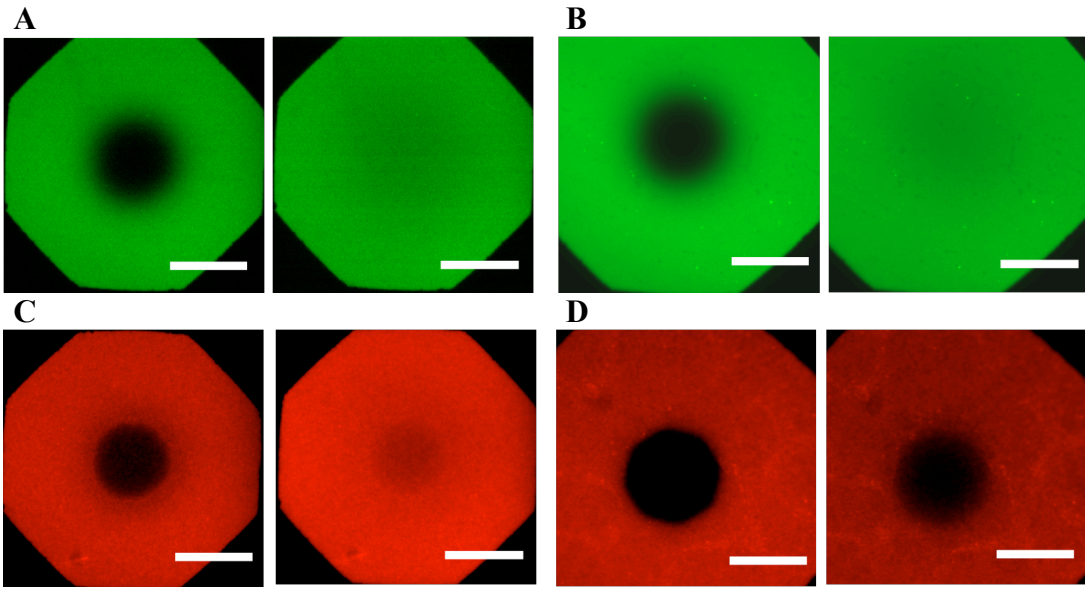

Figure 3.2: Ephrin-modified supported lipid bilayer FRAPs
Fluorescent recovery after photobleach (FRAP) demonstrates that NBD in bilayers (green) is fluid as well as $EA1_m$ and $EA1_d$. **A)** NBD recovery on $EA1_m$-SLB after 5 minutes. **B)** NBD recovery on $EA1_d$-SLB after 5 minutes. **C)** $EA1_m$ recovery on $EA1_m$-SLB after 10 minutes. **D)** $EA1_d$ recovery on $EA1_d$-SLB after 10 minutes. Scale bars equal 50 μm.

of the ligand despite fluid lipids, suggesting that ephrin may have non-specifically bound to the glass substrate. To minimize this non-specific binding, the bilayer was treated with 1 ml of 0.1 mg/ml BSA in PBS before addition of streptavidin. With this treatment, photobleached regions of bare lipids (Figure 3.2A, B), $EA1_m$ (Figure 3.2C) and $EA1_d$ (Figure 3.2D) recovered fluorescence indicating they are fluid, though $EA1_m$ and $EA1_d$ fluorescence recovered at a slower rate than bare lipid fluorescence. Since there are 4 biotin-binding sites per streptavidin, this decrease in fluidity was attributed to cross-linked streptavidin bound to multiple biotinylated lipids, which would create a more slowly diffusing species on the bilayer surface.

3.3.2 SLB-Based EphA2-EA1 System

In order to test the ability of this platform to phenotypically distinguish between metastatic and non-metastatic cells, we observed the differential response of cells to both bare bilayers (SLB) and those displaying ephrin-A1 dimer ($EA1_d$-SLB).

We chose to compare the response of the metastatic cancerous human breast epithelial cell line, MDA-MB-231, with that of the non-metastatic cancerous human breast epithelial cell line, T47D. MDA-MB-231 is a cell line derived from the basal lamina of the breast and these cells express EphA2 on their cell membranes. MDA-MB-231 cells display an invasive, stretched morphology when cultured in Matrigel. T47D is derived from the lumina of the breast and these cells lack EphA2 expression on their cell membranes. These cells display a round, non-invasive morphology when cultured in Matrigel. We applied both cells in serum-rich media (5×10^4 cells/ml) to a SLB and $EA1_d$-SLB. The cells were incubated at 37 ºC, with 5% CO_2 for 13 hr, after which they were visualized by bright field and epifluorescence microscopy. Analysis of membranes revealed attachment of MDA-MB-231 cells to all substrates, but these cells exhibited a much higher degree of cell adhesion and spreading on the bare SLB surface, as judged by

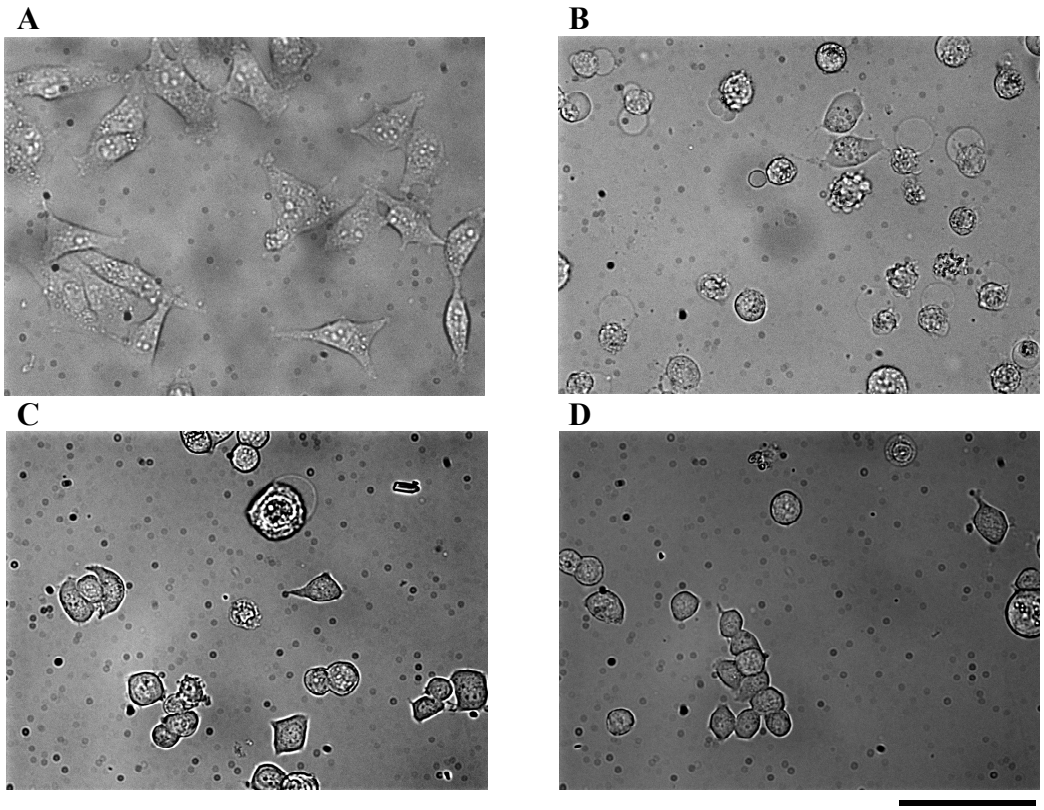

Figure 3.3: Decreased spreading and proliferation of metastatic cells on $EA1_d$-SLB
A) MDA-MB-231 cells cultured on SLB. **B)** MDA-MB-231 cells cultured on $EA1_d$-SLB. **C)** T47D cells cultured on SLB. **D)** T47D cells cultured on $EA1_d$-SLB. Scale bar equals 100 μm.

visual inspection, suggesting that interaction of these cells with bilayer-bound ephrin-A1 triggered a decrease in spreading and proliferation of the MDA-MB-231 cells. This interaction was is in agreement with epifluorescence images that show clustered bilayer-bound ephrin-A1 beneath rounded MDA-MB-231 cells cultured on $EA1_d$-SLB (Figure 3.4A, B). In contrast, T47D cells exhibited the same degree of cell attachment, proliferation and spreading on both the SLB and the ephrin-functionalized substrates (Figure 3.3C, D), suggesting that the T47D cells were unable to interact with the bilayer-bound ephrin-A1, as expected since these cells lack the EphA2 receptor on their cell membrane. These results were further supported when epifluorescence images revealed that T47D cells were unable to initiate clustering of ephrin-A1 on the $EA1_d$-SLB surface (Figure 3.4C, D).

3.3.3 Clustering and Internalization of EA1

When MDA-MB-231 cells were cultured on an $EA1_d$-SLB, clusters of the ligand began to form underneath the cells within 2-3 hours. Furthermore, 16 hours after the cells were added to the substrate, clusters of $EA1_d$ were located within the cells (Figure 3.4A, B, Figure 3.5C, D, and Figure 3.6C). The observed internalization of ephrin-A1 by MDA-MB-231 cells likely proceeds either through a protease-mediated ligand cleavage event, or through endocytosis of the phospholipids to which ephrin:streptavidin complexes are attached, and is discussed further in chapter 4.

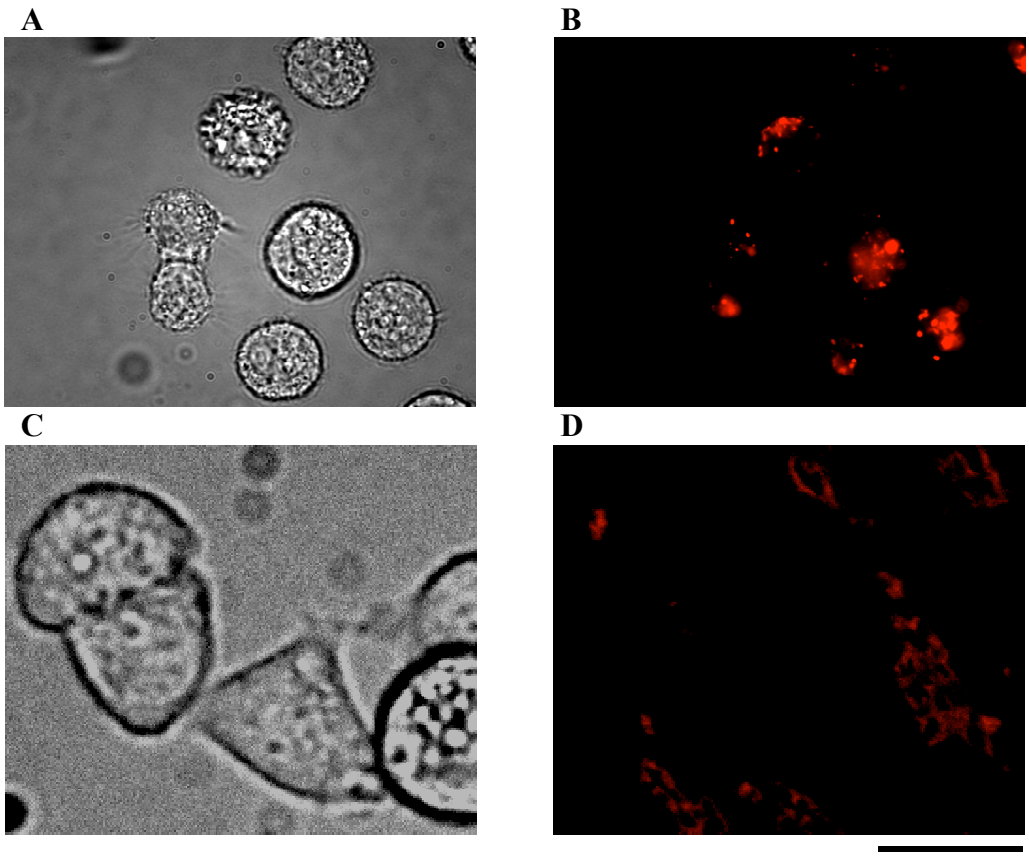

Figure 3.4: EphA2-expressing cells cluster fluid ephrin-A1
A) Bright field and **B)** corresponding epifluorescence images of MDA-MB-231 cells expressing EphA2 after 13 hr incubation on $EA1_d$-SLB at 37 ^oC, with 5% CO_2. **C)** Bright field and **D)** corresponding epifluorescence images of T47D cells lacking EphA2 recorded after 13 hr incubation on $EA1_d$-SLB at 37 ^oC, with 5% CO_2. Scale bar equals 20 μm.

When T47D cells lacking EphA2 were cultured on $EA1_d$-SLBs, neither ligand clustering, nor internalization was observed (Figure 3.4C, D). This suggests that these processes were mediated by the interaction of EA1 on the substrate with EphA2 on the MDA-MB-231 cell membrane.

In contrast, when EA1 was covalently attached to a silica substrate (see section 3.5.3), MDA-MB-231 cells were not able to cluster EA1 or to internalize the ligand (Figure 3.5A, B). Thus the fluidity of the SLB substrate is necessary for cells to cluster EA1. Also, MDA-MB-231 cells are unable to disrupt a covalent attachment between EA1 and the silica substrate, though they are able to disrupt the relatively weak van der Waals interactions that hold neighboring phospholipids together, both in a native cell membrane and in the synthetic supported membrane. From this evidence it is clear that covalent attachment of EA1 to a silica substrate does not provide the necessary biological context for MDA-MB-231 cells to interact with EA1.

3.3.4 Monomeric Ephrin Studies

SLBs were functionalized with the monomer of the extracellular domain of ephrin-A1 ($EA1_m$) to create $EA1_m$-SLBs. Analysis of ephrin-A1 and streptavidin crystal structures,[77,78]

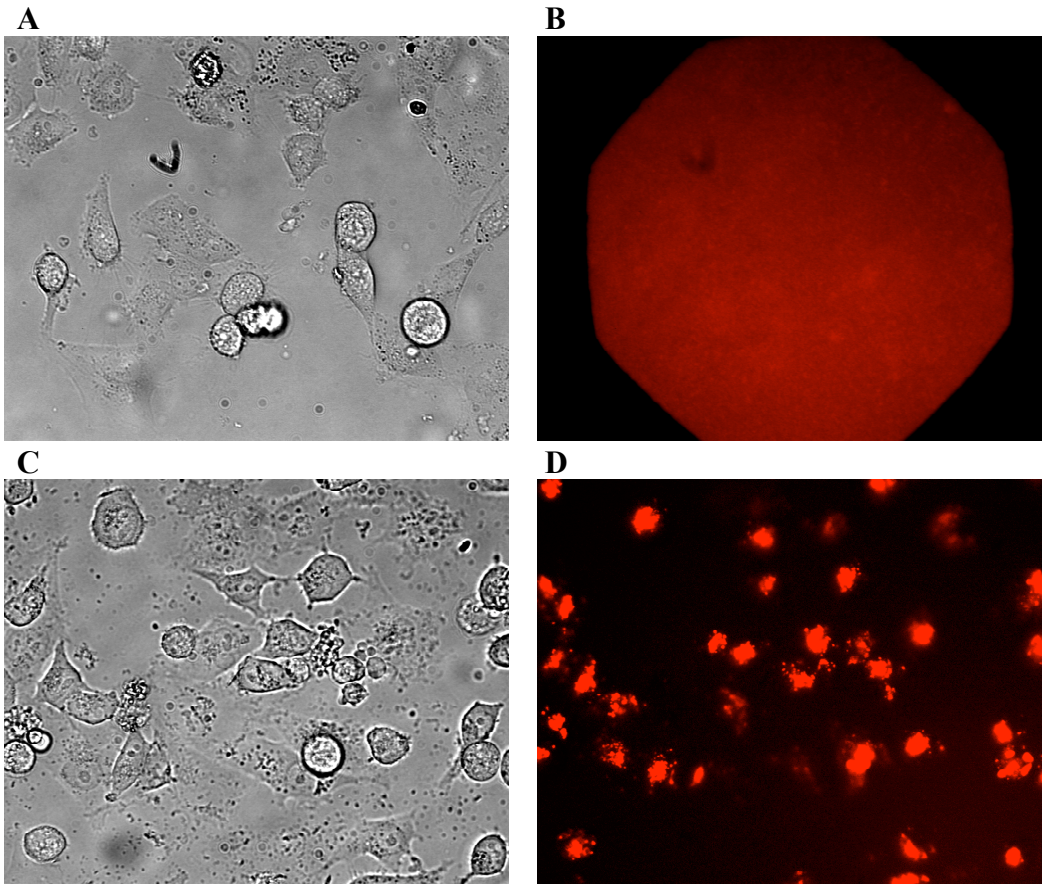

Figure 3.5: Immobile ephrin-A1 is not clustered by cells
A) MDA-MB-231 cells cultured on a silica substrate with 20% surface coverage of covalently attached EA1. **B)** Corresponding epifluorescence image showing Alexa Fluor 594-labeled $EA1_d$. Coverage with $EA1_d$ is homogeneous and localized to the image plane. **C)** MDA-MB-231 cells cultured on $EA1_d$-SLB. **D)** Corresponding epifluorescence image showing Alexa Fluor 594-labeled $EA1_d$. $EA1_d$ is clustered both within and underneath adhered cells. Scale bar equals 20 μm.

suggests that such a tethering technique would result in a population of singly bound ephrin-A1:streptavidin conjugates, due to steric restrictions to doubly bound conjugates.

MDA-MB-231 cells were then cultured on $EA1_m$-SLBs and their behavior compared to that on $EA1_d$-SLBs. After 2 hours, MDA-MB-231 cells were able to cluster $EA1_d$ either in solution or on a bilayer (Figure 3.6). However the cells were only able to cluster bilayer-bound $EA1_m$, not $EA1_m$ in solution. This suggests the monomer is functional on a laterally fluid surface, but not in solution. These results were further supported by western blots of EphA2 after engaging MDA-MB-231 cells with different forms of ephrin-A1 for 2 hours (Figure 3.7). The hypothetical mechanism for EphA2-EA1 signaling proceeds through activation of EphA2 followed by internalization and degradation of the receptor-ligand complex.[79,80] Cells cultured on $EA1_m$-SLBs showed decreased levels of EphA2, similar to cells cultured on $EA1_d$-SLB. Interestingly, when these cells were cultured with monomeric ephrin-A1 in solution, they showed similar levels of EphA2 as did cells on control substrates lacking ephrin. Ephrin-A1 requires the ability to be clustered by EphA2 expressing cells in order to be functional. Presentation in a supported lipid bilayer allows for this clustering, while soluble presentation does not.

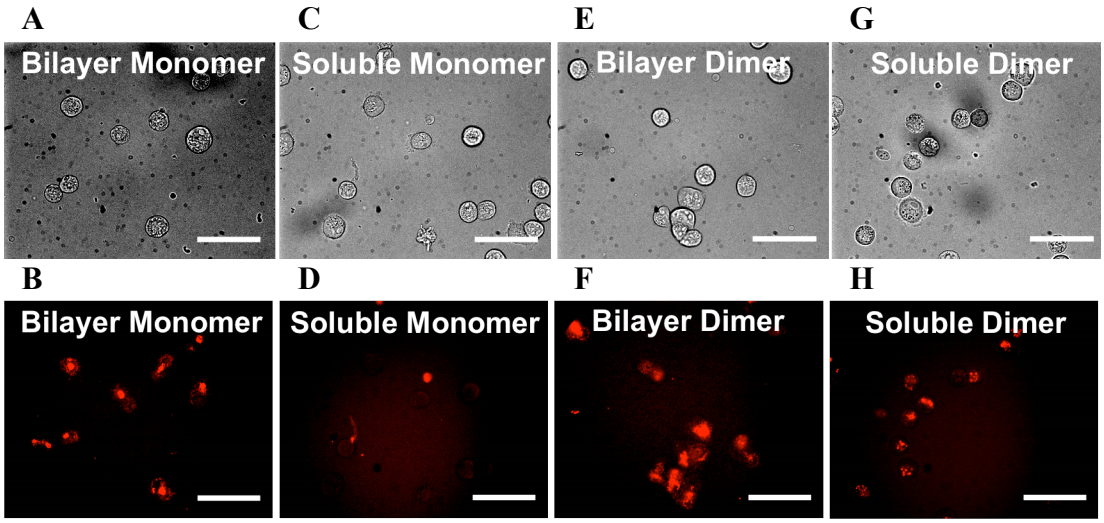

Figure 3.6: Clustering of ephrin-A1 depends on physical context of presentation
A) Bright field and **B)** corresponding epifluorescence image of Alexa Fluor 594-labeled $EA1_m$ showing clustering of the ligand in an $EA1_m$-SLB. **C)** Bright field and **D)** corresponding epifluorescence image of Alexa Fluor 594-labeled $EA1_m$ showing that monomeric ligand is not clustered when presented in solution. **E)** Bright field and **F)** corresponding epifluorescence image of Alexa Fluor 594-labeled $EA1_d$ showing clustering of the ligand in an $EA1_d$-SLB. **G)** Bright field and **H)** corresponding epifluorescence image of Alexa Fluor 594-labeled $EA1_d$ showing that the ligand is clustered when presented in solution. MDA-MB-231 cells were cultured on substrates for 2 hours at 37 ^oC, 5% CO_2, 100% humidity. Scale bars equal 50 μm.

3.4 Discussion

We have demonstrated the utility of fluid SLBs for the presentation of membrane-bound signaling ligands to cells in culture. We found that metastatic cancer cells are able to distinguish between a bare supported lipid bilayer substrate and one displaying fluid, membrane-tethered ephrin-A1 (Figure 3.3 and Figure 3.7). Furthermore, cells respond substantively different to immobile ephrin-A1 than they do to laterally fluid ephrin-A1 (Figure 3.5).

These results suggest that after initial weak cell adhesion which occurs within approximately 30-90 minutes, binding of EphA2 to EA1 leads to the dynamic local enrichment of EA1 molecules beneath the surface of EphA2-expressing metastatic cancer cells. These ligands bind to and activate EphA2 on the MDA-MB-231 cell surface and trigger a signaling cascade that culminates in decreased adhesion to the surface and decreased cell spreading. Non-metastatic T47D cells, lacking EphA2 on their cell surface, are unable to interact with bilayer-bound ephrin-A1, and thus cannot distinguish between the bare SLB and the EA1-SLB (Figure 3.4). This results in no morphological or behavioral response of T47D cells to the ephrin-A1-functionalized membranes.

This fluidity-based membrane-bound ligand display system offers an experimental environment in which one can monitor dynamic reorganization and endocytosis of membrane-bound ligands on a planar platform in the absence of ligands in solution. By eliminating ligands in solution, improved observation of membrane-bound signaling molecules is possible because background fluorescence intensity is minimal in this system. Background intensity can be decreased still further using surface-selective imaging methods such as total internal reflection

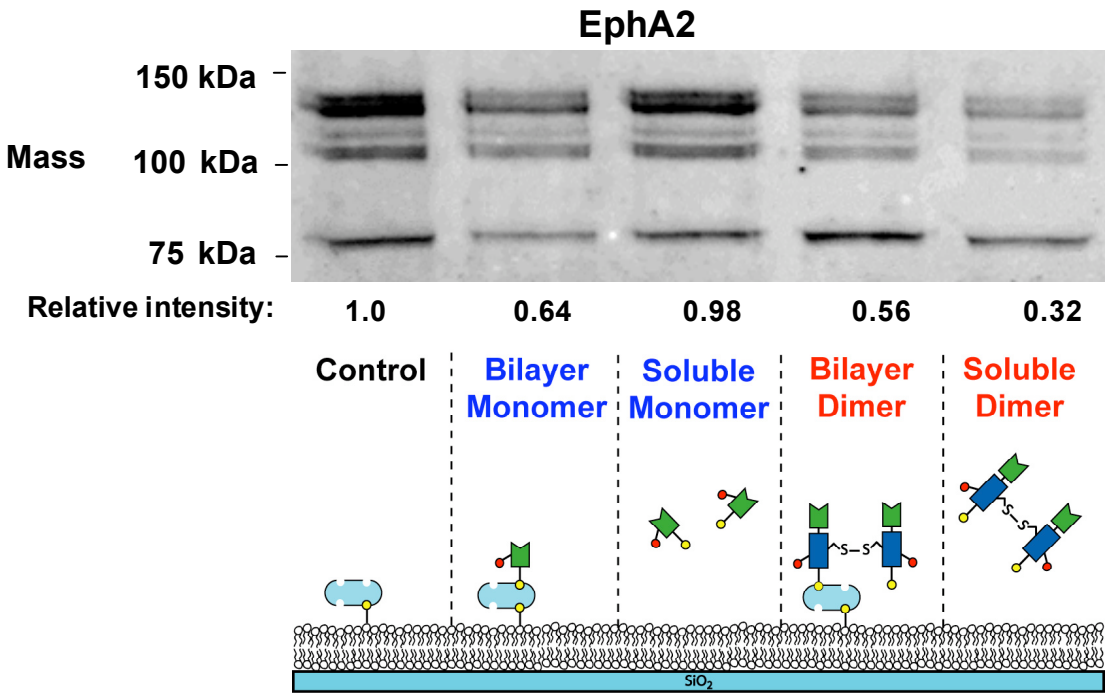

Figure 3.7: EphA2 activity as a function of ligand context
Ephrin-A1 activates EphA2 to a lesser extent (causes less receptor degradation) when presented as a monomer in solution, but its activity is rescued when presented on a fluid supported lipid bilayer. Synthetically cross-linked ephrin-A1 is active both on a fluid supported lipid bilayer and in solution.

fluorescence (TIRF) microscopy to image only proteins within 100 nm of the cell-SLB interface.[39]

Additionally, monomeric $EA1_m$ is only functional when presented in the context of a supported lipid bilayer. This supports the hypothesis that EA1 must be clustered for it to activate EphA2. Clustering can be achieved either through artificial means, as observed in $EA1_d$, or by presentation in a fluid membrane that allows for two-dimensional diffusion. As EA1 is natively presented within the context of the cell membrane, the most physiologically meaningful method of presenting ephrin A1 *in vitro* is the supported lipid bilayer.

The ligand display strategy reported herein provides a method to functionally present natively membrane-bound ligands to live cells. The SLB platform has also been demonstrated to functionally present soluble signaling molecules.[69] We anticipate this strategy will be useful in understanding the biology of ligand-receptor interactions as well as developing patterned membrane-bound ligand-based high-throughput cell screening assays for medical diagnostic and cell biological applications. Future studies may also incorporate patterned extracellular matrix proteins such as fibronectin[36,81] or laminin, allowing for the examination of juxtaposed cell signaling of multiple pathways in a surface array format.

3.5 Methods

3.5.1 Lipid Membrane Preparation

Biotinylated lipid vesicles were prepared using existing methods.[49,69] In short, the desired lipids were dissolved in chloroform, and the chloroform was evaporated using a rotary evaporator. The lipids were thoroughly dried under nitrogen gas and hydrated with 1 mL of water. The hydrated lipids were extruded through 100 nm-sized pore filters and stored at 4 ^{o}C until the day of the experiments. Then, the vesicles (1 mol% biotin-modified DPPE and 99 mol% DMPC purchased from Avanti Polar Lipids, Inc., Alabaster, AL) were allowed to warm to room temperature. They were then ruptured on a piranha-etched microscopic cover glass (Fisher Scientific, Pittsburgh, PA) in 1X PBS solution. The resulting lipid-bilayered glass substrate, immersed in PBS solution, was sealed in an Attofluor cell chamber (Invitrogen Corp., Carlsbad, CA). Excess vesicles were rinsed away with PBS.

3.5.2 Membrane Functionalization

Non-specific binding to the glass surface was blocked by incubating the substrate with 1 ml of 0.1 mg/ml BSA (Sigma-Aldrich, Saint Louis, MO) in PBS at room temperature for 30 minutes. Excess BSA was rinsed away with PBS. 2 ml of a 2 μg/ml solution of streptavidin (Sigma-Aldrich, Saint Louis, MO) in PBS was incubated with the substrate at room temperature for 40 minutes. Unbound streptavidin was rinsed away with PBS. 5 μg of ephrin-A1 dimer ($EA1_d$ purchased from R & D Systems, Minneapolis, MN) or ephrin-A1 monomer ($EA1_m$ donated by Hans-Christian Aasheim) labeled with Alexa Fluor 594 (Invitrogen Corp., Carlsbad, CA) and biotinylated (Sigma-Aldrich, Saint Louis, MO) was added to the substrate and allowed to react for 45 minutes. Unbound $EA1_d$ or $EA1_m$ was rinsed away with PBS. During all rinsing steps, the substrate was kept wet.

3.5.3 Covalent Attachment of EA1 to Substrate

Piranha-etched microscopic coverglass was coated with mercaptopropyl-trimethoxysilane (MPTMS) by vapor deposition for 1 hour at room temperature. The coverglass was then rinsed with ethanol and immersed in a 10% vol/vol solution of succinimidyl-4-(*N*-maleimidomethyl)cyclohexane-1-carboxylate (SMCC) in dimethylsulfoxide (DMSO) for 1 hour. The coverglass was next rinsed with DMSO and then ethanol. A solution of EA1 and BSA mixed in a 20:80 ratio in PBS buffered at pH 7.4 was then added to the coverglass. A single drop of the solution was placed on the coverglass and then sandwiched between a second, etched but bare, coverglass and allowed to incubate for 1 hour and then rinsed in PBS and placed in an Attofluor cell chamber. Cells were then added to the substrate and imaged as described below.

3.5.4 Cell Culture

A human breast cancer epithelial cell line, MDA-MB-231, was cultured in serum-rich media consisting of DMEM media (GIBCO, Invitrogen Corp., Carlsbad, CA), fetal bovine serum (10% vol/vol), L-glutamine (1% vol/vol), and penicillin/streptomycin (1% vol/vol). T47D cells were cultured in serum-rich media consisting of RPMI media (GIBCO, Invitrogen Corp.,

Carlsbad, CA), fetal bovine serum (10% vol/vol), L-glutamine (1% vol/vol), and penicillin/streptomycin (1% vol/vol). The day of the experiments, cells were treated with trypsin-EDTA, centrifuged, counted, and added to each substrate as described previously.

3.5.5 Engagement of Cells to Ephrin-Displaying SLB

After membrane functionalization, cells were added to the substrates. For morphology studies 2 ml of a $2.5x10^4$ cells/ml media were added to the Attofluor cell chamber (for a final concentration of $5x10^4$ cells in ~3 ml total volume). Cells were cultured on substrates for 20 hours. After the incubation period, the cells were imaged using bright field and epifluorescence microscopy.

For western blot experiments, more cells were required and since cells were only cultured for 2 hours, proliferation was not a concern. 2 ml of $1.5x10^5$ cells/ml media were added to the Attofluor cell chamber (for a final concentration of $1.5x10^5$ cells in ~3 ml total volume). Cells were cultured as before for 2 hours and then lysed and their protein mass calculated and normalized. All culturing was performed at 37 ^oC, 5% CO_2, and 100% humidity in sterile conditions.

3.5.6 Western Blotting

Western blots were performed on MDA-MB-231 cells after they had been cultured on SLB, $EA1_m$-SLB and $EA1_d$-SLB for 2 hours. First, each substrate was placed on ice and supernatant from each substrate was collected. Each substrate was then rinsed with 2 ml of cold Dulbecco's PBS and the rinses were added to the supernatant fractions. The combined rinses and supernatant from each substrate were centrifuged at 250 g for 5 minutes at room temperature and the supernatant was aspirated. Each cell pellet was then resuspended in 50 μl of NP-40 buffer. 100 μl of NP-40 buffer was added to each substrate and adhered cells were scraped off the substrate and added to the cell pellet previously resuspended, as was the NP-40 remaining on the substrate surface. Western blots were then run on fractions of the cell lysates.

3.5.7 Optical Microscopy

We used a TE300 Nikon inverted microscope with a mercury arc lamp for epifluorescence illumination and a 100 W halogen lamp for bright field illumination. Bright field and epifluorescence images were taken with a Hamamatsu Orca CCD camera (Hamamatsu Corp., Hamamatsu City, Japan) and a CoolSnap HQ CCD camera (Roper Scientific, Inc., Tucson, AZ). SimplePCI (Compix, Inc. Imaging Systems, Cranberry Township, PA) MetaMorph (Molecular Devices Corp., Downington, PA) and Microsoft Excel software was used to collect and analyze the images, which were then further processed using Adobe Photoshop 7.0. Alexa Fluor 594 was imaged using a Texas Red filter cube. NBD was imaged using an NBD/HPTS filter cube. All filter cubes were purchased from Chroma Technology Corp., Rockingham, VT.

Chapter 4

Restriction of Receptor Movement Alters Cellular Response: Physical Force Sensing by EphA2

4.1 Abstract

Activation of the EphA2 receptor tyrosine kinase by ephrin-A1 ligands presented on apposed cell surfaces plays important roles in development and exhibits poorly understood functional alterations in cancer. Here, we reconstitute this intermembrane signaling geometry between live EphA2-expressing human breast cancer cells and supported membranes displaying laterally mobile ephrin-A1. Receptor-ligand binding, clustering, and subsequent lateral transport within this junction are observed. EphA2 transport can be blocked by physical barriers nanofabricated onto the underlying substrate. This physical reorganization of EphA2 alters the cellular response to ephrin-A1, as observed by changes in cytoskeleton morphology and recruitment of a disintegrin and metalloprotease 10. Quantitative analysis of receptor-ligand spatial organization across a library of 26 mammary epithelial cell lines reveals characteristic differences that strongly correlate with invasion potential. These observations reveal a mechanism for spatio-mechanical regulation of EphA2 signaling pathways.

4.2 Introduction

Mammalian cells exhibit marked sensitivity to physical aspects of their environment, such as compliance,[82] texture,[83] and geometry.[84] Tensional homeostasis between and within cells contributes to proper cell differentiation, development and ultimately survival.[85] Because most cellular decision making occurs via chemical processes, understanding the coupling between physical forces and chemical signaling networks is of fundamental importance. Focal adhesions, which consist of protein assemblies organized at sites where cell-surface integrin receptors bind extracellular matrix ligands, are the most widely studied interface for tensile force transduction.[86] However, the majority of membrane receptors are not associated with focal adhesions. The mechanisms (and even existence) of chemo-mechanical regulatory coupling in these systems remain largely unknown.

It is becoming clear that spatial organization of cell surface receptors can regulate associated signal transduction pathways.[87-90] An important corollary is that mechanical forces acting on ligands can influence receptor spatial organization and, correspondingly, signaling.[22,91,92] Juxtacrine signaling, in which receptor and ligand reside in apposed cell membranes, represents an important class of intercellular communication where physical restriction of ligand spatial organization and movement is evident.[87,93] Here, we reconstitute the juxtacrine signaling geometry between live cells expressing the EphA2 receptor tyrosine kinase and supported membranes displaying laterally mobile ephrin-A1 ligand.

EphA2 is implicated and functionally altered in a number of cancers. In particular, 40% of human breast cancers overexpress the receptor.[94] Upon binding to natively membrane-anchored ephrin-A1, EphA2 undergoes dimerization, transphosphorylation of the cytoplasmic domains, recruitment of a molecular complex with SHC and GRB2 adaptor proteins, and subsequent activation.[16] EphA2 activation stimulates the mitogen activated protein kinase (MAPK) and the phosphoinositide 3-kinase pathways and recruits the c-Cbl adaptor protein and a disintegrin and metalloprotease 10 (ADAM10), both of which regulate receptor degradation.[79,80] Freely soluble ephrin-A1 ligand binds to EphA2 but fails to trigger activation unless the ligand is chemically cross-linked.[27] Despite this observation, most biological and biochemical studies of EphA2 stimulation rely on soluble variants of the ligand.[94] We employ a

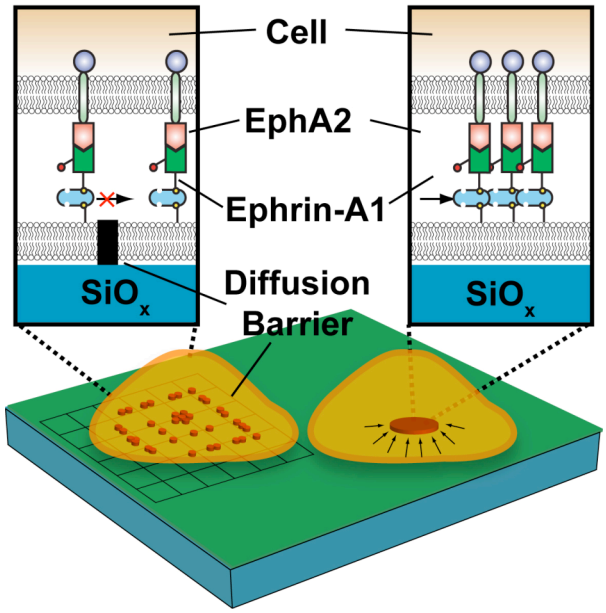

Figure 4.1: Introducing spatial mutations to EphA2
EphA2-expressing mammary epithelial cells are cultured onto a supported membrane displaying laterally mobile, fluorescently labeled ephrin-A1 ligand. Receptors engage ligands, form clusters that coalesce and are transported to the center of the cell-supported membrane junction. Nanofabricated chromium metal lines 10 nm in height and 100 nm in linewidth (left cell) act as diffusion barriers and impede the transport of receptor-ligand complexes, leading to an accumulation of Eph-ephrin clusters at boundaries.

supported membrane presentation of ephrin-A1 (Figure 4.1) that reveals effects of the intrinsic intermembrane physiology on the EphA2 signaling system. This presentation system allows for precise control of membrane chemical composition and lateral organization. Molecules within the supported membrane can be confined within nanoscale corrals by physical barriers to lateral mobility that are prefabricated onto the underlying substrate.[88] In the present study, the barriers restrict ephrin-A1 transport (and thus EphA2 transport in the live cell) in precisely defined ways. We refer to this type of manipulation as a *spatial mutation*;[88,95] it generates chemically identical cells that differ only by the spatial configuration of molecules within the specific signal transduction pathway under study.

4.3 Results

4.3.1 Immediate Ephrin-A1 Microcluster Formation

A fluid supported membrane doped with 0.1% biotin-functionalized lipid was used to generate synthetic cell surfaces presenting laterally mobile ephrin-A1 (Figure 4.1 and Figure 4.2).[69,96] The ligand density on the membrane surface was adjusted to 800 ± 200 molecules/μm^2 (Figure 4.3),[97] which is comparable to the density of EphA2 receptors on the surface of a representative invasive breast cancer cell line, MDA-MB-231 (Figure 4.4). When these cells contact functionalized supported membranes, ephrin-A1 becomes organized into microclusters over the course of 15 min (Figure 4.5A, B). Dimerization and oligomerization of Eph receptors upon ligand stimulation is well-documented,[98,99] and higher-order clusters, such as those we

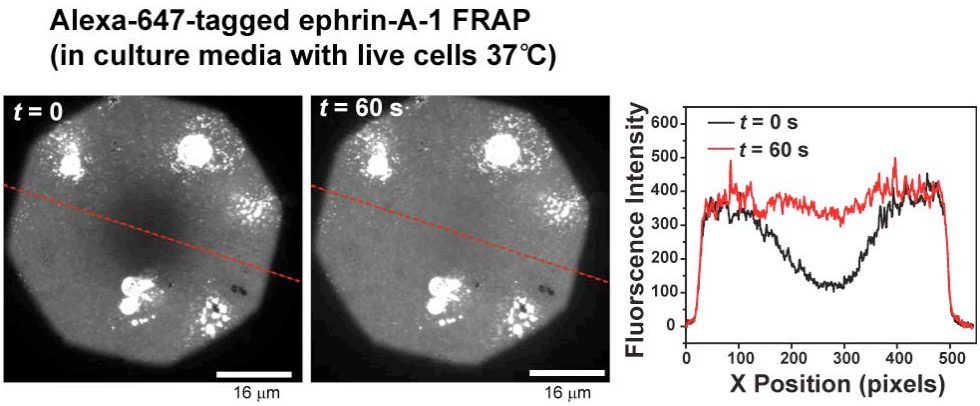

Figure 4.2: Laterally fluid ephrin-A1
Fluorescent recovery after photobleaching (FRAP) was performed at 37 °C, after live MDA-MB-231 cells (bright areas of fluorescence images) had been cultured on the surface for 1 hr. The plot on the right indicates the fluorescence intensities across an identical cross section (dotted red line) through fluorescence images before (black) and after (red) recovery. The bright areas in the image correspond to clusters formed by cells.

observe, have been proposed to exist on the basis of crystallographic studies of the molecular interface in Eph-ephrin complexes.[99,100]

4.3.2 Radial Transport of Eph-Ephrin Clusters

We additionally observe the microclusters to undergo inward radial transport while still bound to the supported membrane, as confirmed by live-cell fluorescence imaging and reflection interference contrast microscopy (RICM), which reveals cell-substrate contact distances (Figure 4.6).[101] Radial transport characteristics can be quantified for a population of cells by averaging the radial distribution of ligand underneath each cell at defined time points (Figure 4.5B and Figure 4.7). Two-color total internal reflection fluorescence microscopy (TIRFM) tracking of ephrin-A1 and enhanced green fluorescent protein (EGFP) β-actin reveals substantial co-movement between image pairs, suggesting association of the actin cytoskeleton with EphA2 clusters (Figure 4.8). Further experiments with a Rho kinase inhibitor (detailed below) confirm that EphA2 transport is driven by actomyosin contractility.

4.3.3 Specificity of EphA2-Ephrin-A1 Binding

The eight different EphA receptors and the five ephrin-A ligands are known to display some promiscuous interactions,[16] but control experiments indicate that ephrin-A1 specifically binds EphA2. First, the EphA2 receptor was highly colocalized with ephrin-A1 (Figure 4.9A). Additionally, when cells were pretreated with EphA2 antibodies that block the binding site for ephrin-A1, no ligand clustering or cell-surface adhesion was observed (Figure 4.9B). Large-scale clustering of EphA2 in live cell junctions was also observed when cells that express ephrin-A1 (ZR-75-1) and cells that express EphA2 (MDA-MB-231) were brought into contact for 30 minutes. Immunostaining of cellular junctions with antibodies specific to either ephrin-A1 or EphA2 indicated accumulation at the contact zone between cells displaying cognate receptor-ligand pairs. Such accumulations resemble those observed in cell-supported membrane experiments (Figure 4.5A, 4.10). Radial transport of receptor-ligand complex was not observed when ephrin-A1-expressing cells contacted EphA2-functionalized supported membranes (Figure

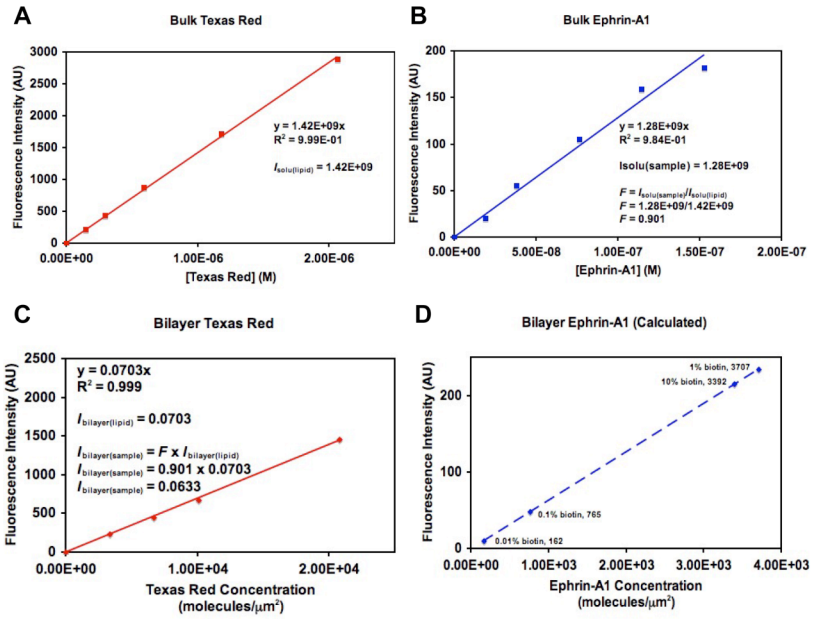

Figure 4.3: Measuring ephrin-A1 density
The density of ephrin-A1 on the supported membrane surface was measured using quantitative fluorescence microscopy. **A**) Texas Red-doped vesicles were used as a bulk concentration calibration standard. **B**) A calibration plot indicating the fluorescence intensities of solutions containing labeled ephrin-A1 protein. **C**) Texas Red-doped supported membranes were used as a surface density calibration standard. **D**) The fluorescence intensities of bilayers functionalized with ephrin-A1 were fit to a re-scaled line to determine the concentration of ephrin-A1 on the bilayer surface.

4.11); thus, receptor translocation is ligand-induced and driven only by the EphA2-expressing cells.

4.3.4 Mixed Supported Membranes

In the preceding experiments, Eph-ephrin binding provided the only physical link between the cell and the supported membrane. RICM confirmed that EphA2 – ephrin-A1 clusters colocalize with the regions of closest intermembrane contact (Figure 4.5C). To determine if the observed inward radial transport may be an indirect consequence of intermembrane anchoring, a cyclic RGD (Arg-Gly-Asp) peptide-lipid conjugate was included in the supported membrane. This peptide serves as a binding partner for integrins on the cell surface,[102] and was presented as a binary mixture with ephrin-A1 on the supported membrane in varying densities. RICM images revealed progressively larger cell – supported membrane contact areas with increasing RGD peptide density, but with no change in EphA2 organization (Figure 4.5D). Immunostaining for β_1, $\alpha_V\beta_3$ and $\alpha_V\beta_5$ integrins, known markers of focal adhesions, did not show colocalization with EphA2 (Figure 4.12). Thus we conclude that the radial transport of EphA2 is selective and independent of integrin-mediated adhesion and signaling.

4.3.5 Ligand Mobility Affects EphA2 Receptor Activity

Importantly, radial transport of ligand-stimulated EphA2 is dependent on the lateral mobility of ephrin-A1 in the supported membrane. Fully saturated 1,2-dipalmitoyl-*sn*-glycero-3 phosphocholine (DPPC) lipids form a non-fluid bilayer in the gel phase at 37 °C and ephrin-A1

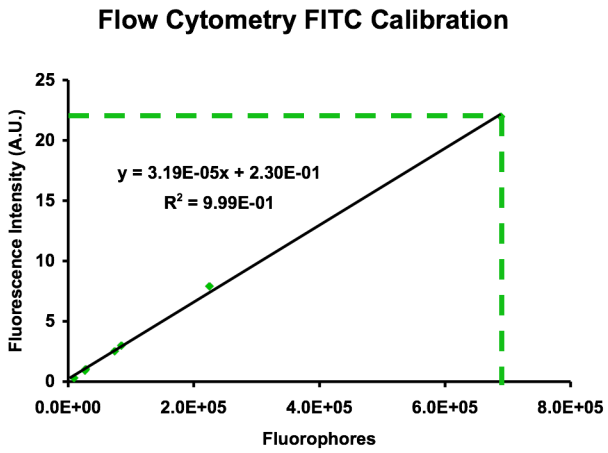

Figure 4.4: Measuring EphA2 receptor density
Flow cytometry calibration using microparticle standards (green markers) and linear fit. Dashed lines mark the measured fluorescence intensity and calculated number of FITC-labeled EphA2 molecules on the surface of MDA-MB-231 cells. The calculated number of EphA2 molecules was divided by the labeling ratio of FITC-labeled secondary antibody and the average surface area per cell to determine the number of EphA2 molecules per μm^2.

displayed on these membranes failed to exhibit microcluster formation or inward transport upon interaction with cells (Figure 4.5E). This correlated with differences in EphA2 signaling as measured by receptor phosphorylation and degradation, which are hallmarks of ligand-induced activation.[79] When identical numbers of cells (~1×10^5) were plated onto fluid and non-fluid supported membranes doped with an identical density of ephrin-A1 binding sites (1:1000 biotin-DPPE), the ephrin-A1 tethered to non-fluid DPPC membranes induced ~50% less EphA2 degradation, and ~40% less tyrosine phosphorylation than did ephrin-A1 tethered to control fluid membranes (Figure 4.5F). Furthermore, on fluid membranes, ephrin-A1 clusters colocalized with the areas of highest tyrosine phosphorylation and radial transport of Eph-ephrin complexes coincided with substantial f-actin reorganization (Figure 4.5C, 4.13).

4.3.6 Cytoskeleton is Responsible for EphA2 Radial Transport

Cytoskeleton reorganization is known to result from ligand-dependent tyrosine phosphorylation of EphA2 and subsequent downstream signaling processes.[103] This ultimately contributes to cell contact-dependent repulsion and tissue patterning.[16] EphA2 can remodel the cytoskeleton through activation of the small guanosine triphosphatase RhoA,[104] a process implicated in the high motility and invasive ability of malignant tumor cells.[105] To explore the effects of this process on EphA2 transport we used the selective Rho-associated kinase inhibitor Y-27632 to block actomyosin contractility.[106] MDA-MB-231 cells treated with inhibitor concentrations ranging from 1 to 50 μM exhibited a dose-dependent decrease in their capacity to transport EphA2-ephrin-A1 complexes to the center of the cell—supported membrane contact junction (Figure 4.5G). This observation indicates that EphA2 transport is actively driven by actomyosin contractile forces.

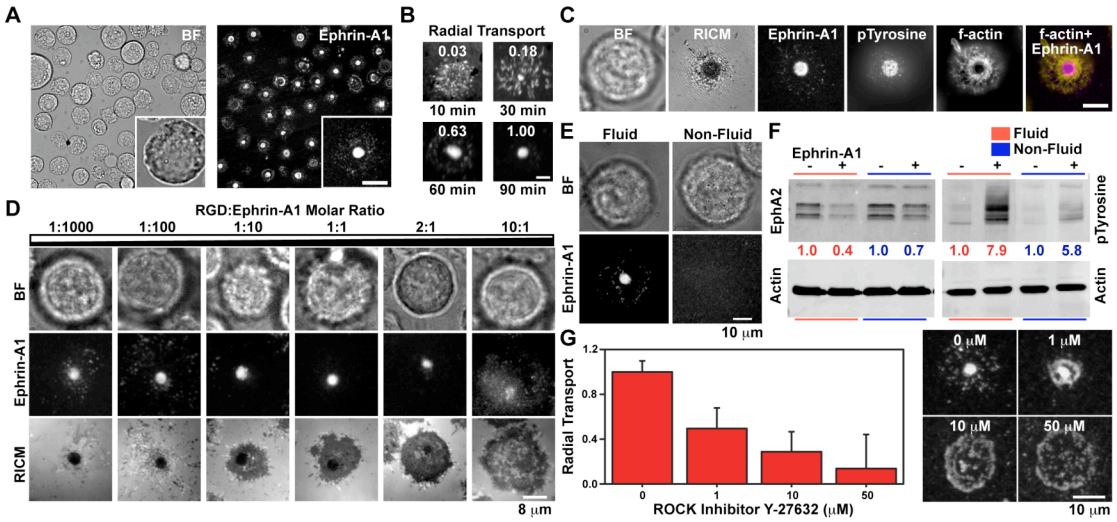

Figure 4.5: Lateral reorganization of ligand-stimulated EphA2
A) Representative bright field and epifluorescence images of MDA-MB-231 cells within 1 hr of interaction with an Alexa Fluor 647—tagged ephrin-A1—functionalized supported membrane. **B**) Dynamics of receptor-ligand reorganization as a function of time. The radial distribution of ephrin-A1 was measured under each cell and the population average value (n=77 cells) is indicated above the fluorescence image for each time point. **C**) The central EphA2 cluster is the region of highest ephrin-A1 concentration, greatest tyrosine phosphorylation and tightest cell adhesion to the substrate, and results in reorganization of the actin cytoskeleton to form a peripheral annulus. Scale bar equals 5 μm in A) to C). **D**) Representative bright field, epifluorescence, and RICM images of cells 1 hr after plating on a supported membrane functionalized with binary mixtures of ephrin-A1 and cyclic RGD peptide. Ephrin-A1 and RGD were incubated in the molar ratios indicated above each panel, and show EphA2 translocation regardless of the area of the cell-supported membrane contact. **E**) Mechanical reorganization of EphA2 requires a fluid membrane. Bilayers composed of 99.9% DPPC and 0.1% Biotin-DPPE are not fluid during cell engagement at 37 °C and, as a result, no long-range EphA2 reorganization is observed on DPPC bilayers. **F**) Western blots of lysates collected from 1×10^5 cells cultured onto fluid and non-fluid membranes. Presentation of fluid ephrin-A1 results in more rapid and complete EphA2 activation than presentation of non-fluid ephrin-A1, as measured by EphA2 degradation and total phosphorylated tyrosine intensities. EphA2 bands are at a mass of ~100 kD. **G)** When cells were treated with the Rho kinase inhibitor Y-27632, a dosage-dependent decrease in Eph-ephrin radial transport was observed (n = 627 cells), demonstrating that the cytoskeleton drives radial transport. Experiments were performed in duplicate, and radial transport was independently normalized to untreated samples from each replicate. Error bars indicate standard error for at least 139 cells at each dosage.

4.3.7 Spatial Mutation of EphA2

To examine the functional consequences of EphA2 transport, we physically manipulated EphA2 spatial organization. Supported membranes were formed on glass substrates with various patterns of metal lines (100-nm linewidth and 10-nm height) prefabricated by electron beam lithography. These create barriers to lateral transport within the supported membrane without otherwise influencing mobility or altering topography (Figure 4.14).[77,107,78] Lipids and membrane-tethered proteins diffuse freely, but cannot cross barriers (Figure 4.15).[22,88,108] Upon binding its supported membrane—bound ephrin-A1 ligand, the EphA2 receptor and other physically associated signaling molecules become subject to the same geometrical constraints to mobility. The approach applies physical perturbations to the living cell exclusively through specific receptor-ligand couplings and the entire ensemble of receptors is uniformly affected. A variety of non-native EphA2 spatial configurations were generated by engaging cells with patterned membranes whose grid pitches ranged from 0.5 to 20 μm (Figure 4.16).

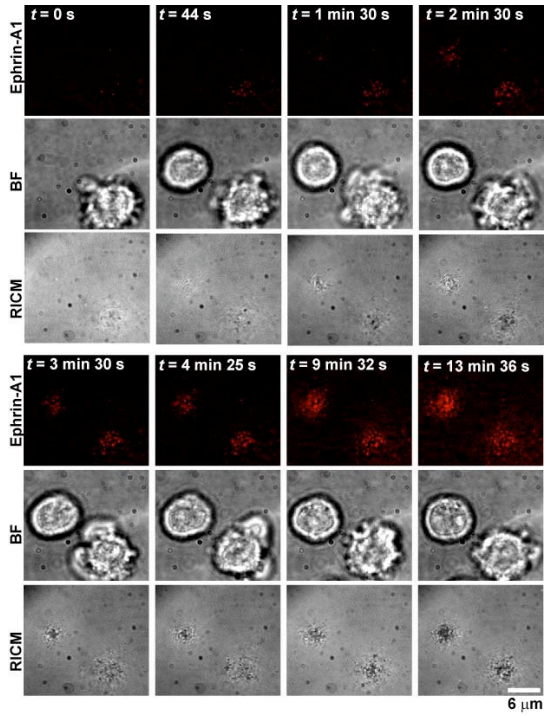

Figure 4.6: Ephrin-A1 transport over time
The corresponding RICM and bright field images are shown for each time point. Microcluster formation begins immediately after cell contact with the supported lipid bilayer, and is accompanied with the formation of tight cell-supported membrane junctions. These clusters grow and coalesce during cell-supported membrane contact.

Immunofluorescence imaging of cells on grid-patterned constraints reveals that the confined EphA2 clusters remain heavily phosphorylated in all cases (unrestricted, 3-, 1-, and 0.5-μm—pitch barriers). EphA2 is locally triggered irrespective of geometrical constraint (Figure 4.16A).

In contrast, the morphology of the f-actin exhibited two discrete states as a function of the degree of physical partitioning forced onto the EphA2 receptor pattern. Cells engaging membranes with 500 nm-pitch barriers displayed a spreading morphology, with f-actin primarily in peripheral lamellipodia. This behavior is similar to that observed in cells cultured on standard glass slides or on RGD-functionalized surfaces without ephrin (Figure 4.17). The actin morphology dramatically changed into an annulus immediately surrounding the EphA2-ephrin-A1 assembly when cells were exposed to substrates with grid barrier pitches of 3 μm or larger (Figure 4.16A). These observed differences in f-actin morphology at identical ephrin-A1 densities indicate that physical resistance to EphA2 receptor transport can change the threshold for ephrin-A1-triggered cytoskeleton reorganization.

The recruitment of effector molecules such as phosphatases or proteases is one mechanism used to dampen EphA2 signaling levels. In particular, ADAM10, a zinc-dependent transmembrane protease, is implicated in the ectodomain trans-shedding of ephrin-As as a consequence of Eph receptor binding.[80] ADAM10 has been shown to weakly associate with Eph receptors at the plasma membrane and to preferentially bind receptor-ligand complexes. Proteolytic cleavage by ADAM10 occurs at the extracellular domain of ephrin-As and is hypothesized to initiate release and endocytosis of the receptor-ligand complex.[80] Disengagement of the physical tether between apposed cells is thought to play a role in the observed Eph-driven cell repulsion, rather than the cell adhesion that might be anticipated due to strong receptor-ligand binding.[80,94] When cells were triggered with fluid ephrin-A1 for 1 hr and

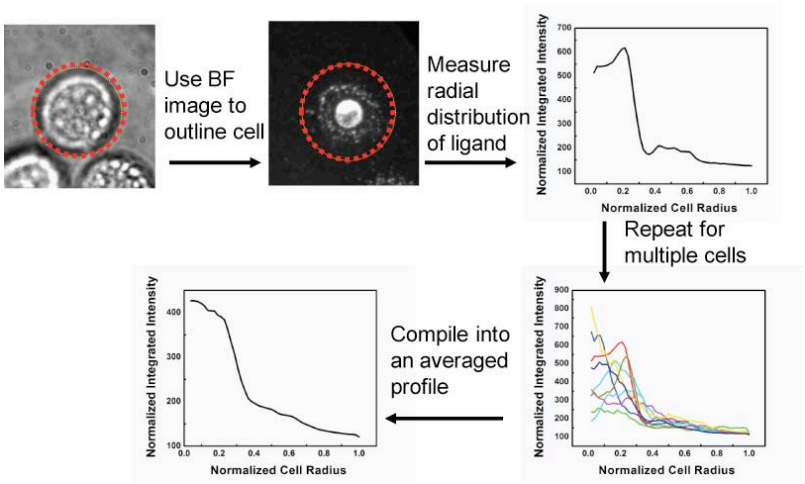

Figure 4.7: Quantifying Eph-ephrin radial transport
The outline of each cell was defined using the bright field image of each cell. The radial distribution of fluorescence intensity was then measured for each cell using software analysis package ImageJ. The radial distributions are then normalized for the cell radius to account for differences in cell size, and then averaged for each unique cell line to generate a signature average radial distribution function.

stained for ADAM10, we observed that ADAM10 was selectively recruited to the cell—supported membrane interface (Figure 4.16B, 4.18). However, when the EphA2 radial transport was mechanically hindered with metal grid patterns, ADAM10 recruitment was substantially reduced and selective colocalization with EphA2 was abrogated at the 60-min time point (Figure 4.16B). Cross-shaped metal patterns with a similar coverage area to that of the grids (4% of surface area) still allow ephrin-A1 radial transport, and do not drastically affect ADAM10 recruitment. This confirms that ADAM10 recruitment can be regulated by physically interfering with EphA2 transport and is not simply diminished by the presence of metal patterns in the supported membrane.

To quantify ADAM10 recruitment to receptor-ligand complexes, TIRFM was used to measure cell surface EphA2 and ADAM10 levels of an identical set of cells (n=477 cells) that displayed a range of receptor spatial mutations. Whereas the amount of EphA2 remained constant, the amount of recruited ADAM10 decreased with the size of the observed EphA2-ephrin-A1 clusters (Figure 4.16B). In addition, the colocalization of ADAM10 with EphA2 (as measured by Pearson correlation coefficient, *r*) also decreased. Control experiments with cross-shaped metal lines and 20-μm—pitch grids all confirm that these results are a consequence of receptor spatial organization and physical constraint. Cells cultured on two-component membranes displaying the cyclic RGD peptide along with ephrin-A1 displayed the same response to spatial mutations, confirming that this phenomenon is independent from RGD-mediated integrin adhesion and signaling (Figure 4.19).

4.3.8 EphA2 Radial Transport Across a Library of Mammary Epithelial Cell Lines

To investigate the generality of ligand-induced EphA2 transport beyond the MDA-MB-231 cell line, we examined a library of breast cancer cell lines. Such cell lines derived from primary tumors have been the most widely used models to elucidate how genes and signaling pathways regulate disease progression.[40] When a panel of cell lines is used as a system, rather

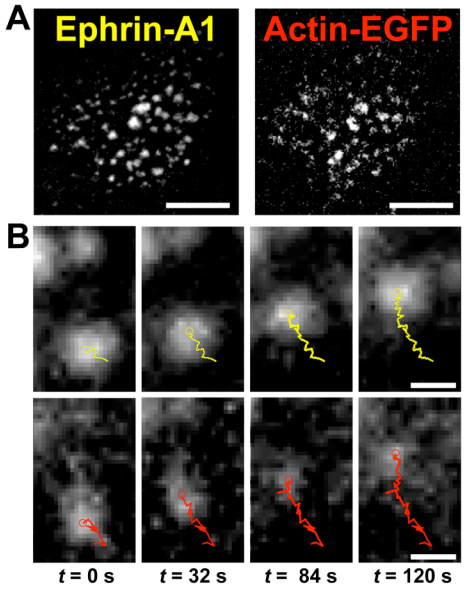

Figure 4.8: Ephrin-A1 moves with actin
A) MDA-MB-231 cells were transfected with actin-EGFP and allowed to engage fluid supported membranes displaying ephrin-A1 labeled with Alexa Fluor 647. Scale bars equal 12 μm. **B)** Actin-EGFP (red) and ephrin-A1 (yellow) clusters were imaged every 4 seconds over 10 minutes. Scale bars equal 2 μm.

than individually, it can serve as a powerful tool to identify and investigate recurrent markers for disease progression.[109] Therefore, the propensity to radially transport the EphA2 receptor was characterized in 26 cell lines.[40] An aliquot of ~50 × 10^3 cells was plated onto ephrin-A1—functionalized supported membranes for 1 hour for each cell line. Live-cell fluorescence microscopy was used to image the resulting distribution of ligand under individual cells and a signature radial distribution function was determined for each cell line. Radial transport was not unique to MDA-MB-231, rather, each cell line tested displayed a distinct and characteristic degree of ligand-induced receptor reorganization (Figure 4.20). The diversity observed in EphA2 transport between different cell lines may result from the wide range of deregulations inherent to this library, as well as variance in EphA2 expression levels. To quantify the EphA2 radial transport phenotype, we parameterized the radial distribution functions for each cell line using linear regression, integration of area under the curve, and the ratio of peak-height to peak-width at half-maximum at time t = 60 min (Figure 4.21). These different scoring methods were robust and led to very similar values across the cell line library.

To identify the molecular signature of this spatial organization phenotype, we next performed large-scale analyses using the wealth of available data for the panel of cell lines. In this analysis, the measured radial transport scores serve as an unconventional *spatial biomarker* unique to each cell line and potentially associated with genomic, proteomic or phenotypic signatures in neoplasia. Invasion potentials, as measured using a modified Boyden chamber assay,[40] were strongly linked (Pearson correlation r = 0.91, $p = 7\times10^{-8}$) to the receptor radial transport phenotype across the library (Figure 4.22A). In contrast, EphA2 mRNA and protein expression levels did not correlate as strongly with invasion potentials, and the correlation values (r) were 0.64 and 0.53, respectively, in agreement with previous reports.[40,73]

Additionally, a system-wide correlation of the spatial organization scores to protein and mRNA expression levels revealed 37 proteins ($p < 0.1$) and 141 mRNA transcripts ($p < 1\times10^{-4}$; 158 probe sets) that are associated with this phenotype (Figure 4.22B, 4.22C, Tables 4.1, 4.2).

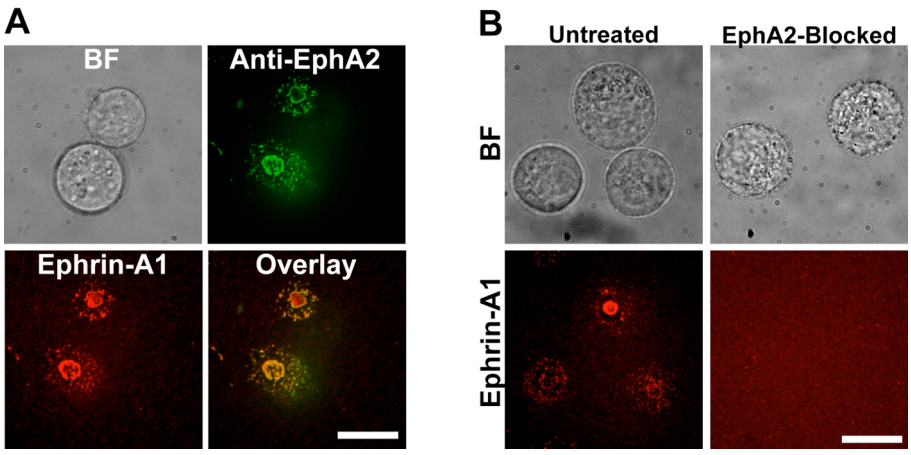

Figure 4.9: Specific EphA-ephrin-A1 binding
A) Receptor-ligand colocalization was characterized using immunofluorescence imaging. Live MDA-MB-231 cells were treated with anti-EphA2 after plating for 15 min at 37 °C on ephrin-A1-presenting supported membranes. **B**) When blocking anti-EphA2 antibodies were used to treat MDA-MB-231 cells, ephrin-A1 was not clustered and cells did not adhere to supported bilayers. Scale bars equal 20 μm.

Searches of the Kyoto Encyclopedia of Genes and Genomes and BioCarta pathway analysis databases [110] revealed that radial transport was associated with the ErbB, p53, integrin, and MAPK signaling pathways (Tables 4.3, 4.4). Notably, all of these pathways have been previously reported to associate with invasiveness and EphA2 signaling,[73] we now show that they also associate with EphA2 spatial organization.

One of the proteins identified through this screen was CD44, a cell membrane-bound glycoprotein involved in cell adhesion and migration.[111] The spatial organization of CD44 upon ephrin-A1 stimulation was found to anti-localize with the assembly of EphA2 (Figure 4.22D), validating the involvement of CD44 in cell-driven EphA2 receptor reorganization. The system-wide correlation analysis does not necessarily provide the mechanistic details leading to EphA2 sorting; instead, it identifies proteins and genes that may serve as surrogate markers to centripetal transport.

4.4 Discussion

The spatial mutation results demonstrate that physical manipulation of EphA2 – ephrin-A1 microcluster organization alters the cellular response to ephrin-A1. There are both spatial and mechanical aspects to these results. The cell applies force, via actomyosin contractility, to ligand-engaged EphA2 receptors. According to Newton's third law, grid barriers that block EphA2 transport in the spatial mutation must necessarily exert opposing forces on the receptor clusters. Spatial organization and mechanical forces are thus interconnected, resulting in an overall sensitivity of the EphA2 signaling pathway to spatio-mechanical aspects of the cellular microenvironment in which ephrin-A1 is displayed.

The discovery that EphA2 translocation was more strongly linked to invasion potential than EphA2 gene or protein expression demonstrates that receptor transport is distinct from expression. This further suggests that beyond the presence of the EphA2 receptor, it is the ability of a cell to move this protein and activate subsequent downstream signaling cascades that is most strongly associated with tissue invasion.

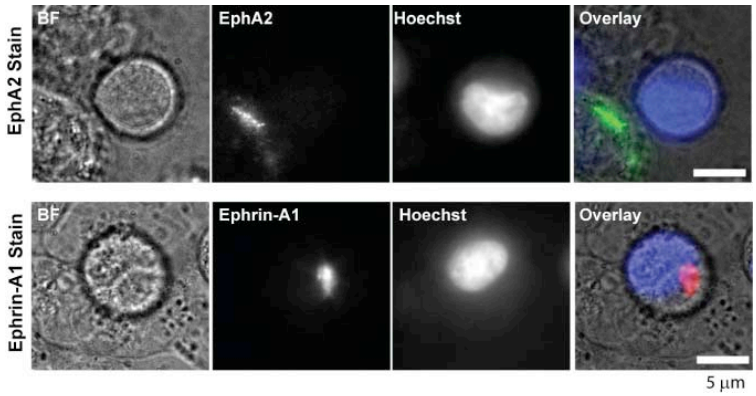

Figure 4.10: EphA2-ephrin-A1 transport *in vivo*
ZR-75-1 cells (labeled with Hoechst 33342 nuclear stain) displaying ephrin-A1 were cultured for 30 minutes on a confluent layer of MDA-MB-231 cells displaying EphA2. Live cells were stained for EphA2 and fixed cells were stained for ephrin-A1, using isotype-matched fluorescent secondary antibodies. Transport of EphA2 and ephrin-A1 to the cell-cell interface was observed.

In conclusion, we report a spatio-mechanical regulation of the EphA2 signaling pathway. Upon fluid membrane-bound ligand stimulation, EphA2 is transported radially inwards by an actomyosin contractile process. Physical interference with this transport, which necessarily involves the imposition of opposing forces on EphA2, alters ligand-induced EphA2 activation as observed by the recruitment of the protease ADAM10 and cytoskeleton morphology. Quantitative measurement of centripetal receptor transport across a library of mammary epithelial cell lines reveals a high correlation with invasion potential and with specific gene and protein expression. These observations suggest that spatio-mechanical aspects of ephrin-A1 expressing cells and their surrounding tissue environment may functionally alter the response of EphA2 signaling systems and could play a contributing role in the onset and progression of cancer.

4.5 Methods

4.5.1 Supported Membrane Preparation

Phospholipid vesicles were prepared using existing methods.[112] In short, the desired lipids were mixed in a chloroform solution and then the chloroform was evaporated using a rotary evaporator. The lipids were thoroughly dried under a stream of N_2 and hydrated with 1.5 mL of DI water. The hydrated lipids were then extruded through 100 nm-sized polycarbonate pore filters and stored at 4 ^{o}C. Fluid bilayers were made from vesicles containing 99.9% DMPC (1,2-dimyristoyl-*sn*-glycero-3-phosphocholine) or DOPC (1,2-dioleoyl-*sn*-glycero-3-phosphocholine), and 0.1% biotin-DPPE (1,2-dipalmitoyl-*sn*-glycero-3-phosphoethanolamine-N-(cap biotinyl)). Fluorescence recovery after photobleach experiments were performed with bilayers containing 3 mol% NBD-PC (1-acyl-2-{12-[(7-nitro-2-1,3-benzoxadiazol-4-yl)amino]lauroyl}-*sn*-glycero-3-phosphocholine), 96.9 mol% DMPC, and 0.1 mol% biotin-DPPE. Quantitative fluorescence standard solutions are described below. Unless otherwise noted, all lipids were acquired from Avanti Polar Lipids, Inc., Alabaster, AL. Vesicles were allowed to warm to room temperature and mixed in a 1:3 ratio with 1× phosphate-buffered saline (PBS; Sigma-Aldrich, Inc., Saint Louis, MO) to a final concentration of 1 mg/ml.

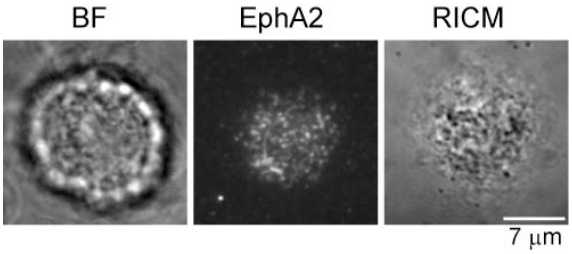

Figure 4.11: Ephrin-A1-expressing cells do not initiate Eph-ephrin transport
When ZR-75-1 cells expressing ephrin-A1 were cultured on a supported membrane functionalized with the extracellular domain of EphA2, they formed microclusters of EphA2, but did not radially transport EphA2-ephrin-A1 complexes.

For experiments performed in 96-well plates, each well was pre-treated with 1 M NaOH for 1 hour and then thoroughly rinsed with DI water. 100 μl of the lipid vesicle solution in PBS was then added to each well and excess vesicles were subsequently rinsed. For experiments performed on microscopic cover glass, substrates were cleaned using a piranha etching protocol (H_2SO_4 and H_2O_2 mixed in a 3:1 ratio) for 15 min, and then rinsed and dried under a stream of N_2. Lipid vesicle solutions were then spread over these substrates. The resulting lipid-bilayer functionalized substrate was immersed in PBS and sealed in an Attofluor cell chamber (Invitrogen Corp., Carlsbad, CA).

Non-fluid supported membranes were generated from lipid vesicles that were composed of 99.9 mol% DPPC and 0.1 mol% biotin-DPPE. In order to facilitate vesicle rupture and spreading, lipid solutions were extruded through 100 and 30 nm-sized pore filters and all solutions and substrates were heated to 50 ^{o}C.

4.5.2 Surface Functionalization

After lipid bilayer deposition, substrates were incubated for 45 min with a 0.01% bovine serum albumin (BSA; Sigma-Aldrich, Inc.) solution to minimize non-specific protein adsorption. The supported membranes were then incubated with a 17 nM solution of streptavidin (Sigma-Aldrich, Inc.) for 45 minutes. For experiments that quantify protein surface density, streptavidin conjugated to Alexa Fluor 488 (Invitrogen Corp.) was substituted for the unlabeled protein. The supported membrane was then thoroughly rinsed and substrates were incubated for 45 min with a 50 nM solution of ephrin-A1 (R&D Systems, Minneapolis, MN), which had been biotinylated (Fisher Scientific, Pittsburgh, PA) and conjugated to Alexa Fluor 594 or Alexa Fluor 647 (both from Invitrogen Corp.). RGD-functionalized supported membranes were generated by incubating streptavidin-functionalized membranes with a cyclic peptide [Arg-Gly-Asp-d-Phe-Lys(Biotin-PEG-PEG)] where PEG = 8-Amino-3,6-Dioxaoctanoic Acid (PCI-3697-PI, Peptides International, Louisville, KY) at the molar concentrations indicated.

In all cell experiments, the PBS solutions were exchanged by rinsing the substrate with DMEM cell media (GIBCO) at 37 °C. Cells were then added to the substrates and allowed to engage and interact with the surface at the conditions indicated.

4.5.3 Electron-beam Lithography

Chromium designs were fabricated on 25 mm diameter round glass coverslips. Coverslips were etched for 2 minutes in piranha solution (3:1 H_2SO_4:H_2O_2), then spin-coated at

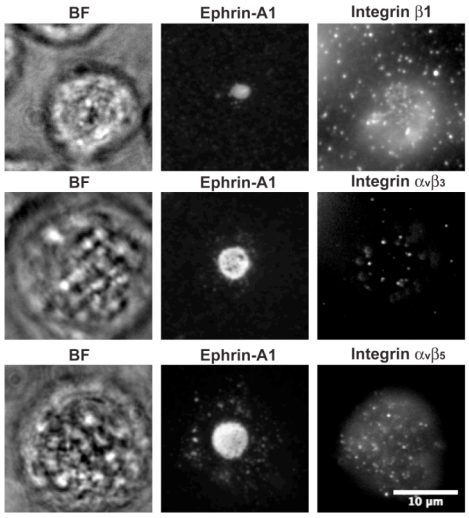

Figure 4.12: Eph-ephrin transport is independent of integrin binding
Integrins β_1, $\alpha_V\beta_3$, and $\alpha_V\beta_5$ all show no significant colocalization with ephrin-A1, based on immunofluorescence. Integrin staining signal outside of cell areas indicates degree of non-specific binding of antibodies to substrate surface.

1000 RPM with EB-resist (ZEP-520A, Zeon) and conductive polymer (Aquasave, Mitsubishi Rayon). Resist was exposed via electron beam lithography (CABL9510CC, Crestec) at 100-150 $\mu C/cm^2$. Patterns fabricated were square grids with spacing 0.5, 1, 3, 5 and 20 μm and crosses with spacing 3 μm. Conductive polymer was removed by deionized water rinse and resist was developed by sonication for 1 minute in isoamyl acetate. Chromium was deposited by electron beam evaporation and resist mask was lifted off by sonication in methylene chloride. Patterns exhibited film thicknesses of 10 nm and grid line widths of 100 nm, as verified by AFM measurements (Figure 4.14A).

4.5.4 Cell culture

Cells were provided by the Gray Lab (Lawrence Berkeley National Laboratory) and cultured using media, supplements, and conditions provided by the Integrative Cancer Biology Program.[113] The day of the experiments, cells were treated with trypsin-EDTA, centrifuged, resuspended in media, counted, and aliquoted as needed. Aliquots were kept in a 37 ^oC, 5% CO_2, 100% humidity incubator until they were added to supported membranes.

4.5.5 Flow Cytometry

EphA2 expression on the surface of MDA-MB-231 cells was measured using flow cytometry. Briefly, cells were detached from cell culture flasks using trypsin-EDTA and incubated for 30 minutes in a 1% solution of bovine serum albumin in PBS to minimize non-specific antibody binding. Cells were incubated for 1 hour in a 1.25-5 μg/ml solution of mouse IgG_{2A} anti-EphA2 antibody (MAB3035, R&D Systems). Primary antibodies were rinsed away with PBS and cells were incubated for 30 minutes in a 5-10 μg/ml solution of goat anti-mouse IgG_{2A} antibody conjugated to fluorescein isothiocyanate (FITC). Secondary antibodies were rinsed away with PBS and cell solutions were analyzed using a Beckman-Coulter EPICS XL

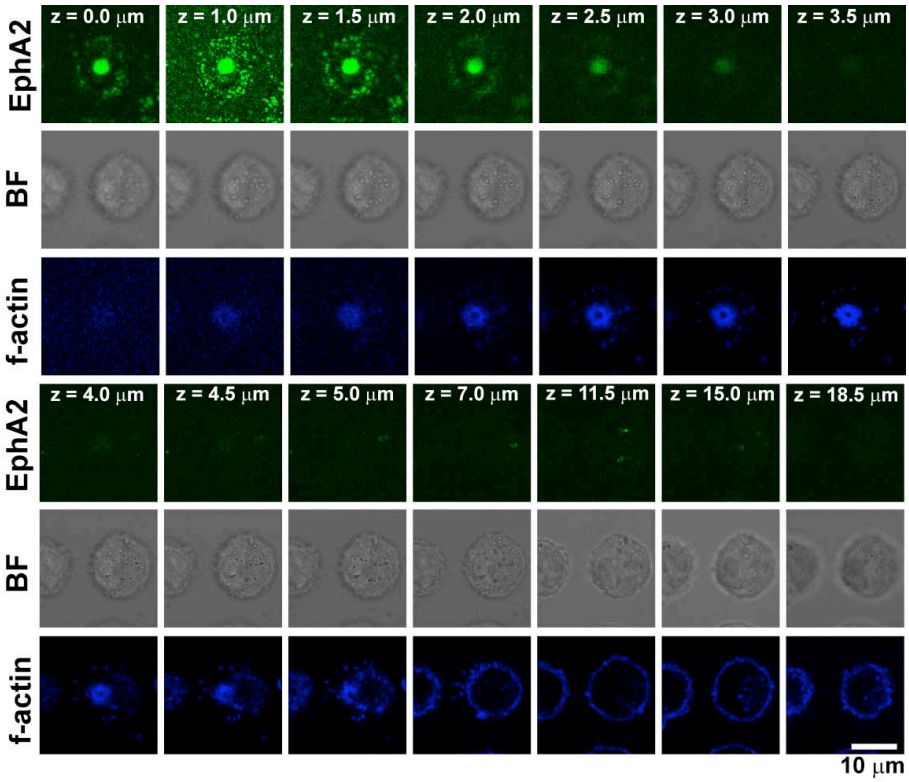

Figure 4.13: Three-dimensional structure of EphA2 and f-actin
MDA-MB-231 cells contacted a fluid supported membrane displaying ephrin-A1 for 1 hr and then were fixed and stained for EphA2 and actin. Z-stack of confocal images. EphA2 was visualized using immunofluorescence and f-actin was visualized using Alexa Fluor 350-conjugated phalloidin. Z-axis step size is 0.5 μm.

Flow Cytometer. Least squares analysis was performed on flow cytometry measurements of silica microspheres conjugated to known quantities of FITC (Bangs Laboratories, Inc., Fishers, IN) to determine the curve that best fit fluorescence intensity vs. number of fluorophores. Flow cytometry measurements of EphA2-labeled cells were then collected and fit to the calibration curve, yielding the average number of fluorophores on each cell (6.43×10^5 fluorophores per cell). This quantity was then divided by the labeling ratio of FITC-conjugated antibody and the average surface area of a cell to determine the average number of EphA2 molecules per μm^2 (~400 EphA2 molecules/μm^2).

4.5.6 Cell Fixing and Membrane Permeabilization

For immunofluorescence experiments cells were cultured on substrates for 1 hour, rinsed with cold Dulbecco's PBS (Invitrogen Corp.), and fixed with 4% paraformaldehyde (EMD Chemicals, Inc., Gibbstown, NJ) in PBS (Invitrogen Corp.) for 12 minutes, unless otherwise noted. When noted, cells were permeabilized with 0.1% Triton-X (EMD Chemicals, Inc.) in PBS for 5 minutes. Cells were then incubated overnight at 4 ^oC in PBS containing 1% BSA to block non-specific antibody binding.

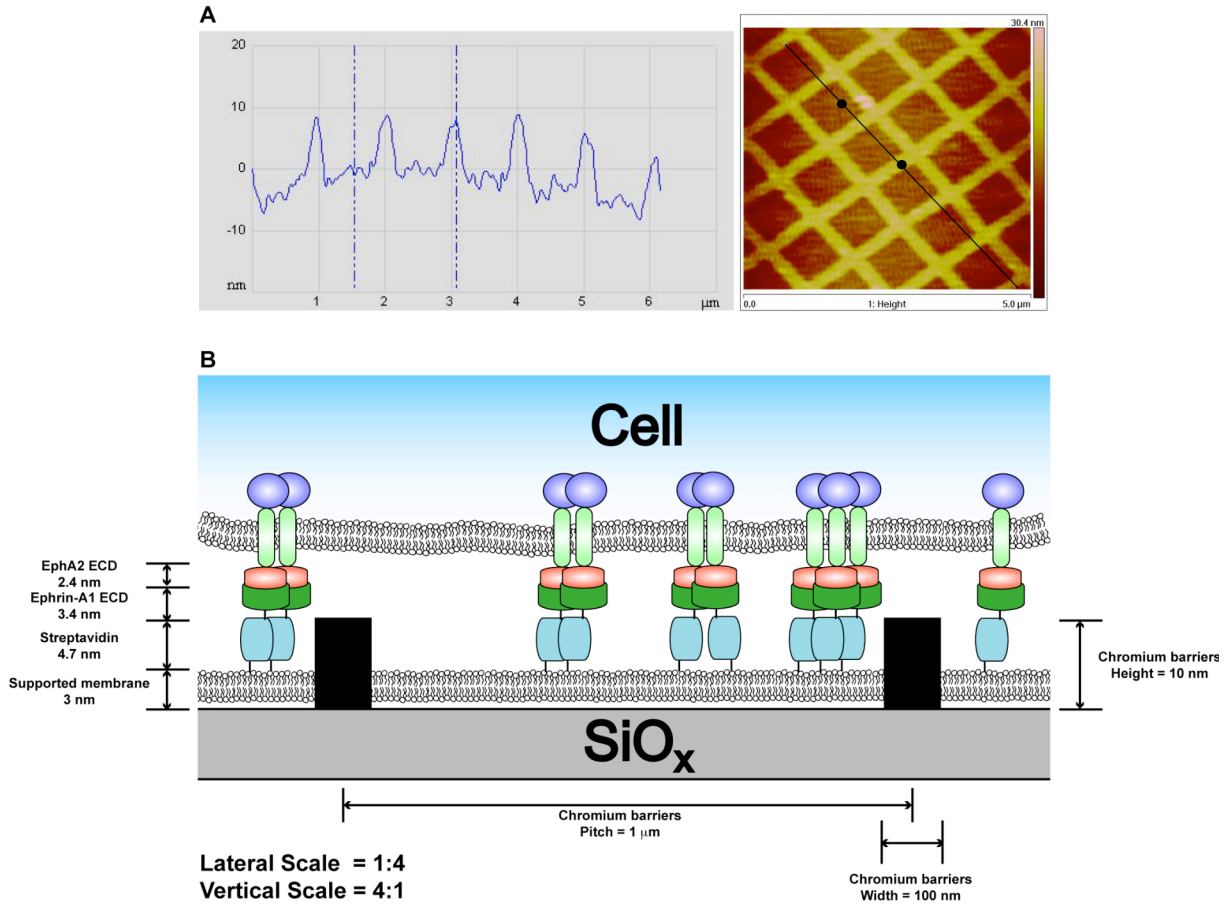

Figure 4.14: Nanopatterned supported membrane interface
The patterned chromium barriers do not alter the topography of the functionalized supported membrane surface. **A)** An atomic force microscope (AFM) image and corresponding line scan of chromium grids with a 1 µm pitch showing barrier heights of approximately 10 nm. Filled circles on AFM image denote points corresponding to dashed lines on line scan. **B)** Schematic diagram of cell-supported membrane interface drawn to scale. References for EphA2 and ephrin-A1 extracellular domains, streptavidin, and supported membrane dimensions are noted in 4.3.7.

4.5.7 Cell Staining

After fixing, cells were stained for 40 minutes with primary antibodies against a variety of target molecules. Anti-integrin $\alpha_V\beta_3$ (MAB3050, R&D Systems Inc.) and anti-integrin $\alpha_V\beta_5$ antibodies (MAB 2528, R&D Systems, Inc.) were incubated at 10 µg/ml and anti-integrin β_1 (sc-9936) was incubated at 2 µg/ml. For EphA2, ephrin-A1, ADAM10, phosphotyrosine, CD44 and F-actin staining, cells were permeabilized before antibody or phalloidin addition. Anti-EphA2 antibody (sc-924) and anti-ADAM10 (sc-48400) antibodies were incubated at 2 µg/ml. Anti-phosphotyrosine (05-321, Millipore, Temecula, CA) and anti-CD44 (sc-51610) antibodies were incubated at 1 µg/ml. For co-culture experiments, fixed cells were incubated with anti-ephrin-A1 (sc-20719) for 20 minutes at 4 µg/ml and live cells were incubated with anti-EphA2 antibody at 20 µg/ml. Unless otherwise noted, antibodies were purchased from Santa Cruz Biotechnology, Inc., Santa Cruz, CA.

After primary antibody incubation, excess antibody was rinsed away with PBS containing 1% BSA and isotype-matched secondary antibodies conjugated to either Alexa Fluor 488 or

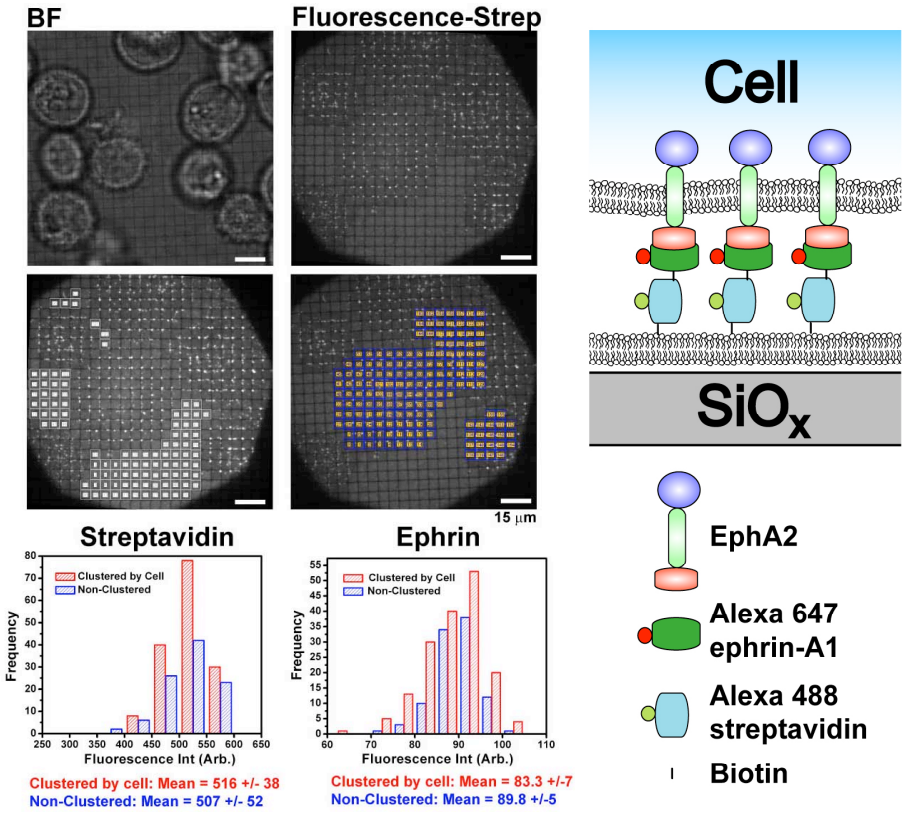

Figure 4.15: Ephrin-A1 remains on supported membrane surface during transport
Fluorescently-labeled ephrin-A1 and streptavidin were both used to functionalize a supported membrane. Cells were allowed to engage the surface for 1 hr, and then the fluorescence intensity was measured and integrated for each Cr-grid defined box. Histograms of integrated measurements are shown (lower) and indicate that the intensities from all boxes are within experimental error.

Alexa Fluor 647 (Invitrogen Corp.) were incubated at a concentration of 2 μg/ml for 20-30 minutes. Excess secondary antibody was rinsed away with PBS.

F-actin was stained using phalloidin conjugated to Alexa Fluor 350, Alexa Fluor 488, or Alexa Fluor 647 (Invitrogen Corp.), according to manufacturer protocols.

For EphA2-blocking studies, cells were pre-treated with anti-EphA2 antibody raised against an epitope on the extracellular domain of EphA2 (MAB3035, R&D Systems, Inc.). Excess antibody was rinsed away with cell culture media, and isotype-specific secondary antibody conjugated to Alexa Fluor 488 was added to the cell solution as before. Excess secondary antibody was rinsed away with cell culture media, and cells were cultured on ephrin-A1-functionalized supported membranes as described earlier.

4.5.8 ROCK Inhibition

Cells were detached from cell culture flasks using trypsin-EDTA and incubated at 37 ^{o}C for 2 hrs in media containing ROCK inhibitor Y-27632 (Sigma-Aldrich, Inc.) at concentrations ranging from 1-50 μM. Trypan blue staining and cell counting indicated no adverse effects in terms of cell viability under these conditions. Cells were cultured in drugged media for one hr on well plates containing Alexa Fluor 647-labeled ephrin-A1 functionalized supported bilayers. Cells were fixed, stained and imaged with epifluorescence microscopy as described above.

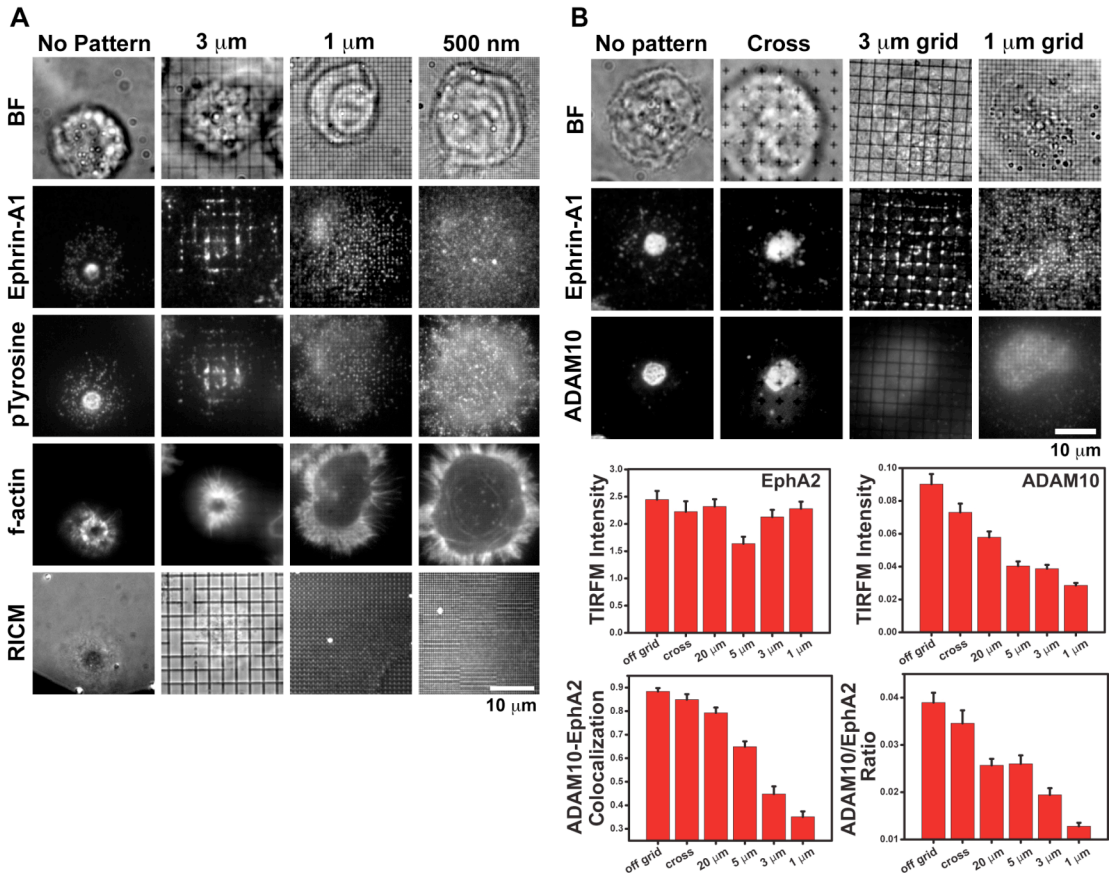

Figure 4.16: The functional consequences of EphA2 spatial mutation
Lateral transport of the EphA2 receptor is hindered by nanoscale chromium lines (10 nm in height and 100 nm in linewidth) prefabricated onto the glass support. MDA-MB-231 cells were allowed to engage the ephrin-A1 functionalized supported membrane for 1 hr, then they were fixed and stained for recruitment of downstream effector molecules. **A**) Irrespective of the presence or the scale of spatial mutations, phoshorylated tyrosine colocalized with ephrin-A1. F-actin adopted an annulus peripheral to the receptor-ligand assembly when EphA2 transport was unrestricted. However, when EphA2 organization was altered, the cytoskeleton assumed a spread morphology with f-actin primarily present in peripheral lamellipodia. The spread actin morphology switched to an annulus surrounding the EphA2-ephrin-A1 assembly when cells were exposed to 3-μm—pitch barriers. **B**) ADAM10 colocalized with the EphA2-ephrin-A1 assembly on unrestricted supported membranes. However, when EphA2 transport was restricted by metal lines on the silica substrate, the measured colocalization decreased and the ratio of ADAM10 to EphA2 also decreased (n = 477 cells). This indicates that mechanical restriction of EphA2 modulates ADAM10 recruitment.

4.5.9 EGFP β-actin Transfection

MDA-MB-231 cells were transfected with a plasmid containing an enhanced green fluorescent protein (EGFP) β-actin fusion construct[114] (construct (2)) using Lipofectamine 2000 (11668-019, Invitrogen Corp.) according to manufacturer protocols. Cells were harvested 24 hrs after transfection.

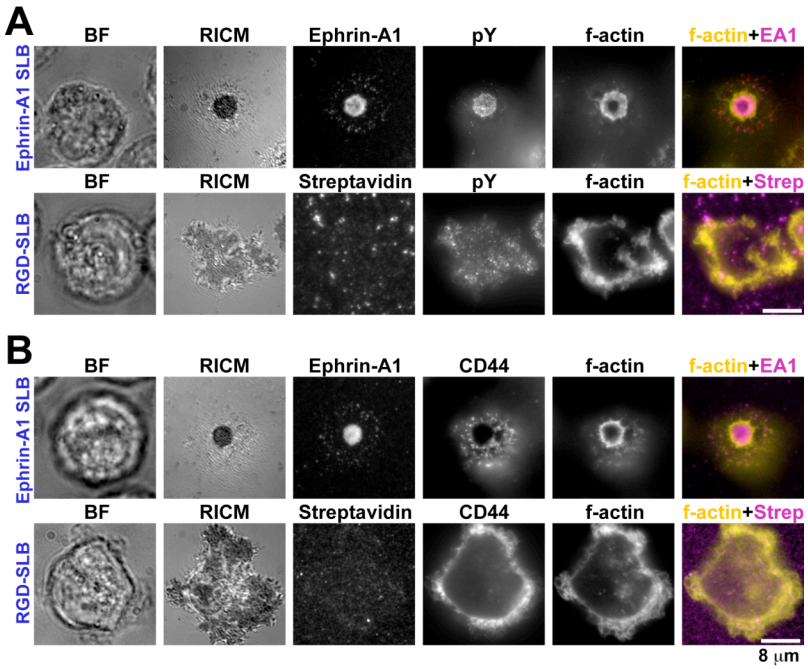

Figure 4.17: Protein localization to EphA2 central assembly is highly specific
Immunofluorescence was used to probe the colocalization of pY and CD44 to EphA2 central assembly. Cyclic-RGD functionalized supported membranes were used as a control promoting cell adhesion. **A**) The central assembly of EphA2-ephrin-A1 is highly phosphorylated. **B**) CD44 anti-localizes with the ephrin-A1 central assembly.

4.5.10 Co-culture Experiments

For the studies to observe ligand and receptor assembly formation at live cell-cell contacts, EphA2-expressing MDA-MB-231 cells were grown in co-culture with ephrin-A1-expressing ZR-75-1 cells. First, MDA-MB-231 cells were cultured to confluency in wells containing RPMI cell media. Then, ZR-75-1 cells were labeled with the nuclear stain Hoechst 33342 (Invitrogen Corp.) at a concentration of 1 μg/ml for 30 minutes, and added to wells containing MDA-MB-231 cells. Cells were grown in co-culture for 30 minutes, at which point ephrin-A1 radial transport was visually complete on supported membranes. Live cells were stained with primary antibodies specific for EphA2 and cells fixed for 20 minutes with 4% paraformaldehyde were stained with primary antibodies specific for ephrin-A1. Cells were then incubated with isotype-matched fluorescent secondary antibodies and imaged using bright field and epifluorescence microscopy, as described above.

4.5.11 Western Blotting

Western blots were performed on lysates collected from ~1 × 10^5 cells cultured on supported lipid membranes for 2 hours. To collect the cell lysates, each sample was placed on ice and supernatant from each substrate was collected. Each substrate was rinsed with 2 ml of cold Dulbecco's PBS and the rinses were added to the supernatant fractions. The combined rinses and supernatant from each substrate were centrifuged at 250 g for 5 minutes at room temperature and the supernatant was aspirated. Each cell pellet was then resuspended in 50 μl of NP-40 buffer. 100 μl of NP-40 buffer was added to each substrate and adhered cells were

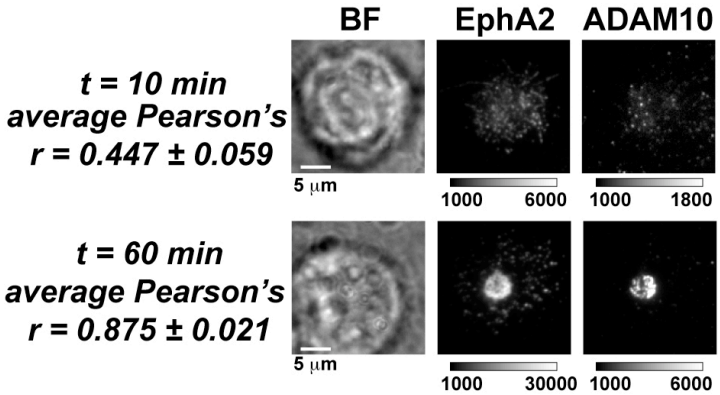

Figure 4.18: EphA2 association with ADAM10 over time
Ephrin-A1 stimulated cells were fixed and stained for ADAM10 and for EphA2 using primary and secondary antibodies. At early time points, the fluorescence intensities of both ADAM10 and EphA2 were very low. However as ligand stimulation proceeds, both the amount of ADAM10 recruited to the interface and the degree of ADAM10 localization to EphA2 (as measured by Pearson's correlation values ± SE), increased.

scraped off the substrate and added to the cell pellet previously resuspended, as was the NP-40 remaining on the substrate surface. The solution was then centrifuged at 15000 g for 15 minutes at 4 ^{o}C and the supernatant was collected and stored in at -80 ^{o}C until the day of blotting.

Western blots were labeled with primary antibodies specific to EphA2 (05-480, Millipore), phosphotyrosine (05-321, Millipore), and actin (sc-1616, Santa Cruz Biotechnology, Inc.). Samples were labeled with isotype-matched secondary antibodies conjugated to Alexa Fluor 680 or Alexa Fluor 780 (Invitrogen Corp.), and imaged using an Odyssey Infrared Scanning System (LI-COR Biotechnology, Lincoln, NE).

4.5.12 Optical Microscopy

We used Nikon Eclipse TE2000-E and TE300 inverted microscopes with mercury arc lamps for epifluorescence illumination and 12 V, 100 W halogen lamps for bright field illumination. Total internal reflection fluorescence (TIRF) illumination was provided using a krypton/argon ion laser for 647 nm excitation, and an argon ion laser (Stabilite 2018 and Model 177 respectively, both from Spectra-Physics, Mountain View, CA) for 488 nm excitation. All epifluorescence microscope images were taken with a Quantix CCD camera and TIRF microscope images were taken using a Cascade 512B EMCCD camera. All cameras were purchased from Roper Scientific, Ottobrunn, Germany. MetaMorph (Molecular Devices Corp., Downington, PA) software was used to drive microscope and collect the images. Alexa Fluor 647 was imaged using a Cy5 filter cube, Alexa Fluor 594 and Texas Red were imaged using a TR filter cube, Alexa Fluor 488 and NBD were imaged using an NBD/HPTS filter cube, and Alexa Fluor 350 and Hoechst 33342 were imaged using a DAPI/Hoechst/AMCA filter cube. Reflection interference contrast microscopy (RICM) images were collected using a dedicated RICM filter cube. All filter cubes were acquired from Chroma Technology Corp., Rockingham, VT. Alexa Fluor 647 Ephrin-A1 and EGFP-actin tracking was performed using a DualView (Photometrics, Tucson, AZ) image splitter fitted with a dual-band pass emission filter interposed between the body of the microscope and the camera. Time-lapse images were collected using a Physitemp TS-4 thermal microscope stage (Physitemp Instruments, Inc., Clifton, NJ), in conjunction with a home-built heating element attached to the microscope objective, to maintain the sample temperature at 37 ^{o}C over the course of the experiment.

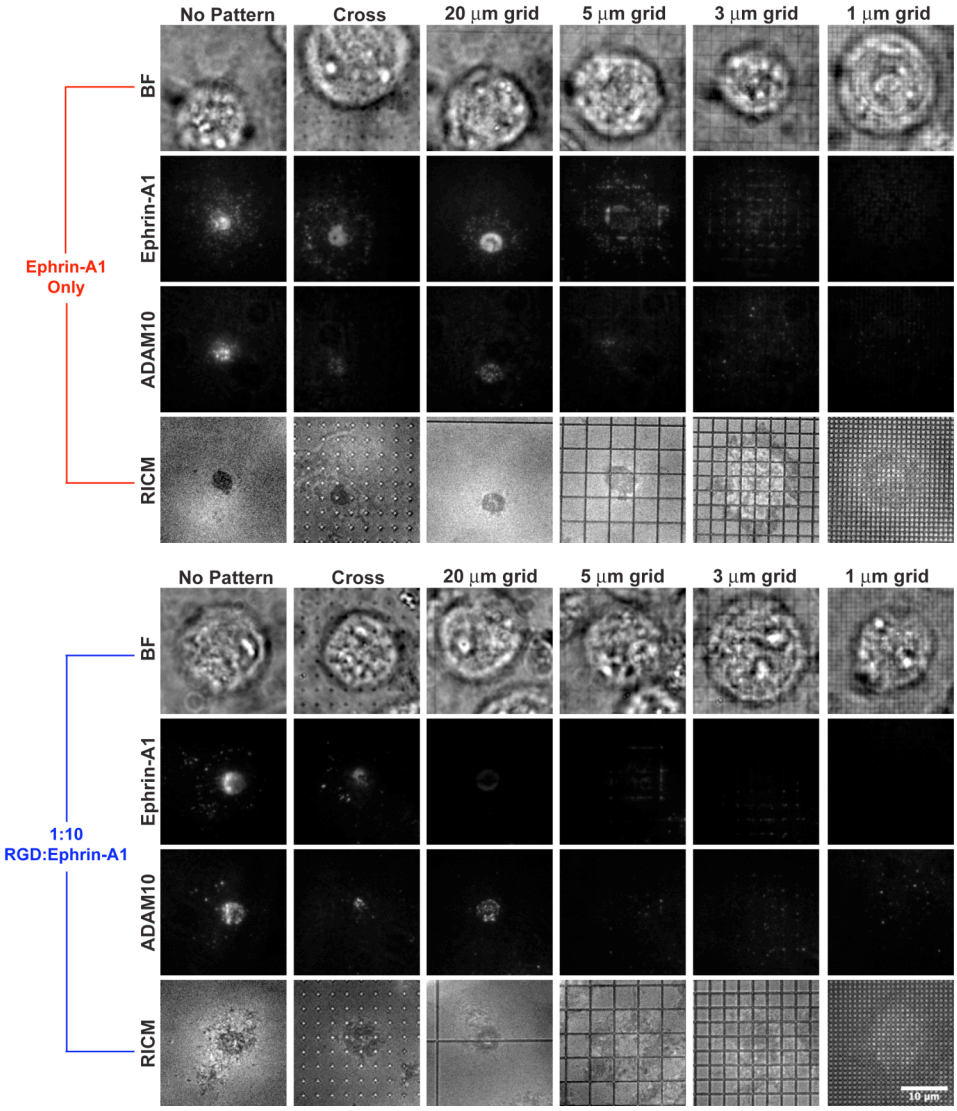

Figure 4.19: ADAM10 recruitment to EphA2 independent of RGD
Selective recruitment of ADAM10 to central assemblies of Eph-ephrin complex is independent of RGD-mediated flattening of the cell-supported membrane interface and subsequent signaling.

4.5.13 Quantitative Epifluorescence Microscopy

The surface density of ephrin-A1 on supported membranes was measured using a recently developed quantitative fluorescence microscopy technique.[97] First, vesicles containing 0.1 mol% TR-DHPE (Texas Red-1,2-dihexanoyl-sn-glycero-3-phosphoethanolamine, Invitrogen Corp.) and 99.9 mol% DMPC (1,2-dimyristoyl-*sn*-glycero-3-phosphocholine) were added to PBS in varying proportions yielding solutions whose final concentrations ranged from 0-0.74 μM Texas Red. These solutions were used to establish a bulk lipid calibration plot where fluorescence intensities, as measured using a Nikon TE300 microscope, were plotted against the concentration of the TR-DHPE. The data were fit to a straight line with a y-intercept of 0 and this slope was designated as $I_{solu(lipid)}$.

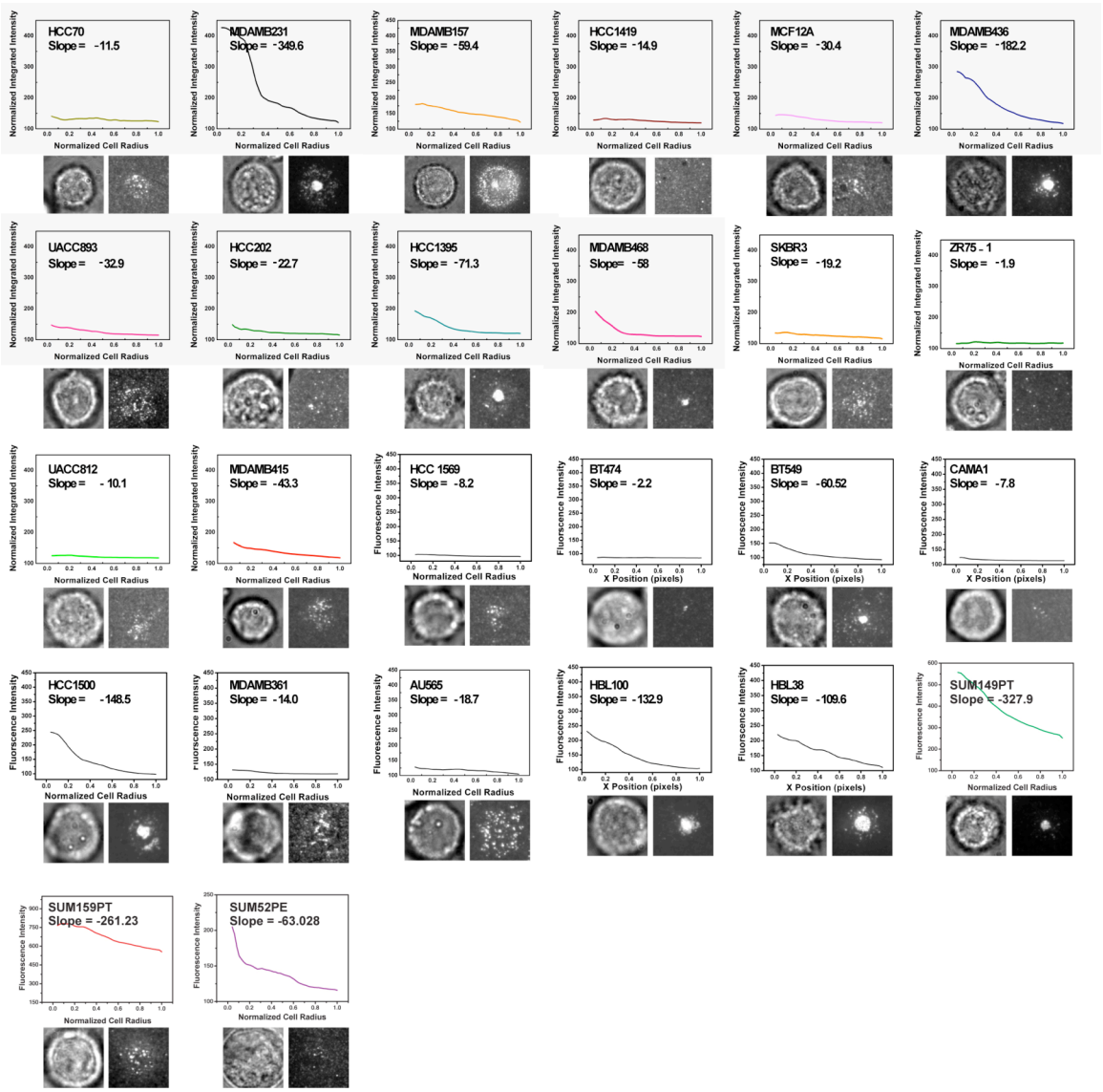

Figure 4.20: Ephrin-A1 radial distributions for 26 unique breast cancer cell lines
Cells were allowed to engage ephrin-A1-functionalized supported membranes for 1 hr.

Subsequently, a bulk protein calibration plot was generated from a serial dilution of Alexa Fluor 594 (Invitrogen)-labeled ephrin-A1 (594-EA1) where the solution concentrations ranged from 0-0.305 μM. Fluorescence from these solutions was measured using the same acquisition settings as the ones used for the lipid vesicle standards. Fluorescence intensity was plotted against [594-EA1] and fit to a straight line with a y-intercept set to 0, and the calculated slope was designated as $I_{solu(sample)}$. From these bulk calibration standards, a scaling factor was calculated to express the difference in fluorescence intensities between fluorescent lipids and proteins: $F = I_{solu(sample)} / I_{solu(lipid)}$.

On the day of the experiment, a surface bilayer calibration curve was generated using lipid membranes that were doped with TR-DHPE at concentrations that ranged from 0 to 0.62 mol% TR-DHPE. Bilayer fluorescence was measured and plotted against the molecular density of Texas Red per μm^2, by using 0.596 nm^2 as the average footprint of each DMPC lipid

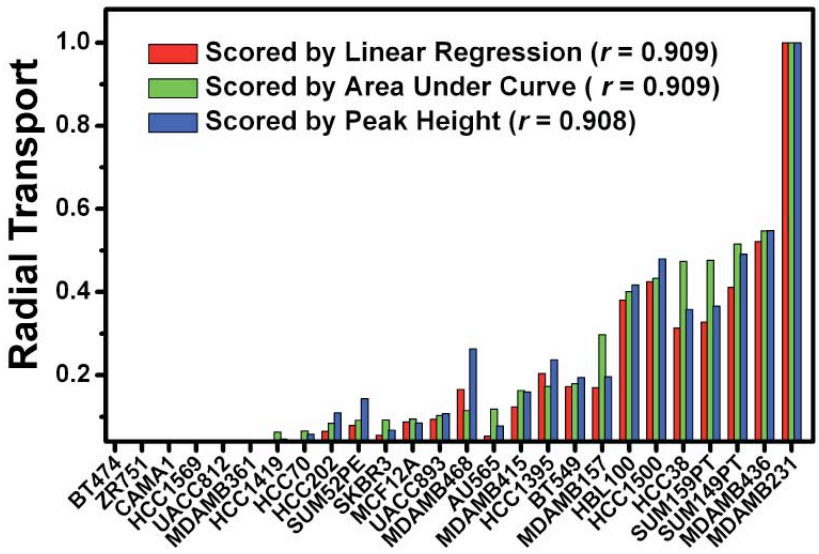

Figure 4.21: Radial transport scores for 26 unique breast cancer cell lines.

molecule.[115] These data were fit to a straight line with a y-intercept of 0, and the calculated slope was labeled as $I_{\text{bilayer(lipid)}}$. The scaling factor was applied to obtain the slope of a line describing fluorescence intensity versus the number of 594-EA1 molecules per μm^2, $I_{\text{bilayer(sample)}} = F \times I_{\text{bilayer(lipid)}}$.

Then, using the same acquisition settings, the fluorescence intensities of unknown bilayers containing 594-EA1 were measured. The measured fluorescence intensities was plotted on a line with slope $I_{\text{bilayer(sample)}}$ and y-intercept 0, allowing for a determination of the corresponding molecular density of 594-EA1 per μm^2. Using this quantitative fluorescence technique, the concentration of 594-EA1 in the bilayer was tuned to 800 ± 200 molecules/μm^2, when the concentration of biotinylated lipids in the bilayer was 0.1 mol%.

4.5.14 Quantitative TIRF Microscopy

In order to account for differences in illumination intensity across the visualized area between 488 nm and 647 nm laser TIRF excitation, a calibration bilayer was used. The calibration bilayer contained 99.9 mol% DOPC and 0.1 mol% biotin-modified DHPE and was incubated for 45 minutes with a 1:1 mixture of Alexa Fluor 488 streptavidin and Alexa Fluor 647 streptavidin, each with a F/P ratio of 2. The bilayer was then rinsed with PBS. Several unique areas of the calibration bilayer were imaged in the 488 nm and 647 nm excitation channels. An average, background-subtracted image was obtained for each channel. Background-subtracted sample images from each channel were divided by the average background-subtracted calibration image for the same channel, yielding sample images with normalized illumination intensities that could be quantitatively compared between the 2 channels for the entire field of view.

The ratio of signal from the ADAM10 channel to signal from the EphA2 channel was calculated independently for each cell. The Pearson's coefficient for these two channels was also calculated independently for each cell. These quantities were obtained using custom macros written in image analysis software package ImageJ (see Appendices A-D). Average values for these quantities are displayed in Figure 4.16B. Error bars denote standard error.

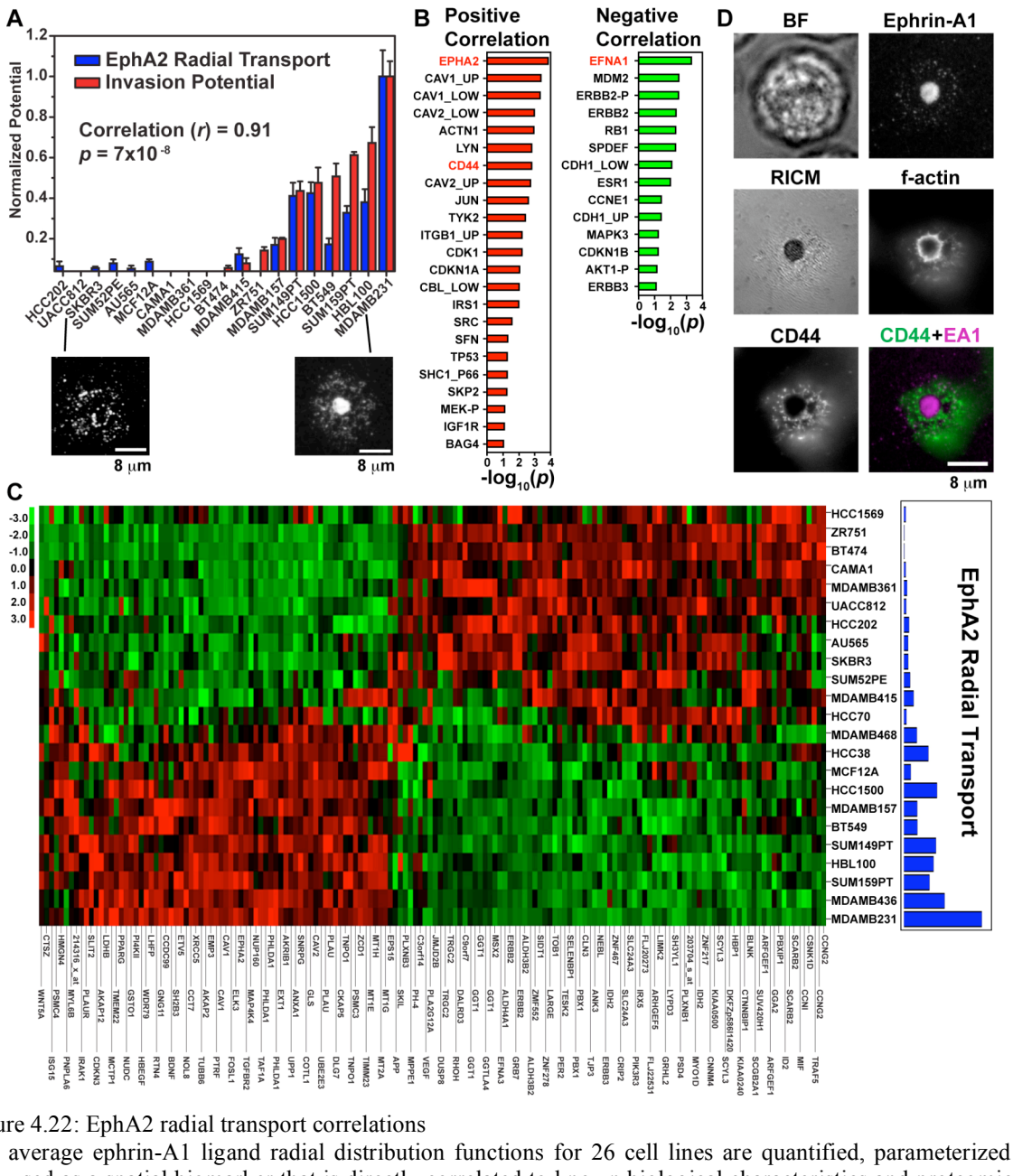

Figure 4.22: EphA2 radial transport correlations

The average ephrin-A1 ligand radial distribution functions for 26 cell lines are quantified, parameterized and then used as a spatial biomarker that is directly correlated to known biological characteristics and proteomic and genomic expression levels. **A**) The average radial distribution function was found to exhibit a strong correlation ($r = 0.91$, $p = 7 \times 10^{-8}$) to invasion potentials, that were determined using modified Boyden chamber analysis. **B**) The proteomic correlates ($p < 0.1$) of EphA2 radial transport are shown in the table with their associated p values, and are grouped based on the type of association (positive or negative). Proteins highlighted in red are those whose role in EphA2 reorganization has been experimentally observed. **C)** Transcriptomic correlates ($p < 1 \times 10^{-4}$; false discovery rate $< 5 \times 10^{-3}$) of EphA2 radial transport are illustrated in a heat map. Unsupervised hierarchical clustering of expression profiles of mRNAs that are predicted to be surrogates of EphA2 radial transport show two distinct clusters of cell lines associated with the phenotype. Red indicates upregulated expression while green indicates downregulated expression. **D**) Representative bright field, epifluorescence immunostaining, and RICM images of a cell 1 hr after plating on a supported membrane functionalized with ephrin-A1. The cell adhesion molecule CD44 was found to be significantly upregulated in protein expression in cells that underwent EphA2 radial transport. This signaling molecule was also found to be antilocalized with EphA2 upon ligand-induced activation.

4.5.15 Radial Transport Analysis

Bright field microscopy was used to determine the area occupied by each cell. The corresponding areas in the fluorescence channel were then analyzed using the Radial Profile plugin from ImageJ, yielding a plot of normalized fluorescence intensities versus radial distance from the cell center. Plots were then normalized for cell size and averaged. Least squares analysis was then performed on the average normalized radial distribution using Origin 7.0 (OriginLab, Northampton, MA), and the slope of the calculated line was used as a score for propensity to radially transport ephrin-A1.

4.5.16 Colocalization Analysis

After culturing cells on substrates for 1 hour, cells were fixed, cell membranes were permeabilized, and target molecules were stained and then imaged using TIRF microscopy as described above.

Areas occupied by cells (20 μm × 20 μm in size) were chosen using bright field images. These same areas were designated as regions of interest in ImageJ and cropped for further analysis. To calculate the ratio of ADAM10/EphA2 signal, the net intensity in the ADAM10 (488 nm excitation) channel was divided by the net intensity in the EphA2 (647 nm excitation) channel (see Appendix C). To calculate the Pearson correlation coefficient, intensity of each pixel in the ADAM10 channel was plotted against pixel number. Similarly, intensity of each pixel in the EphA2 channel was plotted against pixel number. Least squares analysis was performed to fit a straight line to intensity values from each channel. The Pearson correlation coefficient was determined as the correlation coefficient between these two lines (see Appendix D).

4.5.17 Identification of Molecular Predictors of EphA2 Transport

The slope of the radial distribution function characteristic of the receptor reorganization phenotype was correlated with the expression levels of mRNA transcripts and proteins across the panel of breast cancer cell lines[40] using an *in vitro* systems approach. The approach was comprised of evaluating each transcript and protein individually to determine whether it was significantly correlated with EphA2 radial transport, and to identify the signaling pathways that are enriched among these predictors. In these analyses, we used all breast cell lines for which both phenotype and expression data were available. Out of 26 cell lines with measured phenotype data, mRNA expression levels were available for 23 and protein expression levels were available for 18 cell lines. The statistical significance of the correlation was assessed using F-statistic,[116] and the p values were corrected for multiple hypotheses testing using the false discovery rate (FDR) method.[117] Our analysis led to 141 mRNA transcripts ($p < 1 \times 10^{-4}$, FDR < 5×10^{-3}; 158 probesets, Table 4.1) and 37 proteins ($p < 0.1$, Table 4.2) that are significantly associated with the EphA2 reorganization phenotype. We applied the Database for Annotation, Visualization, and Integrated Discovery (DAVID) analysis program to the significant proteins to identify the enriched pathways from the Kyoto Encyclopedia of Genes and Genomes (KEGG; Table 4.3) and BioCarta (Table 4.4) databases.[110] We used a stringent FDR cutoff of 5×10^{-2} to ascertain statistical significance of the pathways. Many mRNAs do not have pathway association, which prevented us from performing equivalent pathway enrichment analysis for the

mRNAs. However, unsupervised hierarchical clustering of mRNA expression levels of the 141 significant genes led to two distinct clusters of breast cell lines – one with large slope (magnitude), and the other with low slope (Figure 4.22C), demonstrating that the mRNAs can collectively predict the EphA2 reorganization phenotype.

Gene ID	EphA2 Radial Transport			Invasion potential		
	p	FDR	Type of Correlation	*p*	FDR	Type of Correlation
ERBB2	4.1E-07	7.6E-04	-	5.5E-04	6.3E-03	-
SCYL3	7.4E-07	7.6E-04	-	2.4E-04	5.1E-03	-
FOSL1	1.0E-06	7.6E-04	+	1.0E-06	1.2E-03	+
SNRPG	1.1E-06	7.6E-04	+	2.5E-03	1.1E-02	+
HBP1	1.1E-06	7.6E-04	-	5.9E-02	5.0E-02	-
ARFGEF1	2.0E-06	9.2E-04	-	1.4E-01	8.6E-02	-
PLXNB1	2.6E-06	9.2E-04	-	1.5E-05	2.7E-03	-
PHLDA1	2.7E-06	9.2E-04	+	1.1E-04	4.5E-03	+
ALDH4A1	3.0E-06	9.2E-04	-	1.2E-02	2.2E-02	-
TIMM23	3.2E-06	9.2E-04	+	4.7E-03	1.4E-02	+
KIAA0240	3.2E-06	9.2E-04	-	3.6E-03	1.3E-02	-
PLAU	3.4E-06	9.2E-04	+	4.1E-03	1.3E-02	+
GGT1	4.2E-06	9.2E-04	-	1.2E-01	7.5E-02	-
MT1G	4.4E-06	9.2E-04	+	5.0E-03	1.5E-02	+
MT2A	4.4E-06	9.2E-04	+	3.2E-03	1.2E-02	+
CCNG2	4.5E-06	9.2E-04	-	3.0E-01	1.4E-01	-
ARFGEF1	4.8E-06	9.2E-04	-	1.7E-01	9.6E-02	-
CSNK1D	5.2E-06	9.2E-04	-	4.1E-05	3.7E-03	-
CRIP2	5.3E-06	9.2E-04	-	1.1E-03	7.6E-03	-
CKAP5	6.1E-06	9.2E-04	+	3.6E-03	1.3E-02	+
PBXIP1	6.1E-06	9.2E-04	-	1.1E-02	2.1E-02	-
NEBL	6.4E-06	9.2E-04	-	6.7E-05	3.9E-03	-
UBE2E3	6.9E-06	9.2E-04	+	5.3E-03	1.5E-02	+
ERBB3	7.1E-06	9.2E-04	-	1.5E-04	4.6E-03	-
SH3YL1	7.3E-06	9.2E-04	-	2.5E-04	5.2E-03	-
DKFZp586I1420	7.7E-06	9.2E-04	-	8.4E-03	1.8E-02	-
SCYL3	7.7E-06	9.2E-04	-	7.7E-04	6.8E-03	-
PTRF	7.8E-06	9.2E-04	+	5.4E-04	6.3E-03	+
ZCD1	8.2E-06	9.2E-04	+	6.7E-03	1.7E-02	+
CAV2	8.3E-06	9.2E-04	+	2.5E-04	5.2E-03	+
PHLDA1	8.9E-06	9.2E-04	+	4.1E-03	1.3E-02	+
GRB7	9.3E-06	9.2E-04	-	7.0E-04	6.8E-03	-
MYO1D	9.3E-06	9.2E-04	-	7.9E-03	1.8E-02	-
PI4KII	9.4E-06	9.2E-04	+	1.3E-02	2.2E-02	+
GGT1	1.0E-05	9.2E-04	-	5.1E-02	4.6E-02	-
GRHL2	1.0E-05	9.2E-04	-	4.8E-03	1.4E-02	-
FLJ22531	1.1E-05	9.2E-04	-	1.9E-02	2.7E-02	-
ZNF217	1.1E-05	9.2E-04	-	6.1E-03	1.6E-02	-
TAF1A	1.1E-05	9.2E-04	+	4.3E-02	4.2E-02	+
CCNG2	1.1E-05	9.2E-04	-	2.0E-01	1.1E-01	-
CAV1	1.1E-05	9.2E-04	+	1.3E-03	8.3E-03	+
GLS	1.2E-05	9.3E-04	+	4.1E-03	1.3E-02	+
DALRD3	1.2E-05	9.3E-04	-	5.9E-04	6.4E-03	-
TGFBR2	1.2E-05	9.3E-04	+	2.9E-04	5.5E-03	+
PSD4	1.3E-05	9.8E-04	-	1.2E-03	8.0E-03	-
MT1H	1.4E-05	1.0E-03	+	1.6E-02	2.5E-02	+
CNNM4	1.4E-05	1.0E-03	-	8.7E-05	3.9E-03	-
PBX1	1.5E-05	1.0E-03	-	7.3E-03	1.7E-02	-

MAP4K4	1.7E-05	1.2E-03	+	3.4E-02	3.6E-02	+
SCGB2A1	1.7E-05	1.2E-03	-	3.9E-03	1.3E-02	-
EPHA2	1.8E-05	1.2E-03	+	6.3E-05	3.9E-03	+
ELK3	2.0E-05	1.3E-03	+	1.2E-03	8.0E-03	+
C3orf14	2.0E-05	1.3E-03	-	1.0E-02	2.0E-02	-
BDNF	2.1E-05	1.3E-03	+	1.5E-03	8.7E-03	+
ERBB2	2.1E-05	1.3E-03	-	2.7E-03	1.1E-02	-
DLG7	2.2E-05	1.3E-03	+	1.7E-03	8.9E-03	+
TMEM22	2.2E-05	1.3E-03	+	7.1E-03	1.7E-02	+
SELENBP1	2.2E-05	1.3E-03	-	9.1E-05	4.0E-03	-
BLNK	2.2E-05	1.3E-03	-	1.7E-03	9.0E-03	-
SLC24A3	2.3E-05	1.3E-03	-	9.6E-04	7.3E-03	-
EFNA3	2.4E-05	1.3E-03	-	1.3E-02	2.2E-02	-
MPPE1	2.5E-05	1.3E-03	-	1.6E-03	8.7E-03	-
CCNI	2.5E-05	1.3E-03	-	1.2E-02	2.2E-02	-
MIF	2.5E-05	1.3E-03	-	9.1E-03	1.9E-02	-
CTSZ	2.5E-05	1.3E-03	+	9.9E-03	2.0E-02	+
PLXNB3	2.5E-05	1.3E-03	-	2.9E-03	1.1E-02	-
SCARB2	2.7E-05	1.3E-03	-	6.6E-02	5.3E-02	-
IRX5	2.7E-05	1.3E-03	-	1.9E-03	9.4E-03	-
SUV420H1	2.7E-05	1.3E-03	-	1.2E-03	8.1E-03	-
PLAU	2.8E-05	1.3E-03	+	3.2E-03	1.2E-02	+
CTNNBIP1	2.8E-05	1.3E-03	-	7.7E-02	5.8E-02	-
ZNF552	2.9E-05	1.3E-03	-	3.7E-02	3.8E-02	-
TRAF5	3.0E-05	1.3E-03	-	1.9E-02	2.7E-02	-
ZNF467	3.0E-05	1.3E-03	-	1.4E-04	4.6E-03	-
PBX1	3.0E-05	1.3E-03	-	5.3E-03	1.5E-02	-
ZNF278	3.0E-05	1.3E-03	-	2.4E-03	1.1E-02	-
LHFP	3.0E-05	1.3E-03	+	4.6E-04	6.1E-03	+
EXT1	3.2E-05	1.4E-03	+	2.1E-02	2.9E-02	+
CCDC99	3.3E-05	1.4E-03	+	6.2E-04	6.6E-03	+
TNPO1	3.3E-05	1.4E-03	+	2.0E-04	4.9E-03	+
IDH2	3.6E-05	1.5E-03	-	1.2E-03	8.0E-03	-
LARGE	3.7E-05	1.5E-03	-	5.4E-04	6.2E-03	-
XRCC5	4.1E-05	1.6E-03	+	5.2E-04	6.1E-03	+
UPP1	4.1E-05	1.6E-03	+	2.6E-03	1.1E-02	+
MT1E	4.1E-05	1.6E-03	+	2.1E-03	9.9E-03	+
NUP160	4.1E-05	1.6E-03	+	1.6E-02	2.4E-02	+
LYPD3	4.2E-05	1.6E-03	-	7.2E-05	3.9E-03	-
EMP3	4.2E-05	1.6E-03	+	5.9E-04	6.4E-03	+
ALDH3B2	4.2E-05	1.6E-03	-	7.4E-04	6.8E-03	-
PHLDA1	4.3E-05	1.6E-03	+	1.6E-03	8.8E-03	+
PER2	4.3E-05	1.6E-03	-	8.0E-05	3.9E-03	-
AKAP12	4.4E-05	1.6E-03	+	1.5E-04	4.6E-03	+
MSX2	4.4E-05	1.6E-03	-	3.1E-02	3.5E-02	-
WDR79	4.7E-05	1.7E-03	+	1.8E-02	2.6E-02	+
COTL1	4.7E-05	1.7E-03	+	2.2E-04	4.9E-03	+
ETV5	4.8E-05	1.7E-03	+	3.4E-03	1.2E-02	+
SCARB2	4.8E-05	1.7E-03	-	1.1E-01	7.3E-02	-
HMGN4	4.9E-05	1.7E-03	+	1.1E-02	2.1E-02	+
TJP3	4.9E-05	1.7E-03	-	9.1E-06	2.6E-03	-

IDH2	5.0E-05	1.7E-03	-	8.8E-04	7.1E-03	-
PIK3R3	5.0E-05	1.7E-03	-	1.0E-03	7.5E-03	-
RTN4	5.1E-05	1.7E-03	+	4.4E-04	6.1E-03	+
HBEGF	5.1E-05	1.7E-03	+	1.9E-04	4.9E-03	+
MYL6B	5.1E-05	1.7E-03	+	9.5E-02	6.6E-02	+
AKR1B1	5.2E-05	1.7E-03	+	1.8E-04	4.9E-03	+
LIMK2	5.2E-05	1.7E-03	-	4.2E-04	6.1E-03	-
ANK3	5.4E-05	1.7E-03	-	7.4E-04	6.8E-03	-
PLA2G12A	5.5E-05	1.7E-03	-	1.4E-02	2.3E-02	-
KIAA0500	5.5E-05	1.7E-03	-	1.1E-03	7.9E-03	-
LDHB	5.5E-05	1.7E-03	+	9.2E-03	1.9E-02	+
Transcribed locus	5.5E-05	1.7E-03	+	8.3E-03	1.8E-02	+
GGA2	5.6E-05	1.7E-03	-	4.9E-02	4.4E-02	-
PLAUR	5.7E-05	1.7E-03	+	2.9E-02	3.3E-02	+
SIDT1	5.8E-05	1.7E-03	-	2.9E-05	3.4E-03	-
TRGC2	5.8E-05	1.7E-03	-	6.5E-02	5.2E-02	-
TNPO1	5.9E-05	1.7E-03	+	8.8E-03	1.9E-02	+
SH2B3	5.9E-05	1.7E-03	+	2.3E-03	1.0E-02	+
ANXA1	5.9E-05	1.7E-03	+	3.1E-03	1.2E-02	+
SLIT2	6.0E-05	1.7E-03	+	1.7E-02	2.6E-02	+
DUSP8	6.2E-05	1.7E-03	-	5.7E-03	1.5E-02	-
EPS15	6.2E-05	1.7E-03	+	2.2E-04	4.9E-03	-
ID2	6.3E-05	1.7E-03	-	6.9E-02	5.4E-02	-
TRGC2	6.3E-05	1.7E-03	-	1.4E-01	8.4E-02	-
AKAP2	6.4E-05	1.8E-03	+	3.0E-03	1.2E-02	+
GGTLA4	6.5E-05	1.8E-03	-	1.7E-01	9.6E-02	-
GGT1	6.6E-05	1.8E-03	-	3.6E-02	3.7E-02	-
MCTP1	6.7E-05	1.8E-03	+	3.3E-03	1.2E-02	+
SKIL	6.7E-05	1.8E-03	-	3.3E-01	1.6E-01	-
VEGF	7.0E-05	1.8E-03	-	1.2E-02	2.2E-02	-
CLN3	7.1E-05	1.8E-03	-	4.3E-03	1.4E-02	-
WNT5A	7.2E-05	1.9E-03	+	2.4E-03	1.1E-02	+
ARHGEF5	7.3E-05	1.9E-03	-	1.1E-05	2.6E-03	-
GSTO1	7.4E-05	1.9E-03	+	3.4E-03	1.2E-02	+
IRAK1	7.5E-05	1.9E-03	+	7.8E-02	5.9E-02	+
PH-4	7.6E-05	1.9E-03	-	4.3E-04	6.1E-03	-
CCT7	7.7E-05	1.9E-03	+	5.7E-03	1.5E-02	+
GGT1	7.8E-05	1.9E-03	-	1.4E-01	8.4E-02	-
SLC24A3	7.8E-05	1.9E-03	-	3.0E-04	5.6E-03	-
C9orf7	8.1E-05	2.0E-03	-	1.2E-03	8.0E-03	-
RREB1	8.2E-05	2.0E-03	-	8.3E-03	1.8E-02	-
CAV1	8.3E-05	2.0E-03	+	2.5E-03	1.1E-02	+
TUBB6	8.3E-05	2.0E-03	+	3.1E-02	3.5E-02	+
FLJ20273	8.4E-05	2.0E-03	-	1.0E-02	2.0E-02	-
APP	8.5E-05	2.0E-03	-	1.6E-02	2.5E-02	-
CDKN3	8.7E-05	2.0E-03	+	6.4E-03	1.6E-02	+
GNG11	8.7E-05	2.0E-03	+	7.8E-04	6.8E-03	+
NUDC	8.9E-05	2.0E-03	+	4.9E-03	1.5E-02	+
PPARG	8.9E-05	2.0E-03	+	9.9E-03	2.0E-02	+
NOL8	8.9E-05	2.0E-03	+	9.0E-03	1.9E-02	+
RHOH	9.1E-05	2.0E-03	-	2.4E-02	3.0E-02	-

TOB1	9.1E-05	2.0E-03	-	1.9E-04	4.9E-03	-
ISG15	9.1E-05	2.0E-03	+	7.2E-03	1.7E-02	+
ALDH3B2	9.4E-05	2.1E-03	-	3.4E-04	5.6E-03	-
PSMC3	9.5E-05	2.1E-03	+	2.1E-02	2.9E-02	+
PSMC4	9.8E-05	2.1E-03	+	6.3E-01	2.5E-01	+
PNPLA6	9.8E-05	2.1E-03	+	3.7E-02	3.8E-02	+
TESK2	9.8E-05	2.1E-03	-	2.5E-02	3.1E-02	-
JMJD2B	9.9E-05	2.1E-03	-	1.5E-03	8.6E-03	-

Table 4.1: Gene transcripts correlated with EphA2 transport
141 mRNA transcripts (158 probesets) displayed significant correlation ($p < 1 \times 10^{-4}$, FDR $< 5 \times 10^{-3}$) with EphA2 radial transport phenotype. Their respective correlations with invasion potential are also shown. All selected mRNA biomarkers display the same type of correlation with the EphA2 reorganization phenotype as with invasion potential.

Protein ID	EphA2 Radial Transport		Invasion potential	
	p	Type of Correlation	*p*	Type of Correlation
EPHA2	1.5E-04	+	9.8E-03	+
CAV1_UP	4.2E-04	+	2.1E-02	+
CAV1_LOW	4.6E-04	+	2.3E-02	+
EFNA1	5.0E-04	-	3.5E-01	+
CAV2_LOW	1.1E-03	+	1.9E-02	+
ACTN1	1.2E-03	+	4.3E-02	+
LYN	1.5E-03	+	1.6E-01	+
CD44	1.5E-03	+	1.6E-03	+
CAV2_UP	1.8E-03	+	5.8E-03	-
JUN	2.6E-03	+	5.5E-03	-
MDM2	3.1E-03	-	3.9E-02	-
ERBB2-P	3.2E-03	-	9.9E-04	-
TYK2	4.0E-03	+	3.1E-01	+
ERBB2	4.6E-03	-	6.6E-03	+
RB1	4.9E-03	-	1.8E-01	+
SPDEF	4.9E-03	-	6.1E-03	+
ITGB1_UP	6.3E-03	+	2.7E-02	-
CDK1	6.4E-03	+	1.0E-02	+
CDH1_LOW	8.6E-03	-	2.9E-01	-
CDKN1A	8.9E-03	+	7.7E-01	+
CBL_LOW	9.5E-03	+	5.2E-02	+
IRS1	1.0E-02	+	6.8E-02	+
ESR1	1.0E-02	-	8.6E-02	-
SRC	2.7E-02	+	9.2E-01	+
CCNE1	3.9E-02	-	3.9E-01	-
CDH1_UP	4.0E-02	-	1.9E-01	-
SFN	4.9E-02	+	4.1E-01	+
TP53	5.3E-02	+	1.1E-02	-
SHC1_P66	5.5E-02	+	1.2E-01	-
SKP2	5.6E-02	+	6.2E-01	+
MAPK3	6.0E-02	-	4.3E-01	+
CDKN1B	6.1E-02	-	4.8E-01	-
AKT1-P	7.4E-02	-	3.7E-01	-
MEK-P	7.7E-02	+	8.8E-01	+
IGF1R	8.1E-02	+	1.9E-01	+
ERBB3	8.2E-02	-	3.8E-03	+
BAG4	9.4E-02	+	2.7E-03	+

Table 4.2: Proteins correlated with EphA2 transport
37 proteins displayed significant correlation ($p < 0.1$) with EphA2 radial transport phenotype. Their respective correlations with invasion potential are also shown. All selected protein biomarkers display the same type of correlation with the EphA2 reorganization phenotype as with invasion potential.

KEGG Pathway	*p*	FDR	Genes
ErbB signaling pathway	1.3E-09	1.6E-08	CDKN1A, ERBB2, SRC, JUN, CDKN1B, AKT1, SHC1, ERBB3, MAPK3, CBL,
Prostate cancer	1.6E-09	2.0E-08	RB1, CDKN1A, ERBB2, MDM2, TP53, CCNE1, CDKN1B, AKT1, IGF1R, MAPK3,
Chronic myeloid leukemia	1.1E-08	1.3E-07	RB1, CDKN1A, MDM2, TP53, CDKN1B, AKT1, SHC1, MAPK3, CBL,
Glioma	5.9E-08	7.4E-07	RB1, CDKN1A, MDM2, TP53, AKT1, SHC1, IGF1R, MAPK3,
Bladder cancer	1.3E-07	1.6E-06	RB1, CDKN1A, ERBB2, MDM2, TP53, CDH1, MAPK3,
Melanoma	1.6E-07	2.0E-06	RB1, CDKN1A, MDM2, TP53, CDH1, AKT1, IGF1R, MAPK3,
Focal adhesion	1.8E-07	2.3E-06	ERBB2, CAV1, SRC, CAV2, ACTN1, JUN, AKT1, ITGB1, SHC1, IGF1R, MAPK3,
Cell cycle	5.0E-06	6.3E-05	RB1, SKP2, CDKN1A, MDM2, SFN, TP53, CCNE1, CDKN1B,
Small cell lung cancer	1.4E-05	1.7E-04	RB1, SKP2, TP53, CCNE1, CDKN1B, AKT1, ITGB1,
Adherens junction	8.7E-05	1.1E-03	ERBB2, SRC, CDH1, ACTN1, IGF1R, MAPK3,
Endometrial cancer	2.5E-04	3.2E-03	ERBB2, TP53, CDH1, AKT1, MAPK3,
Non-small cell lung cancer	2.9E-04	3.7E-03	RB1, ERBB2, TP53, AKT1, MAPK3,
p53 signaling pathway	8.2E-04	1.0E-02	CDKN1A, MDM2, SFN, TP53, CCNE1,
Pancreatic cancer	1.1E-03	1.3E-02	RB1, ERBB2, TP53, AKT1, MAPK3,
Colorectal cancer	1.9E-03	2.4E-02	TP53, JUN, AKT1, IGF1R, MAPK3,

Table 4.3: KEGG pathways correlated with EphA2 transport
15 KEGG pathways displayed significant correlation (FDR $< 5 \times 10^{-2}$) with EphA2 radial transport phenotype.

Biocarta Pathway	*p*	FDR	Genes
Influence of Ras and Rho proteins on G1 to S Transition	3.0E-05	4.0E-04	RB1, CDKN1A, CCNE1, CDKN1B, AKT1, MAPK3,
Cell Cycle G1/S Check Point	4.5E-05	6.0E-04	RB1, SKP2, CDKN1A, TP53, CCNE1, CDKN1B,
p53 Signaling Pathway	8.3E-05	1.1E-03	RB1, CDKN1A, MDM2, TP53, CCNE1,
Multiple antiapoptotic pathways from IGF-1R signaling lead to BAD phosphorylation	1.7E-04	2.3E-03	AKT1, SHC1, IGF1R, MAPK3, IRS1,
Integrin Signaling Pathway	1.9E-04	2.6E-03	CAV1, SRC, JUN, ITGB1, SHC1, MAPK3,
IGF-1 Signaling Pathway	2.1E-04	2.8E-03	JUN, SHC1, IGF1R, MAPK3, IRS1,
PTEN dependent cell cycle arrest and apoptosis	2.1E-04	2.8E-03	CDKN1B, AKT1, ITGB1, SHC1, MAPK3,
Trefoil Factors Initiate Mucosal Healing	2.6E-04	3.5E-03	ERBB2, AKT1, ITGB1, SHC1, MAPK3,
Role of ERBB2 in Signal Transduction and Oncology	2.6E-04	3.5E-03	ERBB2, ESR1, SHC1, ERBB3, MAPK3,
Regulation of p27 Phosphorylation during Cell Cycle Progression	9.4E-04	1.3E-02	RB1, SKP2, CCNE1, CDKN1B,
Erk1/Erk2 Mapk Signaling pathway	1.2E-03	1.6E-02	SRC, ITGB1, SHC1, IGF1R, MAPK3,
Sprouty regulation of tyrosine kinase signals	1.5E-03	2.0E-02	SRC, SHC1, MAPK3, CBL,
IL-2 Receptor Beta Chain in T cell Activation	2.4E-03	3.2E-02	AKT1, SHC1, MAPK3, IRS1, CBL,

Table 4.4: Biocarta pathways correlated with EphA2 transport
13 Biocarta pathways displayed significant correlation (FDR $< 5 \times 10^{-2}$) with EphA2 radial transport phenotype.

Chapter 5

Future Directions

5.1 Abstract

The work described in the preceding chapters has revealed the importance of physical characteristics of the microenvironment to receptor-ligand binding processes and subsequent signaling events. The systems discussed here are not the only ones in which such factors have been shown to play a role in signaling. In fact, it is becoming evident that receptor organization on the cell surface is a common mechanism that cells use to regulate intercellular signaling events necessary for the maintenance of tissue homeostasis. Prior to this work, the examination of regulatory roles for receptor organization in cell signaling was experimentally inaccessible due to the chemical and physical complexity of cell membranes. The techniques developed in this study allow detailed investigation into the mechanisms by which signaling cascades sense and respond to physical parameters of the microenvironment. Finally, the results discussed here reveal new mechanistic details about the EphA2 signaling pathway, specifically regarding how it responds to ligand mobility and spatial organization. In the following sections I will describe new questions uncovered by this study, which serve as potential directions for future exploration.

5.2 The Study of Signaling at Intercellular Interfaces

The cell membrane is a diverse chemical interface and the intercellular communication it is responsible for maintaining requires a complex integration of many signaling systems acting in concert. To make sense of the vast array of potential signaling outputs that may arise from many receptors on its surface, the cell must utilize several regulatory mechanisms. One such mechanism is the dynamic lateral reorganization of signaling molecules on the membrane surface in response to stimuli, to create areas of enhanced local receptor concentration. If signaling events are at all cooperative, this may allow the cell to selectively amplify certain signaling outputs, while dampening others.

The direct observation of such reorganization events on the cell membrane is experimentally challenging due to the heterogeneous and dynamic nature of the cell membrane. To address this difficulty, the Groves lab has pioneered the use of nanopatterned supported membranes to study signaling regulation through spatial reorganization.[20,88,95] In this work, we coupled the use of spatial mutations with several biochemical readouts of signaling events to determine which facets of different signal transduction cascades were responsive to ligand fluidity and spatial organization. The areas patterned using the fabrication techniques described here are often too small to provide enough cellular material for standard biochemical assays. For this reason, techniques that can be performed at the single-cell level are preferable for use with nanofabricated substrates.

Microscopy-based signaling readouts couple especially well to the use of nanopatterned supported membranes because the planar nature of these surfaces creates a well-defined cell-supported membrane interface suitable for high resolution microscopy. Recent advances in the choices of fluorescent proteins, dyes, and microscopy techniques mean that future studies will enjoy ever-shrinking temporal and spatial resolution limits. This means one can reasonably foresee direct observation of the dynamics of receptor-ligand binding events in the cell-supported membrane interface in real time and at the molecular scale.

5.3 Molecular Physiology of EphA2 Mechano-Sensing

The strong link between EphA2 lateral transport and tissue invasion, described in chapter 4, has emerged as a topic of broad significance. Invasive cells are known to interact with their environment in an abnormal fashion, and Eph receptors direct cell guidance. For these reasons, the association between EphA2 expression and cancer metastasis seems logical, but this is the first evidence of altered EphA2 mechano-sensing in invasive cells.[118] Future work will focus on determining the specific elements of the EphA2 signal transduction pathway that are responsive to physical aspects of the microenvironment, at the molecular scale. The work described in chapter 4 highlights many target biomolecules that are implicated in this altered response, and future work will elucidate the mechanism by which these downstream effectors, and likely others, contribute to EphA2 transport.

As discussed in chapter 4, the connection between EphA2 transport in response to fluid membrane-bound ligand and tissue invasion makes this an especially exciting system to study. Understanding which elements of the EphA2 signaling cascade are responsive to factors such as ligand mobility and spatial organization may allow us to more precisely direct the cellular response to ephrin-A1. This, in turn, may lend insight into the process by which invasive cells are able to elude homeostatic regulatory mechanisms to leave their host tissues and colonize distant sites within the body. Future work in this area will focus on determining which biomolecules downstream of EphA2 activation are responsive to physical parameters of the signaling microenvironment.

Bibliography

1. Lutolf, M.P. & Hubbell, J.A. Synthetic biomaterials as instructive extracellular microenvironments for morphogenesis in tissue engineering. *Nature Biotechnology* **23**, 47-55 (2005).
2. Singh, A.B. & Harris, R.C. Autocrine, paracrine and juxtacrine signaling by EGFR ligands. *Cellular Signalling* **17**, 1183-1193 (2005).
3. Bruce Alberts et al. *Molecular Biology of the Cell*. (Garland Science: 2007).
4. Ramarao, M.K. & Cohen, J.B. Mechanism of nicotinic acetylcholine receptor cluster formation by rapsyn. *Proceedings of the National Academy of Sciences of the United States of America* **95**, 4007-4012 (1998).
5. Le Borgne, R. & Schweisguth, F. Notch Signaling: Endocytosis Makes Delta Signal Better. *Current Biology* **13**, R273-R275 (2003).
6. Tsuchida, J., Ueki, S., Takada, Y., Saito, Y. & Takagi, J. The 'ligand-induced conformational change' of alpha 5 beta 1 integrin. Relocation of alpha 5 subunit to uncover the beta 1 stalk region. *Journal of Cell Science* **111**, 1759-1766 (1998).
7. Dustin, M.L., Bromley, S.K., Davis, M.M. & Zhu, C. Identification of self through two-dimensional chemistry and synapses. *Annual Review of Cell and Developmental Biology* **17**, 133-157 (2001).
8. Israelachvili, J. *Intermolecular and Surface Forces*. (Academic Press: 1992).
9. Singer, S. & Nicolson, G. The fluid mosaic model of the structure of cell membranes. *Science* **175**, 720-731 (1972).
10. Hanahan, D. & Weinberg, R.A. The hallmarks of cancer. *Cell* **100**, 57-70 (2000).
11. ElShamy, W. Epithelial to mesenchymal transition, cell surface receptors activation and intracellular communications in cancer metastasis. *Cancer Therapy* **3**, 443-460 (2005).
12. Birchmeier, W. & Behrens, J. Cadherin expression in carcinomas: role in the formation of cell junctions and the prevention of invasiveness. *Biochimica et Biophysica Acta* **1198**, 11-26 (1994).
13. Frixen, U.H. et al. E-cadherin-mediated cell-cell adhesion prevents invasiveness of human carcinoma cells. *The Journal of Cell Biology* **113**, 173-185 (1991).
14. Yarden, Y. & Sliwkowski, M.X. Untangling the ErbB signalling network. *Nature Reviews Molecular Cell Biology* **2**, 127-137 (2001).
15. Pasquale, E.B. Eph receptor signalling casts a wide net on cell behaviour. *Nature Reviews*

Molecular Cell Biology **6**, 462-75 (2005).
16. Kullander, K. & Klein, R. Mechanisms and functions of Eph and ephrin signalling. *Nature Reviews Molecular Cell Biology* **3**, 475-86 (2002).
17. Britten, C.D. Targeting ErbB receptor signaling: A pan-ErbB approach to cancer. *Molecular Cancer Therapeutics* **3**, 1335-1342 (2004).
18. Carles-Kinch, K., Kilpatrick, K.E., Stewart, J.C. & Kinch, M.S. Antibody targeting of the EphA2 tyrosine kinase inhibits malignant cell behavior. *Cancer Research* **62**, 2840-2847 (2002).
19. Monks, C.R.F., Freiberg, B.A., Kupfer, H., Sciaky, N. & Kupfer, A. Three-dimensional segregation of supramolecular activation clusters in T cells. *Nature* **395**, 82-86 (1998).
20. Manz, B.N. & Groves, J.T. Spatial organization and signal transduction at intercellular junctions. *Nature Reviews Molecular Cell Biology* **11**, 342-52
21. Engelman, D.M. Membranes are more mosaic than fluid. *Nature* **438**, 578-580 (2005).
22. Hartman, N.C., Nye, J.A. & Groves, J.T. Cluster size regulates protein sorting in the immunological synapse. *Proceedings of the National Academy of Sciences of the United States of America* **106**, 12729-12734 (2009).
23. Schlessinger, J. Ligand-Induced, Receptor-Mediated Dimerization and Activation of EGF Receptor. *Cell* **110**, 669-672 (2002).
24. Pabbisetty, K.B. et al. Kinetic analysis of the binding of monomeric and dimeric ephrins to Eph receptors: Correlation to function in a growth cone collapse assay. *Protein Science* **16**, 355-361 (2007).
25. Mossman, K.D., Campi, G., Groves, J.T. & Dustin, M.L. Altered TCR signaling from geometrically repatterned immunological synapses. *Science* **310**, 1191-1193 (2005).
26. Gureasko, J. et al. Membrane-dependent signal integration by the Ras activator Son of sevenless. *Nature Structural and Molecular Biology* **15**, 452-461 (2008).
27. Davis, S. et al. Ligands for EPH-related receptor tyrosine kinases that require membrane attachment or clustering for activity. *Science* **266**, 816-9 (1994).
28. Poliakov, A., Cotrina, M. & Wilkinson, D.G. Diverse roles of eph receptors and ephrins in the regulation of cell migration and tissue assembly. *Developmental Cell* **7**, 465-80 (2004).
29. Sackmann, E. Supported membranes: scientific and practical applications. *Science* **271**, 43-48 (1996).
30. Grakoui, A. et al. The immunological synapse: A molecular machine controlling T cell activation. *Science* **285**, 221-227 (1999).
31. Nye, J.A. & Groves, J.T. Kinetic Control of Histidine-Tagged Protein Surface Density on Supported Lipid Bilayers. *Langmuir* **24**, 4145-4149 (2008).
32. Rabuka, D., Forstner, M.B., Groves, J.T. & Bertozzi, C.R. Noncovalent Cell Surface Engineering: Incorporation of Bioactive Synthetic Glycopolymers into Cellular Membranes. *Journal of the American Chemical Society* **130**, 5947-5953 (2008).
33. Groves, J.T. & Dustin, M.L. Supported planar bilayers in studies on immune cell adhesion and communication. *Journal of Immunological Methods* **278**, 19-32 (2003).
34. Groves, J.T. & Boxer, S.G. Micropattern Formation in Supported Lipid Membranes. *Accounts of Chemical Research* **35**, 149-157 (2002).
35. Kane, R.S., Takayama, S., Ostuni, E., Ingber, D.E. & Whitesides, G.M. Patterning proteins and cells using soft lithography. *Biomaterials* **20**, 2363-2376 (1999).
36. Jackson, B.L. & Groves, J.T. Hybrid Protein−Lipid Patterns from Aluminum Templates. *Langmuir* **23**, 2052-2057 (2007).

37. Demond, A.L., Mossman, K.D., Starr, T., Dustin, M.L. & Groves, J.T. T cell receptor microcluster transport through molecular mazes reveals mechanism of translocation. *Biophysical Journal* **94**, 3286-3292 (2008).
38. Groves, J.T. Bending Mechanics and Molecular Organization in Biological Membranes. *Annual Review of Physical Chemistry* **58**, 697-717 (2007).
39. Groves, J.T., Parthasarathy, R. & Forstner, M.B. Fluorescence imaging of membrane dynamics. *Annual Review of Biomedical Engineering* **10**, 311-338 (2008).
40. Neve, R.M. et al. A collection of breast cancer cell lines for the study of functionally distinct cancer subtypes. *Cancer Cell* **10**, 515-527 (2006).
41. Feldmann, M. & Steinman, L. Design of effective immunotherapy for human autoimmunity. *Nature* **435**, 612-9 (2005).
42. Chen, E.H. & Olson, E.N. Unveiling the mechanisms of cell-cell fusion. *Science* **308**, 369-73 (2005).
43. Groves, J.T. Learning the chemical language of cell-surface interactions. *Science Signaling: Signal Transduction Knowledge Environment* **2005**, pe45 (2005).
44. Irvine, D.J., Hue, K.A., Mayes, A.M. & Griffith, L.G. Simulations of cell-surface integrin binding to nanoscale-clustered adhesion ligands. *Biophysical Journal* **82**, 120-132 (2002).
45. Groves, J.T., Mahal, L.K. & Bertozzi, C.R. Control of cell adhesion and growth with micropatterned supported lipid membranes. *Langmuir* **17**, 5129-5133 (2001).
46. Schmeichel, K.L. & Bissell, M.J. Modeling tissue-specific signaling and organ function in three dimensions. *Journal of Cell Science* **116**, 2377-2388 (2003).
47. Wu, M., Holowka, D., Craighead, H.G. & Baird, B. Visualization of plasma membrane compartmentalization with patterned lipid bilayers. *Proceedings of the National Academy of Sciences of the United States of America* **101**, 13798-13803 (2004).
48. Douglass, A.D. & Vale, R.D. Single-molecule microscopy reveals plasma membrane microdomains created by protein-protein networks that exclude or trap signaling molecules in T cells. *Cell* **121**, 937-950 (2005).
49. Groves, J.T. & Dustin, M.L. Supported planar bilayers in studies on immune cell adhesion and communication. *Journal of Immunological Methods* **278**, 19-32 (2003).
50. Tirrell, M., Kokkoli, E. & Biesalski, M. The role of surface science in bioengineered materials. *Surface Science* **500**, 61-83 (2002).
51. Jensen, T.W. et al. Lipopeptides incorporated into supported phospholipid monolayers have high specific activity at low incorporation levels. *Journal of the American Chemical Society* **126**, 15223-15230 (2004).
52. Chen, C.S., Mrksich, M., Huang, S., Whitesides, G.M. & Ingber, D.E. Geometric control of cell life and death. *Science* **276**, 1425-1428 (1997).
53. Alberts, B. & National Center for Biotechnology Information (U.S.) *Molecular biology of the cell*. **4th**, (Garland ; NCBI: New York, N.Y. Bethseda, MD, 2002).
54. Ziauddin, J. & Sabatini, D.M. Microarrays of cells expressing defined cDNAs. *Nature* **411**, 107-110 (2001).
55. Wheeler, D.B. et al. RNAi living-cell microarrays for loss-of-function screens in Drosophila melanogaster cells. *Nature Methods* **1**, 127-32 (2004).
56. Bailey, S.N., Sabatini, D.M. & Stockwell, B.R. Microarrays of small molecules embedded in biodegradable polymers for use in mammalian cell-based screens. *Proceedings of the National Academy of Sciences of the United States of America* **101**, 16144-9 (2004).
57. Sackmann, E. & Tanaka, M. Supported membranes on soft polymer cushions: fabrication,

characterization and applications. *Trends in Biotechnology* **18**, 58-64 (2000).
58. Groves, J.T. Molecular organization and signal transduction at intermembrane junctions. *Angewandte Chemie International Edition* **44**, 3524-38 (2005).
59. Yee, C.K., Amweg, M.L. & Parikh, A.N. Direct photochemical patterning and refunctionalization of supported phospholipid bilayers. *Journal of the American Chemical Society* **126**, 13962-72 (2004).
60. Holden, M.A., Jung, S.Y., Yang, T., Castellana, E.T. & Cremer, P.S. Creating fluid and air-stable solid supported lipid bilayers. *Journal of the American Chemical Society* **126**, 6512-3 (2004).
61. Kam, L. & Boxer, S.G. Spatially selective manipulation of supported lipid bilayers by laminar flow: Steps toward biomembrane microfluidics. *Langmuir* **19**, 1624-1631 (2003).
62. Zhang, S.G. Beyond the Petri dish. *Nature Biotechnology* **22**, 151-152 (2004).
63. Olayioye, M.A., Neve, R.M., Lane, H.A. & Hynes, N.E. The ErbB signaling network: receptor heterodimerization in development and cancer. *European Molecular Biology Organization Journal* **19**, 3159-3167 (2000).
64. Sawano, A., Takayama, S., Matsuda, M. & Miyawaki, A. Lateral propagation of EGF signaling after local stimulation is dependent on receptor density. *Developmental Cell* **3**, 245-257 (2002).
65. Ichinose, J., Murata, M., Yanagida, T. & Sako, Y. EGF signalling amplification induced by dynamic clustering of EGFR. *Biochemical and Biophysical Research Communications* **324**, 1143-1149 (2004).
66. Forstner, M.B., Yee, C.K., Parikh, A.N. & Groves, J.T. Lipid lateral mobility and membrane phase structure modulation by protein binding. *Journal of the American Chemical Society* **128**, 15221-7 (2006).
67. Tocanne, J.F., Dupoucezanne, L. & Lopez, A. Lateral Diffusion of Lipids in Model and Natural Membranes. *Progress in Lipid Research* **33**, 203-237 (1994).
68. Kopfstein, L. & Christofori, G. Metastasis: cell-autonomous mechanisms versus contributions by the tumor microenvironment. *Cellular and Molecular Life Sciences* **63**, 449-468 (2006).
69. Nam, J.M., Nair, P.M., Neve, R.M., Gray, J.W. & Groves, J.T. A fluid membrane-based soluble ligand-display system for live-cell assays. *ChemBioChem* **7**, 436-40 (2006).
70. Koo, L.Y., Irvine, D.J., Mayes, A.M., Lauffenburger, D.A. & Griffith, L.G. Co-regulation of cell adhesion by nanoscale RGD organization and mechanical stimulus. *Journal of Cell Science* **115**, 1423-1433 (2002).
71. Surawska, H. The role of ephrins and Eph receptors in cancer. *Cytokine & Growth Factor Reviews 15* **6**, 419-433 (2004).
72. Nakamoto, M. & Bergemann, A.D. Diverse roles for the Eph family of receptor tyrosine kinases in carcinogenesis. *Microscopy Research and Technique* **59**, 58-67 (2002).
73. Macrae, M. et al. A conditional feedback loop regulates Ras activity through EphA2. *Cancer Cell* **8**, 111-118 (2005).
74. Zelinski, D.P., Zantek, N.D., Stewart, J.C., Irizarry, A.R. & Kinch, M.S. EphA2 overexpression causes tumorigenesis of mammary epithelial cells. *Cancer Research* **61**, 2301-2306 (2001).
75. Noblitt, L.W. et al. Decreased tumorigenic potential of EphA2-overexpressing breast cancer cells following treatment with adenoviral vectors that express EphrinA1. *Cancer Gene Therapy **11***, 757-766 (2004).

76. Baksh, M.M. et al. Neuronal Activation by GPI-Linked Neuroligin-1 Displayed in Synthetic Lipid Bilayer Membranes. *Langmuir* **21**, 10693-10698 (2005).
77. Hendrickson, W.A. et al. Crystal structure of core streptavidin determined from multiwavelength anomalous diffraction of synchrotron radiation. *Proceedings of the National Academy of Sciences of the United States of America* **86**, 2190-2194 (1989).
78. Himanen, J.P. et al. Ligand recognition by A-class Eph receptors: crystal structures of the EphA2 ligand-binding domain and the EphA2/ephrin-A1 complex. *European Molecular Biology Organization Reports* **10**, 722-8 (2009).
79. Walker-Daniels, J., Riese, D.J. & Kinch, M.S. c-Cbl-dependent EphA2 protein degradation is induced by ligand binding. *Molecular Cancer Research* **1**, 79-87 (2002).
80. Janes, P.W. et al. Adam meets Eph: An ADAM substrate recognition module acts as a molecular switch for ephrin cleavage in trans. *Cell* **123**, 291-304 (2005).
81. Kam, L. & Boxer, S.G. Cell adhesion to protein-micropatterned-supported lipid bilayer membranes. *Journal of Biomedical Materials Research* **55**, 487-495 (2001).
82. Discher, D.E., Janmey, P. & Wang, Y.L. Tissue cells feel and respond to the stiffness of their substrate. *Science* **310**, 1139-1143 (2005).
83. Dalby, M.J. et al. The control of human mesenchymal cell differentiation using nanoscale symmetry and disorder. *Nature Materials* **6**, 997-1003 (2007).
84. Nelson, C.M., VanDuijn, M.M., Inman, J.L., Fletcher, D.A. & Bissell, M.J. Tissue geometry determines sites of mammary branching morphogenesis in organotypic cultures. *Science* **314**, 298-300 (2006).
85. Butcher, D.T., Alliston, T. & Weaver, V.M. A tense situation: forcing tumour progression. *Nature Reviews Cancer* **9**, 108-122 (2009).
86. Chen, C.S. Mechanotransduction - a field pulling together? *Journal of Cell Science* **121**, 3285-3292 (2008).
87. Qi, S.Y., Groves, J.T. & Chakraborty, A.K. Synaptic pattern formation during cellular recognition. *Proceedings of the National Academy of Sciences of the United States of America* **98**, 6548-6553 (2001).
88. Mossman, K.D., Campi, G., Groves, J.T. & Dustin, M.L. Altered TCR signaling from geometrically repatterned immunological synapses. *Science* **310**, 1191-3 (2005).
89. Andrews, N.L. et al. Actin restricts Fc epsilon RI diffusion and facilitates antigen-induced receptor immobilization. *Nature Cell Biology* **10**, 955-963 (2008).
90. Hurtley, S. Location, Location, Location. *Science* **326**, 1205-1205 (2009).
91. Scott, J.D. & Pawson, T. Cell signaling in space and time: where proteins come together and when they're apart. *Science* **326**, 1220-1224 (2009).
92. Hynes, R.O. The extracellular matrix: not just pretty fibrils. *Science* **326**, 1216-1219 (2009).
93. Marquardt, T. et al. Coexpressed EphA receptors and ephrin-A ligands mediate opposing actions on growth cone navigation from distinct membrane domains. *Cell* **121**, 127-139 (2005).
94. Lackmann, M. & Boyd, A.W. Eph, a protein family coming of age: more confusion, insight, or complexity? *Science Signaling: Signal Transduction Knowledge Environment* **1**, re2 (2008).
95. Groves, J.T. Spatial mutation of the T cell immunological synapse. *Current Opinion in Chemical Biology* **10**, 544-50 (2006).
96. Groves, J.T., Ulman, N. & Boxer, S.G. Micropatterning fluid lipid bilayers on solid supports. *Science* **275**, 651-653 (1997).

97. Galush, W.J., Nye, J.A. & Groves, J.T. Quantitative fluorescence microscopy using supported lipid bilayer standards. *Biophysical Journal* **95**, 2512-2519 (2008).
98. Himanen, J.P. et al. Crystal structure of an Eph receptor-ephrin complex. *Nature* **414**, 933-938 (2001).
99. Day, B. et al. Three distinct molecular surfaces in ephrin-A5 are essential for a functional interaction with EphA3. *The Journal of Biological Chemistry* **280**, 26526-26532 (2005).
100. Himanen, J.P. et al. Repelling class discrimination: ephrin-A5 binds to and activates EphB2 receptor signaling. *Nature Neuroscience* **7**, 501-509 (2004).
101. Verschueren, H. Interference Reflection Microscopy in Cell Biology - Methodology and Applications. *Journal of Cell Science* **75**, 279-301 (1985).
102. Humphries, J.D., Byron, A. & Humphries, M.J. Integrin ligands at a glance. *Journal of Cell Science* **119**, 3901-3903 (2006).
103. Carter, N., Nakamoto, T., Hirai, H. & Hunter, T. EphrinA1-induced cytoskeletal re-organization requires FAK and p130(cas). *Nature Cell Biology* **4**, 565-573 (2002).
104. Taddei, M.L. et al. Kinase-dependent and -independent roles of EphA2 in the regulation of prostate cancer invasion and metastasis. *The American Journal of Pathology* **174**, 1492-1503 (2009).
105. Friedl, P. & Wolf, K. Tumour-cell invasion and migration: diversity and escape mechanisms. *Nature Reviews Cancer* **3**, 362-374 (2003).
106. Provenzano, P.P., Inman, D.R., Eliceiri, K.W., Trier, S.M. & Keely, P.J. Contact guidance mediated three-dimensional cell migration is regulated by Rho/ROCK-dependent matrix reorganization. *Biophysical Journal* **95**, 5374-5384 (2008).
107. Leonenko, Z.V., Finot, E., Ma, H., Dahms, T.E.S. & Cramb, D.T. Investigation of temperature-induced phase transitions in DOPC and DPPC phospholipid bilayers using temperature-controlled scanning force microscopy. *Biophysical Journal* **86**, 3783-3793 (2004).
108. Groves, J.T. & Boxer, S.G. Micropattern formation in supported lipid membranes. *Accounts of Chemical Research* **35**, 149-157 (2002).
109. Vargo-Gogola, T. & Rosen, J.M. Modelling breast cancer: one size does not fit all. *Nature Reviews Cancer* **7**, 659-672 (2007).
110. Dennis, G. et al. DAVID: Database for annotation, visualization, and integrated discovery. *Genome Biology* **4**, - (2003).
111. Ponta, H., Sherman, L. & Herrlich, P.A. CD44: From adhesion molecules to signalling regulators. *Nature Reviews Molecular Cell Biology* **4**, 33-45 (2003).
112. Groves, J.T., Boxer, S.G. & McConnel, H.M. Electric field-induced reorganization of two-component supported bilayer membranes. *Proceedings of the National Academy of Sciences of the United States of America* **94**, 13390-13395 (1997).
113. http://icbp.lbl.gov/breastcancer/celllines.php Integrative Cancer Biology Program. at <http://icbp.lbl.gov/breastcancer/celllines.php>
114. Ballestrem, C., Wehrle-Haller, B. & Imhof, B.A. Actin dynamics in living mammalian cells. *Journal of Cell Science* **111 (Pt 12)**, 1649-1658 (1998).
115. Nagle, J.F. & Tristram-Nagle, S. Structure of lipid bilayers. *Biochimica et Biophysica Acta-Reviews on Membranes* **1469**, 159-195 (2000).
116. Das, D., Nahle, Z. & Zhang, M.Q. Adaptively inferring human transcriptional subnetworks. *Molecular Systems Biology* - (2006).
117. Storey, J.D. & Tibshirani, R. Statistical significance for genomewide studies. *Proceedings*

of the National Academy of Sciences of the United States of America **100**, 9440-9445 (2003).
118. Paszek, M. & Weaver, V. Enforcing Order on Signaling. *Science* **327**, 1335-1336 (2010).

Appendix A

Measuring Illumination

```
// This ImageJ macro averages n frames in a stack
// input file format <name>.stk
// outputs file in format <name>-average.tif
// subtracts background from image, outputs file <name>-average-background.tif

dir = getDirectory("Choose File Directory");
Dialog.create("Calibration File");
Dialog.addString("Name of file(no extension): ","488");
Dialog.addString("Channel: ","488");
Dialog.show();
name=Dialog.getString();
channel=Dialog.getString();
setBatchMode(true);
open(dir+name+".stk");
frames=nSlices;
print(frames);
run("Stack to Images");
imageCalculator("Add create 32-bit", channel+"-0001",channel+"-0002");
saveAs("Tiff", dir+"temp.tif");
selectImage(channel+"-0001");
close();
selectImage(channel+"-0002");
close();
if (frames>2){
  for (i=3; i<=frames; i++){
    if (i<10){
      imageCalculator("Add create 32-bit", "temp.tif",channel+"-000"+i);
      selectImage("temp.tif");
      close();
      selectImage("temp-1.tif");
      saveAs("Tiff", dir+"temp.tif");
      selectImage(channel+"-000"+i);
      close();}
    else{
          imageCalculator("Add create 32-bit","temp.tif",channel+"-00"+i);
          selectImage("temp.tif");
          close();
          selectImage("temp-1.tif");
          saveAs("Tiff", dir+"temp.tif");
      selectImage(channel+"-00"+i);
      close();}
  print(i);}
}
selectImage("temp.tif");
run("Divide...", "value="+frames);
saveAs("Tiff",dir+name+"-average.tif");
```

```
run("Set Measurements...", "  mean redirect=None decimal=3");
makeRectangle(11, 453, 65, 54);
run("Measure");
noise=getResult('Mean',nResults-1);
run("Select All");
run("Subtract...", "value="+noise);
saveAs("Tiff",dir+name+"-average-background.tif");
File.delete(dir+"temp.tif");
run("Close All Without Saving");
```

Appendix B

Separating Channels,

Calibrating for Uneven Illumination

```
// This ImageJ macro converts all the stacks in a folder to TIFF
// Subtracts background from each channel
// Divides background-subtracted image by background-subtracted calibration image
// for corresponding channel
// BF images (#1 in the stack) are made into 8-bit TIFF
// Two dialog boxes are displayed. Select the raw data source directory in the first
// Select the calbration files directory (generated by Appendix A file) in the second
// Requires cell ROIs to be saved beforehand in “roi” sub-directory within source directory
// Creates “processed” folder for output files

 dir1 = getDirectory("Choose Source Directory ");
 dir2 = dir1+"processed";
 if (File.isDirectory(dir2)==0){
        File.makeDirectory(dir2);}
 list1 = getFileList(dir1);
 roidir = dir1+"roi";
 list2 = getFileList(roidir);
 calibdir = getDirectory("Where are the calibration files?");
 Dialog.create("Calibration File");
 Dialog.addString("488 raw file (no extension): ","488");
 Dialog.addString("647 raw file (no extension): ","647");
 Dialog.show();
 name488=Dialog.getString();
 name647=Dialog.getString();
 setBatchMode(true);
 open(calibdir+name488+"-average-background.tif");
 open(calibdir+name647+"-average-background.tif");
 run("Set Measurements...", "  mean redirect=None decimal=3");
 k = 0;
 l = list1.length-1;
 for (i=10; i<=(l*10); i+=10) {
        showProgress(k+1, list2.length);
        if ((!File.exists(roidir+"/"+(k+1)+".zip")) && (!File.exists(roidir+"/"+(k+1)+".roi"))){
                print("Stack "+(k+1)+" data not formatted correctly");}
        else{
                open(dir1+(k+1)+".stk");
                if (nSlices!=3){
                        print("Stack "+(k+1)+" has the wrong number of frames!");}
                else{
                        run("Stack to Images");
                        for (j=3;j>0;j--){
                                selectWindow((k+1)+"-000"+j);
                                if (j==1){
                                resetMinAndMax();
                                        run("8-bit");}
                                else{
```

```
                                        makeRectangle(11, 453, 65, 54);
                                        run("Measure");
                                        noise=getResult('Mean',nResults-1);
                                        run("Select All");
                                        run("Subtract...", "value="+noise);}
                                saveAs("TIFF", dir2+"/"+i+j);
                                name = toString(i+j);
                                if (j==3){
                                        imageCalculator("Divide create 32-bit",
name+".tif",name488+"-average-background.tif");
                                        saveAs("TIFF", dir2+"/(flat)"+i+j);}
                                if (j==2){
                                        imageCalculator("Divide create 32-bit",
name+".tif",name647+"-average-background.tif");
                                        saveAs("TIFF", dir2+"/(flat)"+i+j);}}
                                close();}
                        }
        k++;}
  selectImage(name488+"-average-background.tif");
  close();
  selectImage(name647+"-average-background.tif");
  close();
```

Appendix C

Cropping Areas with Cells and Calculating Ratio of Signal in Two Channels

```
// This ImageJ macro takes tif files of the format: bf(11), red(12), green(13)
// (generated by Appendix B file)
// and roi or zip files for cells in each image
// Crops the cells in each image and saves 8-bit versions of each
// Calculates the adam10/epha2 ratio for each cell
// Three dialog boxes are displayed. Select the raw data source directory in the first
// Creates “16bit” subdirectory for full bit-depth images used for analysis
// Creates “8bit” subdirectory for 8-bit images used for presentation
// In second box, choose whether 1.5x lens was used-must be noted during data collection
// In third box, enter treatment—grid pitch or drugging conditions
// Outputs Excel spreadsheet with mean red and green signal intensities and
// ratio of the two for each cell
// Note, this macro can analyze up to 1000 cells, if more are needed
// change “ratio = newArray(1000)” line accordingly

  dir1 = getDirectory("Where is the raw data?");
  processed = dir1+"processed";
  dir16 = dir1+"16bit";
  if (File.isDirectory(dir16)==0){
        File.makeDirectory(dir16);}
  dir8 = dir1+"8bit";
  if (File.isDirectory(dir8)==0){
        File.makeDirectory(dir8);}
  roidir = dir1+"roi";
  list = getFileList(dir1);
  roilist=getFileList(roidir);
  l=roilist.length;
  Dialog.create("Magnification");
  Dialog.addCheckbox("1.5x ", false);
  Dialog.show();
  highmag=Dialog.getCheckbox();
  if (highmag==true){
        resolution = 115;}
  else{
        resolution = 165;}
  exact = 20000/resolution;
  width = round(exact);
  height = width;
  Dialog.create("Spatial Mutation");
  Dialog.addString("Grid pattern? ","Unrestricted");
  Dialog.show();
  table=Dialog.getString();
  tablename="["+table+"]";
  run("Set Measurements...", "  mean redirect=None decimal=3");
  j=0;
  n=0;
```

```
ratio =newArray(1000);
run("Table...", "name="+tablename+" width=350 height=250");
print(tablename,"\\Clear");
print(tablename, "\\Headings:Cell"+"\t"+"EphA2"+"\t"+"ADAM10"+"\t"+"Ratio");
setBatchMode(true);
tempi=0;
for (i=10; i<=(l*10);i+=10){
        showProgress(j+1, l);
        name=split(roilist[j],".");
        tempi=name[0];
        tabletemp=tempi;
        tempi*=10;
        roiManager("Open",roidir+"/"+roilist[j]);
        numcells=roiManager("count");
        j++;
        for (k=0;k<numcells;k++){
                n++;
                count=toString(k+1);
                for (m=1; m<=3;m++){
                        if (m!=1) open(processed+"/(flat)"+tempi+m+".tif");
                        else open(processed+"/"+tempi+m+".tif");
                        roiManager("select",k);
                        run("Crop");
                        if (m!=1){
                                run("Measure");
                                if (m==2){
                                        epha2=getResult('Mean',nResults-1);

        saveAs("TIFF",processed+"/"+tabletemp+"cell"+count+"EphA2");}
                                else if (m==3){
                                        adam10=getResult('Mean',nResults-1);

        saveAs("TIFF",processed+"/"+tabletemp+"cell"+count+"ADAM10");
                                        ratio[n-1]=adam10/epha2;
                                        namej=toString(tabletemp);
                                        print(tablename, "\\Update"+n-1+":"+tabletemp+"-
"+count+"\t"+epha2+"\t"+adam10+"\t"+ratio[n-1]);
                                        imageCalculator("Divide create 32-bit",
namej+"cell"+count+"ADAM10.tif",namej+"cell"+count+"EphA2.tif");

        saveAs("TIFF",processed+"/"+tabletemp+"cell"+count+"ratio");
                                        run("8-bit");
                                        saveAs("TIFF",dir8+"/"+tabletemp+"cell"+count+"ratio");
                                        close();
                                        selectWindow(namej+"cell"+count+"ADAM10.tif");
                                        resetMinAndMax();
```

```
                                        run("16-bit");

        saveAs("TIFF",dir16+"/"+tabletemp+"cell"+count+"ADAM10");
                                        resetMinAndMax();
                                        run("8-bit");

        saveAs("TIFF",dir8+"/"+tabletemp+"cell"+count+"ADAM10");
                                        close();
                                        selectWindow(namej+"cell"+count+"EphA2.tif");
                                        resetMinAndMax();
                                        run("16-bit");

        saveAs("TIFF",dir16+"/"+tabletemp+"cell"+count+"EphA2");
                                        resetMinAndMax();
                                        run("8-bit");

        saveAs("TIFF",dir8+"/"+tabletemp+"cell"+count+"EphA2");
                                        close();}
                                        }
                        else{
                                resetMinAndMax();
                                saveAs("TIFF",dir8+"/"+tabletemp+"cell"+count+"bf");}
                }
        }
        roiManager("reset");}
selectWindow(table);
saveAs("Text",dir1+table+" Mean Intensities and Ratio.xls");
```

Appendix D

Calculating Pearson's Coefficient for Two Channels

```
// This ImageJ macro takes 16-bit tif files that have been cropped
// (generated by Appendix C file) and
// calculates the red-green Pearson's coefficient for each cell
// Displays two dialog boxes. Select the raw data source directory in the first
// In second box, choose whether 1.5x lens was used-must be noted during data collection
// In third box, enter treatment—grid pitch or drugging conditions
// Outputs Excel spreadsheet with Pearson’s coefficient between red and green channels
// for each cell

  dir1 = getDirectory("Where is the raw data?");
  dir16=dir1+"/16bit/";
  list = getFileList(dir16);
  l=list.length;
  Dialog.create("Magnification");
  Dialog.addCheckbox("1.5x ", false);
  Dialog.show();
  highmag=Dialog.getCheckbox();
  if (highmag==true){
        resolution = 115;}
  else{
        resolution = 165;}
  exact = 20000/resolution;
  width = round(exact);
  height = width;
  Dialog.create("Spatial Mutation");
  Dialog.addString("Grid pattern? ","Unrestricted");
  Dialog.show();
  table=Dialog.getString()+" Pearson's Coefficients";
  tablename="["+table+"]";
  run("Table...", "name="+tablename+" width=350 height=250");
  print(tablename,"\\Clear");
  print(tablename, "\\Headings:Cell\tPearson's Coefficient");
  setBatchMode(true);
  cell=0;
  for (i=0; i<l;i+=2){
        open(dir16+list[i]);
        cellname=split(list[i],"cell");
        cellname2=split(cellname[1],"ADAM");
        heightA=getHeight();
        widthA=getWidth();
        EphA2=newArray(heightA*widthA);
        ADAM10=newArray(heightA*widthA);
        locationA=0;
        for (j=0; j<heightA; j++){
              for (k=0; k<widthA; k++){
                    EphA2[locationA]=getPixel(j,k);
```

```
                locationA++;
        }
}
close();
open(dir16+list[i+1]);
locationB=0;
for (j=0; j<heightA; j++){
        for (k=0; k<widthA; k++){
                ADAM10[locationB]=getPixel(j,k);
                locationB++;
        }
}
close();
num=0;
den1=0;
den2=0;
coeff=newArray(6);
count=0;
sumA=0;
sumB=0;
sumAB=0;
sumsqrA=0;
EphA2mean=0;
ADAM10mean=0;
for (m=0; m<EphA2.length; m++){
        if (EphA2[m]>=0 && ADAM10[m]>=0){
                sumA+=EphA2[m];
        sumB+=ADAM10[m];
        sumAB+=EphA2[m]*ADAM10[m];
        sumsqrA+=EphA2[m]*EphA2[m];
        count++;}
}
EphA2mean=sumA/count;
ADAM10mean=sumB/count;
for (m=0; m<EphA2.length; m++){
        if (EphA2[m]>=0 && ADAM10[m]>=0){
        num+=(EphA2[m]-EphA2mean)*(ADAM10[m]-ADAM10mean);
        den1+=(EphA2[m]-EphA2mean)*(EphA2[m]-EphA2mean);
        den2+=(ADAM10[m]-ADAM10mean)*(ADAM10[m]-ADAM10mean);}
}
//0:a, 1:b, 2:corr coeff, 3: , 4: den1, 5: den2
coeff[0]=(count*sumAB-sumA*sumB)/(count*sumsqrA-(sumA*sumA));
coeff[1]=(sumsqrA*sumB-sumA*sumAB)/(count*sumsqrA-(sumA*sumA));
coeff[2]=num/(sqrt(den1*den2));
coeff[3]=num;
coeff[4]=den1;
```

```
        coeff[5]=den2;
        print(tablename,
"\\Update"+cell+":"+cellname[0]+"_"+cellname2[0]+"\t"+d2s(coeff[2],4));
        cell++;
 }
selectWindow(table);
saveAs("Text",dir1+table+".xls");
```